HAL
open science

Functionalized carbon nanotubes for detecting traces of benzene vapors employing screen-printed resistive and resonant transducers

Pierrick Clément

To cite this version:

Pierrick Clément. Functionalized carbon nanotubes for detecting traces of benzene vapors employing screen-printed resistive and resonant transducers. Electronics. Université de Bordeaux; Universitat Rovira i Virgili (Tarragone, Espagne), 2015. English. NNT : 2015BORD0127 . tel-01233027

HAL Id: tel-01233027

https://theses.hal.science/tel-01233027

Submitted on 24 Nov 2015

HAL is a multi-disciplinary open access archive for the deposit and dissemination of scientific research documents, whether they are published or not. The documents may come from teaching and research institutions in France or abroad, or from public or private research centers.

L'archive ouverte pluridisciplinaire **HAL**, est destinée au dépôt et à la diffusion de documents scientifiques de niveau recherche, publiés ou non, émanant des établissements d'enseignement et de recherche français ou étrangers, des laboratoires publics ou privés.

THÈSE EN COTUTELLE PRÉSENTÉE

POUR OBTENIR LE GRADE DE

DOCTEUR DE

L'UNIVERSITÉ DE BORDEAUX

ET DE L'UNIVERSITÉ ROVIRA I VIRGILI

ÉCOLE DOCTORALE UBX

ÉCOLE DOCTORALE DU PARTENAIRE

SPÉCIALITÉ : ELECTRONIQUE

Par Pierrick CLEMENT

Functionalized carbon nanotubes for detecting traces of benzene vapors employing screen-printed resistive and resonant transducers

Soutenue le 24 septembre 2015

Membres du jury :

Dr. Maria PILAR PINA, Universidad de Zaragoza – INA	Présidente
Pr. Philippe MENINI, Université de Toulouse Paul Sabatier – LAAS	Rapporteur
Pr. Eduard LLOBET, Universitat Rovira i Virgili – MINOS	Directeur de thèse
Dr. Hélène DEBEDA, Université de Bordeaux – IMS	Directrice de thèse

Titre: Nanotubes de carbone fonctionnalisés pour la détection de traces de vapeurs de benzène à l'aide de transducteurs résistifs et résonants sérigraphiés

Résumé: Ce travail de thèse porte sur l'optimisation des propriétés de nanotubes de carbone pour la détection de gaz. Pour cette application, les nanotubes de carbone ont été déposés sur deux types de transducteur sérigraphiés, résistif et résonant. Les nanotubes de carbone à multi-parois traités par plasma d'oxygène (O-MWCNTs) ont été le point de départ de ces travaux. Les performances de ces nanomatériaux déposés par air-brushing sur le transducteur de type résistif comportant deux électrodes de platine interdigitées préalablement déposées sur un substrat d'alumine ont été étudiées en présence de composés organiques volatils (COVs). Par comparaison aux réponses obtenues sous éthanol et acétone, une meilleure sensibilité et un meilleur temps de recouvrement ont été observés en présence de benzène et de toluène. Les nanotubes de carbone O-MWCNTs ont été ensuite déposés sur une micropoutre piézoélectrique sérigraphiée. Cette dernière, à base de PZT placé entre 2 électrodes, permet simultanément l'actionnement et la mesure de sa fréquence de résonance. De plus, le remplacement de l'électrode supérieure de géométrie rectangulaire par deux électrodes interdigitées a permis la mesure simultanée de la résistance des nanotubes de carbone et de la fréquence de résonance. Grâce à cette nouvelle génération de transducteur, la variation de résistance de la couche de nanotubes de carbone et la variation de masse ont pu être mesurés en présence de COVs mais aussi de monoxyde de carbone et de dioxyde d'azote. Sous forte concentration de vapeurs/gaz, la prise de masse de la couche sensible entraîne des variations de fréquence négatives. En revanche, à plus faible concentration, des variations de fréquence positives ont été observées. Ce phénomène est attribué à une modification de la rigidité de la poutre résonante

suite à l'adsorption sur la poutre de l'espèce à détecter en faible quantité. La mesure simultanée de la résistance des O-MWCNTs de type-p a de plus permis la discrimination du caractère oxydant ou réducteur des gaz/vapeurs. Finalement, face à la difficulté de détecter le benzène à faible concentration, une approche basée sur la reconnaissance moléculaire « host-guest » a été proposée. Afin de promouvoir des interactions spécifiques avec le benzène, les MWCNTs ont été fonctionnalisés avec une molécule de type quinoxaléine en conformation de cavité. Ainsi, la mesure de la résistance de ce nanomatériau hybride a permis la détection de 2,5 ppb de benzène sous air sec avec une limite de détection (LOD) proche de 600 ppt. Ces résultats remarquables démontrent les potentialités des nanotubes de carbone fonctionnalisés pour la détection de faibles traces de composés aromatiques.

Mots clés: nanotubes de carbone, capteur, résistif, résonant, piézoélectrique, benzène, reconnaissance moléculaire

Title: Functionalized carbon nanotubes for detecting traces of benzene vapors employing screen-printed resistive and resonant transducers

Abstract: Multiwall carbon nanotubes (MWCNTs) base sensitive layers have been deposited onto different transducer substrates for gas sensing application. Oxygen plasma treated MWCNTs, so-called O-MWCNTs, have been a building block for developing other gas sensitive nanomaterials. At first, O-MWCNTs have been studied as resistive gas sensors. Volatile organic compounds (VOCs) such as benzene, toluene, ethanol, methanol and acetone have been used to characterize this sensitive layer. The sensors show good sensitivity and excellent baseline recovery in the presence of benzene or toluene vapors compared to the others tested VOCs. O-MWCNTs have been studied as adsorbent nanomaterials deposited on PZT piezoelectric resonant cantilevers fabricated by multilayer screen-printing. In the second step, a modification of the rectangular top electrode to become an interdigitated electrode was implemented in order to have a sensor transducer employing two transduction mechanisms. This configuration allowed us to measure, for a single device, the resistance change of the carbon nanotube film and the resonance frequency shift of the PZT cantilever upon exposure to VOCs. The sensing properties of such systems have been studied for benzene, CO, and NO2 contaminants. Positive and negative shifts of the resonance frequency are observed at low and high gas concentrations, respectively. These are attributed to stress or to mass effects becoming dominant at low or high gas concentration levels. Monitoring the resistance of the p-type O-MWCNT film helps discriminating gases/ vapours according to their oxidizing or reducing character. The interest of the double transduction has been demonstrated in the detection of CO. Finally, in front of the difficulty to detect benzene at low concentrations, a different approach based on the host-guest molecular recognition is proposed. To promote specific interaction toward benzene, quinoxaline-walled

thioether-legged deep cavitand functionalized MWCNTs are used. The detection of 2.5 ppb of benzene in dry air is demonstrated with a limit of detection (LOD) near 600 ppt. These remarkable results show the potentiality of functionalized carbon nanotubes in aromatic vapor sensing at traces level.

Keywords: carbon nanotubes, sensor, resistive, resonant, piezoelectric, benzene, molecular recognition

Unité de recherche

[IMS, UMR 5218, 351 Cours de la Libération, 33405 Talence]

Acknowledgement

Firstly, I would like to express my sincere gratitude to my advisors Prof. Eduard Llobet, Dr. Hélène Debéda and Dr. Claude Lucat for their excellent guidance, support and availability. They always carried me when talking about new ideas and dedicated lot of time for my writing. Also, this thesis has been possible thanks to their respective knowledge and collaboration.

I also thank the CTP funding under grants no. 2011CTP00015 (Catalonia) and no. 369831/36982 (Aquitaine) that financially supported this thesis.

I would like to thank Pr. Pablo Ballester for his collaboration with the use of cavitand as recognition part of the sensor. In that sense, I really thank my colleague and friend Dr. Sasa Korom for his time with the synthesis of the cavitand and all his precious advices related to results interpretation.

I deeply trust that without a strong technical support, a PhD student cannot extend his personal skills and loose lot of time so I would to thank Dr. Raul Calavia Boldu, the Jordi Mare team (Badi, Jaume, …), the electronic microscopy team of Merce Moncusí Mercadé (Lukas, Rita, Marianna). I thank also Dr. Isabelle Favre and Jonathan Argillos for precious help in the microcantilever fabrication and their kindness.

My sincere thanks go to my teacher Stéphane Pagneux, who in critical point of my life, trusted in me and teach me chemistry with passion, that I have received afterwards. In that way, I would like to thank Dr. Franck Berger who gives me the opportunity to go in Spain and know the laboratory of Pr. Eduard Llobet.

Many thanks to Dr. Carla Bittencourt and her student Carla Struzzi for their XPS analysis and relevant comments.

I thank Prof. Nantakan Muensit and Dr. Chalongrat Daengngam for their kind reception by two times in the Prince of Songkhla University (Thailand). We had very interesting talks that have emerged ideas in this thesis.

Of course, I could not have imagined better good time without my labmates. So I sincerely thank Raul, Sergio, Oriol, Enrique, Rosa, Fatima, Giovanni, Marc, Ariadna and Angel. I do not forget my old friends with which I have shared my life, so thank you to Julien, Alexis, Ali and Patrick.

I express my deepest gratitude to all my family for their support and their kindness since always. I will never thanks enough my parents, that taught me what is life, human values and their unconditional love which helped me thousands times.

Finally, I thank Esther for her encouragement, patience and help during these four years. Her advices and love has been a key point for the success of this thesis.

Dedicated to my parents:

Daniel Clément

&

Marie-Brigitte Clément

And to my sister:

Amélie Paris

Table of content

General introduction 1

CHAPTER I: State of the art 5

1.1. Introduction 5

1.2. Overview of benzene toxic vapour 7

1.2.1. Benzene properties and emanation origin 7

1.2.2. Current techniques for analysing benzene vapours 8

1.3. Solid state gas sensors 10

1.3.1. Resistive gas sensors 10

1.3.2. Resonant cantilever based gas sensors 13

1.4. Carbon nanotubes as sensitive layer 16

1.4.1. Functionalized CNTs gas sensors 17

1.4.2. Metal decorated CNT gas sensors 19

1.5. Benzene detection based on CNT composites as gas sensitive interface 20

References 22

CHAPTER II: Transducers fabrication, CNTs deposition and experimental gas sensing setup 29

2.1. Transducer fabrication 29

2.1.1. Generalities on the screen-printing technique 29

2.1.2. Fabrication of the resistive transducer 31

2.1.3. Fabrication of the resonant transducer 33

2.1.4. Microstructural characterization 38

2.2. O-MWCNTs deposition method 39

2.2.1. On the resistive transducer 39

2.2.2. On the cantilever transducer 42

2.3. Gas sensing test setup 43

2.3.1. Sensor test chamber design and fabrication 43

2.3.2. Setup for gas sensing characterization 48

2.4. Conclusion 51

References 52

CHAPTER III: Benchmark study of oxygen functionalized MWCNTs as gas sensing interface 55

3.1. Overview 55

3.1.1. Oxygen functionalization methods 56

3.1.2. Structural and electronic properties changing 57

3.1.3. Gas sensing interaction mechanism 58

3.2. Gas sensor fabrication 60

3.2.1. MWCNTs synthesis and functionalization 60

3.2.2. Impedance spectroscopy characterization 63

3.3. Gas sensing properties of O-MWCNTs 64

3.3.1. VOCs detection 64

3.3.2. Discussion 69

3.4. Conclusion 73

References 75

CHAPTER IV: Piezoelectric resonant cantilever gas sensor with double transduction 79

4.1. Electromechanical characterization of the microcantilever 80

4.1.1. Configuration of electrical connections 80

4.1.2. Polarization step.....82

4.1.3. Electro-mechanical characterization 84

4.1.4. Theory correlation of experimental observation 91

4.2. Microcantilever preparation for gas sensing tests 100

4.2.1. Effect of CNTs deposition 100

4.2.2. Electrical measurement processing.....101

4.3. Results and discussion 102

4.3.1. Temperature effect.....102

4.3.2. Detection of volatile compounds at room temperature 104

4.3.3. Effect of humidity.....109

4.4. Conclusion.....109

References.....111

CHAPTER V: Cavitand functionalized MWCNTs for sensitive benzene detection.....113

5.1. Motivation.....113

5.2. Anchoring of the cavitand on MWCNTs.....116

5.2.1. Experimental section.....116

5.2.2. Step by step characterization 119

5.2.3. Stability study of thioether-Au bond with temperature.....124

5.3. Gas sensing properties.....126

5.3.1. High sensitivity to benzene.....126

5.3.2. Gas sensing mechanism 131

5.3.3. Humidity effect.....135

5.3.4. Case of NO_2 138

5.4. Conclusion 141

References 143

General conclusion 151

Annex I 155

Annex II 158

Annex III 166

General introduction

The detection of gases and (bio)chemical species with the help of miniaturized sensors is, nowadays, at the center of research efforts, especially for industrial applications (petro chemistry, aeronautic, transport, …), food quality control, disease diagnostic or air and water quality surveillance. Benzene, among other volatile organic compounds (VOCs) is recognized for its high toxicity, so its accurate detection is of paramount importance. In this domain, the use of resonant sensors is attracting interest and, very recently, sensor microsystems based on piezoelectric thick films alone or screen printed on silicon cantilevers are getting promising results. This thesis has as starting point the results of a previous project, which allowed the realization of a detection platform using screen-printed microcantilevers from piezoelectric material (PZT) to generate unusual, in-plane 31-longitudinal vibrations modes. To achieve a low detection limit (<ppm), microcantilevers were coated with different organic and inorganic adsorbing materials. The best results for a reversible detection of benzene at room temperature were obtained with active carbon. These interesting results push us, in the framework of this thesis, to continue optimizing the sensing platform in view of detecting very low benzene concentrations (few tens of ppb). Nevertheless, the previously used active carbon compounds lack of intrinsic selectivity and, therefore, have been replaced by carbon nanotubes. This nanomaterial offers the advantage of being

easily modified employing different strategies in order to obtain higher and more specific interaction with the toxic volatile target to be detected. Additionally, an improvement in the sensitivity and the viability of the detection platform is sought by optimizing the piezoelectric properties of the transducer. Finally, a modification will be brought to the platform in order to measure the conductivity of the sensitive layer additionally to the resonance frequency of the piezoelectric cantilever with the objective to improve selectivity. The manuscript of this thesis is divided in five chapters as follows:

Chapter I presents a general description related to the risks of benzene exposure with the presentation of the conventional analytical techniques for monitoring the environment. Then, it reviews the latest technologies used in gas sensing devices and focuses in benzene detection.

Chapter II describes, at first, the fabrication of the transducers used for the gas sensing application considered in this Thesis. Then, an experimental section describes how transducers are coated with the active layer. Finally the study of the design and fabrication of the test chamber with the different coupled elements for the gas sensing characterization is presented.

Chapter III gives a preliminary study of the gas sensing properties of oxygen functionalized multiwall carbon nanotubes as resistive gas sensors. The study is focused on the structure and electronic properties of these nanotubes with their gas sensing characterization towards different volatile contaminants.

Chapter IV proposes to enhance sensitivity and selectivity by measuring both the resonance frequency shift of a CNT coated piezoelectric cantilevers and the resistance change of CNT films upon the adsorption of gas species. Also, the piezoelectric properties of this new device are compared to the previous one (simple transduction).

Chapter V presents a different approach to enhance the interaction between benzene molecules and the sensitive layer, which is based on host-guest molecular recognition. To achieve this objective, a cavitand, which plays the role to trap benzene, is grafted onto the outer wall of multiwall carbon nanotubes and simple, resistive gas sensors employing this hybrid nanomaterial are fabricated and tested.

CHAPTER I: State of the art

In this chapter, we will give a general description related to the risks of benzene exposure. Also, conventional analytical techniques for monitoring the environment will be presented. Then we will focus on the latest technologies used in gas sensing devices to improve benzene detection.

1.1. Introduction

Current interests in environmental protection are focused in outdoor and indoor air quality. Harmful gases present in the atmosphere can spoil our environment and cause disease or death to humans and other living organisms. Gas pollutants can be classified as primary or secondary. Primary pollutants are generated from processes (natural or industrial) such as volcanic eruption or gas from motor vehicle exhaust for example. Major primary pollutants include:

- Nitrogen oxides (NO_x) that are principally generated from high temperature combustion.
- Carbon monoxide (CO) that is a byproduct of incomplete combustion from fuel such as natural gas or wood but its major source comes from motor vehicle exhaust.
- Sulfur oxides (SO_x) that are produced by volcanic activity and various industrial processes.

- Ammonia (NH_3) that is emitted from livestock and agricultural processes with the incorporation in foodstuffs and fertilizers.
- Volatile organic compounds (VOCs) that are well known since they are emitted basically from human activity. They are organic compounds with a very high vapor pressure at room temperature. Among them aromatic compounds such as BTEX (Benzene, Toluene, Ethylbenzene and Xylene) are known to be very toxic at low concentrations and prolonged exposure.

Secondary pollutants are not generated directly and are formed in the air when primary pollutants react or interact. they principally include:

- Ozone (O_3) that is formed in presence of NO_x and VOCs. In the stratosphere, it constitutes an important role with the Ozone layer by filtering some electromagnetic waves at high energy (UV,…). But at high concentration in air, it forms a smog with other constituents and actuate as a high oxidizing agent with other chemical compounds.
- Particulate matter (PM) that is formed from combustion reactions. The presence of ammonia has a role in the formation of particulate matter. PM is responsible for the onset of serious pulmonary diseases.

The European Commission has developed an extensive body of legislation which establishes health based standards [1] and objectives for a number of pollutants in air summarized in **Table 1.**

Table 1: Health based standards of pollutants in air

Pollutant	Concentration limit in air	Averaging periode
SO_2	47.5 ppb	24 hours
NO_2	21.2 ppb	1 year
CO	8.7 ppm	8 hours daily
C_6H_6	1.6 ppb	1 year
O_3	61.1 ppb	8 hours daily
$PM_{2.5}$*	25 $\mu g.m^{-3}$	1 year

$PM_{2.5}$= PM with diameter < 2.5 µm

1.2. Overview of benzene toxic vapour

1.2.1. Benzene properties and emanation origin

Benzene is a non-polar six-membered ring aromatic hydrocarbon with molecular formula C_6H_6, with dimensions of ca. 6.0 x 3.5 Å and a volume of 120 $Å^3$. It belongs to the BTEX (Benzene, Toluene, Ethylbenzene and Xylene) group of compounds. The components of this group feature similar structures but quite different toxicological properties. Benzene is present in the petrochemical industry, land reclamation, petroleum coke oven operators, petrol stations, motor vehicle repair stations, roadside works and many other industries.[2] Cigarette smoking is another important source of exposure to benzene.[3] It is listed among the most harmful VOCs. It generates highly flammable and toxic vapours and is recognized as a human carcinogen by the US Environmental Protection Agency and by the European Commission. Long term exposures to relatively low concentrations of benzene over months or years lead to severe hemotoxic effects such as aplastic anaemia and pancytopenia and to

acute non-lymphocytic leukaemia.[4-6] In the last ten years, the permissible exposure limit has been lowered from 10 ppm to 100 ppb.[7] According to the Directive 2008/50/EC of the European Parliament and of the Council of May 2008, the limit value for the annual average exposure to benzene is 5 $\mu g.m^{-3}$ (1.6 ppb).[8]

1.2.2. Current techniques for analysing benzene vapours

Nowadays, several methods for detecting benzene traces are in use. They provide fairly accurate and selective gas reading. Most of them involve pumping of the sample and subsequent analysis by employing colorimetric detector tubes, gas chromatography (GC) coupled to a detector like flame ionisation detector (GC-FID) or mass spectrometer (GC-MS), nuclear magnetic resonance (NMR) and Fourier transform infrared spectroscopy (FTIR). These methods are bulky, expensive and do not allow for implementing a continuous monitoring of benzene traces. Furthermore, they require specially skilled and knowledgeable operators. In the last few years, pre-concentration methods and GC equipment have been improved in terms of miniaturization and with a LOD reaching the ppb level for benzene.[9-11] However, such systems are still limited by their long response time, high power consumption and high cost. Alternatively, the use of portable photoionization detectors (PID) has been reported as well (Photovac, Raesystems, Draeger), but PID devices are not selective to benzene and give a total reading for VOCs. The photoionization measurement process consists of the illumination by high energy UV (Ultra Violet) light of a molecule. The photons absorbed provoke the ionization of the molecule. Ions can be detected by applying an electric field. The resulting current measured depends

of the concentration of the molecule ionized. Sensing principle is shown in **Figure 1**.

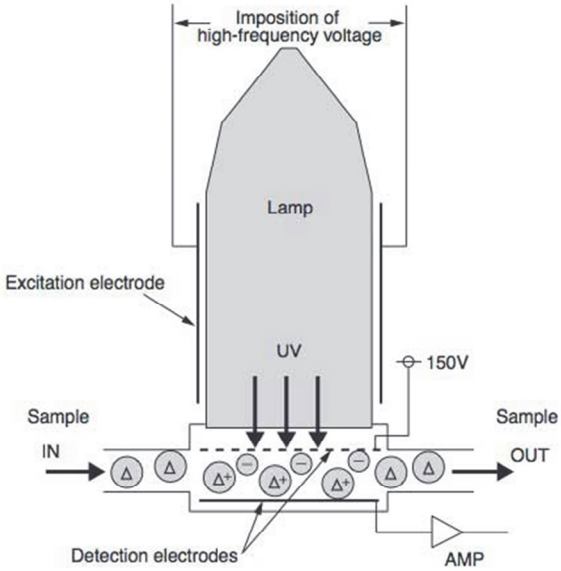

Figure 1: Operating principle of a photoionization detector

The lack of selectivity of such a device is clearly dependant on the choice of the ionization lamp. One option to make PID more selective for benzene is to utilize a single-use, disposable and rather expensive filter at the inlet port of the device what would result in a dramatic cost increase of running benzene measurements. Human activity may result in active exposure to benzene and would clearly benefit from affordable, portable, highly sensitive and selective detectors able to run continuous measurements. Keeping this in mind, scientists have intensified their research in another kind of detection systems that can be used for gas identification and control. These are solid state gas sensors and their principle consists of a sensing layer that allows recognizing the target gas with which it interacts and a transducer to

transform the chemical/physical interaction into an electrical or optical signal.

1.3. Solid state gas sensors

A characteristic of solid state gas sensors is the reversible interaction of the gas with the surface of the solid state material. Several physical effects are used to achieve the detection of gases. In addition to the conductivity change of gas sensing material, the detection of this interaction (transduction) can be performed by measuring the change of the capacitance, work function, mass, optical characteristics or reaction energy released by the gas/solid interaction.[12] The sensing layer can be organic (polymers, complexes,…) and inorganic (metal oxide semi-conductors, electrolytes…). Nowadays, a wide variety of solid state gas sensor has been studied with interdisciplinary science such as chemistry, electronics, biology and many more. In the context of the thesis we will focus on layers of CNTs (carbon nanotubes) as sensitive nanomaterials coating either resonant (cantilevers) or non-resonant (resistive) transducers.

1.3.1. Resistive gas sensors

Resistive sensors (chemoresistors) are among the most commonly used gas sensors. Resistive gas sensors are based on the change in resistance that undergo sensitive layers upon gas exposure. The most typical sensitive layers are semiconductor metal oxides and organic semiconductors.[13] For metal oxides, the most common sensing material used in resistive gas sensing is SnO_2. Also, other metal

oxides such as ZnO, TiO_2, WO_3 and In_2O_3 have been investigated. Recently, intensive researches have been focused on the design of monocrystalline and nanostructured metal oxides in order to enhance sensitivity and stability.[14] A general rule linked to the use of metal oxides as gas sensitive layers consists of the formation of nanosized grains that partially adhere to each other. Then, they interact with oxygen to form active oxygen species that alter the electrical charge at that grain surface. By reaction with combustible gases, oxygen active species are depleted, which result in an alteration of the resistance of the device. For example, SnO_2 behaves as an n-type semiconductor due to oxygen vacancies in the crystal structure. As a result, two electrons at a tin atom become free.[13] When tin dioxide is exposed to ambient oxygen, oxygen molecules adsorb at the interface and each oxygen molecule captures electrons via the conduction band of the semiconductor forming adsorbed anionic oxygen species such as O_2^-, O^- and O^{2-} which depend strongly on the operating temperature.[15] Then, gas molecules can interact with such oxygen reactive species resulting in the surface depletion of charge carriers as shown in **Figure 2.**

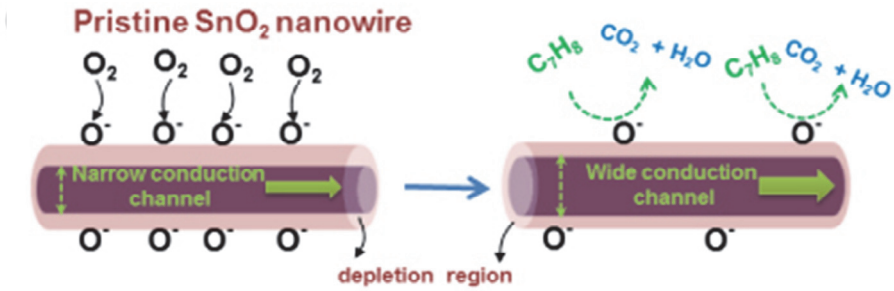

Figure 2: Formation of a charged layer by oxygen chemisorption and the effect of a reducing gas, adapted from [16]

Besides metal oxides, organic semiconductors have merged as a new class of gas sensing material. Unlike traditional inorganic sensors, they present innate porosity and a wide range of morphologies are provided adjusting directly synthesis or post-synthesis parameters. Additionally, they can operate at room temperature which is an advantage for very low power consumption. For example, Gaudillat P. *et al.* have shown superior performance of polymer-phtalocyanine hybrid material for ammonia sensing in high humidity atmospheres. They could detect 30 ppm of ammonia in 10-70% of relative humidity (R.H).[17] Also, Dan Y. *et al.* have shown sensitive performance of poly(3,4-ethylenedioxythiophene) /poly(styrenesulfonate) (PEDOT/PSS) with relative resistance changes of 10.5%, 9% and 4% towards acetone, methanol and ethanol, respectively.[18] Another similar class of compounds based on carbon material are carbon nanotubes (CNTs). They have become the most studied carbon nanomaterial for developing gas sensors.[19] The electronic properties of CNTs have been found to be extremely sensitive to their local environment with a high specific area. Furthermore, gas sensing properties can be tuned thanks to the modification of their external wall as shown in **Figure 3.**

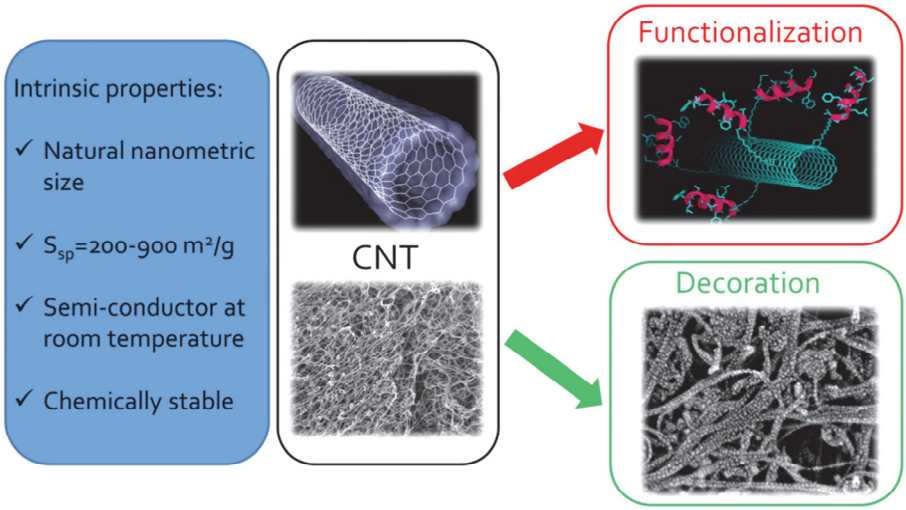

Figure 3: Possible modifications of CNTs

For all these intrinsic properties, CNTs have been chosen as sensitive layer for the development of benzene gas sensing. Details on their electronic properties and gas sensing mechanism are shown later in chapter III.

1.3.2. Resonant cantilever based gas sensors

First interests in the use of cantilevers as potential chemical or physical sensor come from advances in the study of AFM (Atomic Force Microscopy) probes. During the last two decades, microelectromechanical systems (MEMS) have facilitated the development of sensors that involve transduction of mechanical energy. Bimorph effect is observed with an AFM probe when it is covered with a metallic layer on one side and, afterwards, has been exploited for humidity, temperature [20] and chemical [21] sensor applications. Then, several studies based on the bimorph effect or chemically induced strain effect have been investigated.[22] One of

the first systems based on silicon microcantilevers consisted of gas sensors arrays coated with a layer of different polymers allowing to detect simultaneously changes in surface strain induced by adsorption of alcohols that could be distinguished.[15] For chemical sensing, the microcantilever is generally coated with a sensitive layer with the aim to adsorb with more affinity the target species. Then, the adsorbed element can be detected by measuring the quasi-static deflexion (static mode) or the shift of the resonance frequency (dynamic or resonant mode) of the microcantilever.

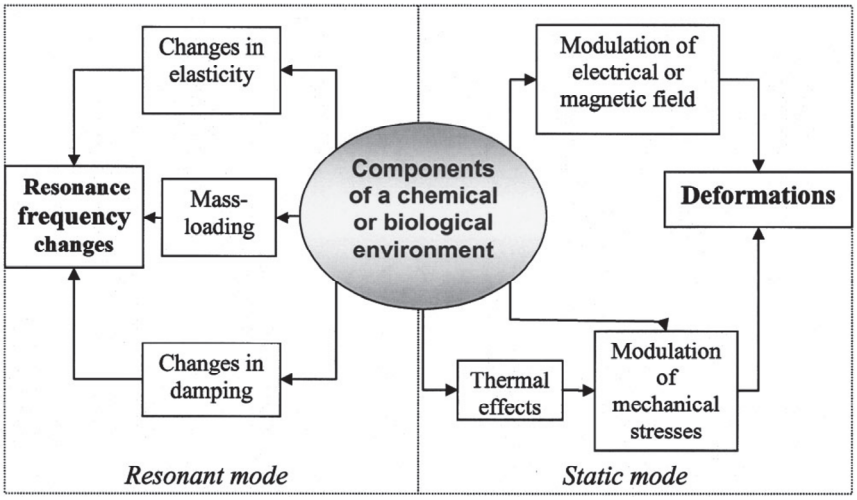

Figure 4: Conversion of input stimuli into output signals by cantilever transducers is associated with a number of transduction mechanisms. Depending on the measured parameter—structural deformations or resonance frequency changes—the mode of sensor operation can be referred to as either static or resonant. Each of these modes, in turn, can be associated with different transduction scenarios.[23]

The measured parameter chosen is directly related to the cantilever deflection or the resonance frequency and the mode of the cantilever operation can be referred to as either static or resonant. Each of these

modes, in turn, can be associated with different transduction scenarios (**Figure 4.**). For static cantilever deflection, transduction takes place by external forces exerted on the cantilever or intrinsic stresses generated on the cantilever surface (or within the cantilever). On the other hand, for cantilever sensors operating in dynamic mode, variation of the resonance frequency depends upon the attached mass as well as viscoelastic properties of the cantilever and the medium.

The bending and the changes of the cantilever resonance frequency can be monitored by several techniques like optical beam deflection,[24] piezoresistivity,[25] piezoelectricity,[26] interferometry,[27] capacitance [28] and electron tunneling [29] for the most important. Previous works have shown that screen-printed piezoelectric cantilevers based on PZT ($PbZr_xTi_{1-x}O_3$) can be an alternative technology to the silicon micromachining for cantilever gas sensors.[30] The advantage of piezoelectric material is that it can be used both for actuating and transducing as a result from mechanical or electrical stimuli. Thus, it allows a simplification of the fabrication process of the microcantilevers and of their actuation/detection mode. All these properties show that PZT printed microcantilevers are good candidates for chemical sensors in gas sensing applications. Also, CNTs (carbon nanotubes) have been chosen as sensitive layer deposited on the cantilever because, as 1D nanomaterial, they present high specific area for gas adsorption.

1.4. Carbon nanotubes as sensitive layer

Carbon nanotubes (CNTs) belong to the family of fullerene structures. Theses allotropes of carbon have been re-discovered by Iijima in 1991 [31] and particular interest has been devoted in many applications of this new class of nanomaterial.[32-34] Their structure arises from the folding of a graphene sheet (planar structure of hexagonal carbon rings), rolled-up into a seamless cylinder with diameter of few nm and length from 1 to 100 µm. CNTs are chiral structures and can be classified in two groups: single wall carbon nanotube (SWCNT) with on single outer wall and multiwall carbon nanotubes (MWCNTs) with multiple concentrically nestled walls (with interlayer graphite distance of 0.34 nm) as shown in **Figure 5.**

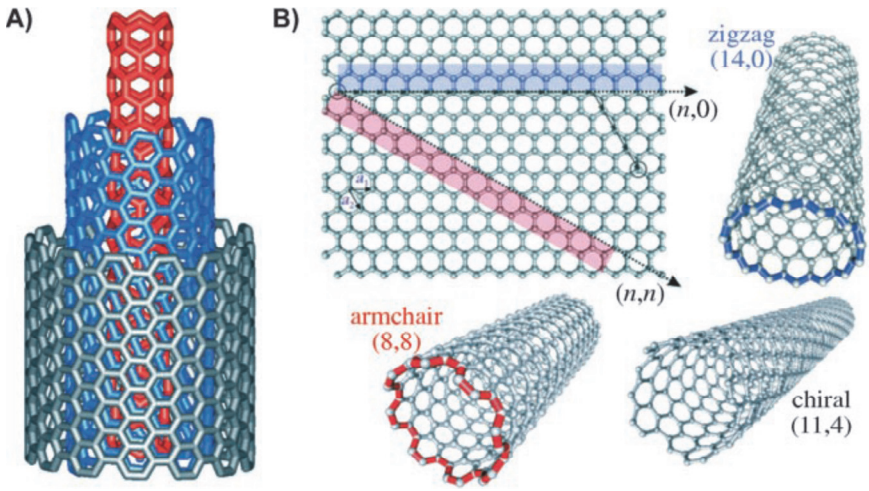

Figure 5: A) Conceptualized depiction of a multiwalled carbon nanotube (MWNT) with concentrically nestled walls. A single-walled carbon nanotube (SWNT) consists of one wall, or the innermost (red) CNT. B) Schematic depiction of the roll-up vectors (n,m) of a CNT, showing armchair (n=m), chiral (n≠m), and zigzag (n,0) SWNTs [35]

SWCNTs can be either metallic or semiconducting depending to the roll-up vector. If n-m=3q (where q is an integer or zero) it is a metallic SWCNT and when n-m≠3q, it is a semiconducting SWCNT. As far as coaxial SWCNTs (i.e. MWCNTs), calculation have shown that each of the SWCNTs tends to maintain its own behaviour, yet tube interactions may occur that are likely to modify the electronic behaviour for specific relative positions of the superimposed graphene lattices.[36, 37] However, this is specifically sensitive for tubes with relatively small diameters.[38] As soon as radii of curvature are larger than 7 nm (almost always the case for MWCNTs), the band gap energy of the semiconducting SWCNTs is lower than the thermal energy at room temperature, meaning that all MWCNTs whose outer diameter is larger than 14 nm exhibit a metallic behaviour.[39] As mentioned in 1.2.1, pristine (without chemical modifications) CNTs present several advantages to compensate their lack of specificity to different gaseous analytes and also the low sensitivity towards gases that do not interact with CNTs. Functionalization and decoration of CNTs walls can tune the reactivity / interaction with a target gas. Some of such modifications are presented below and their sensing properties are compared to those of pristine CNTs.

1.4.1. Functionalized CNTs gas sensors

Indeed, functionalization of CNTs walls allows creating specific interactions with the target analyte and can also improve the dynamic sensing. The functionalization can be distinguished in two

approaches: covalent functionalization and non-covalent functionalization. These two pathways differ by the type of the linkage of the functional entity used to functionalize the CNTs wall. The non-covalent functionalization is principally based on the use of multiple weak forces such as Van der Walls and π-stacking interactions for the complexation of a supramolecule and the CNTs wall.[33] This method is non-destructive because the physical properties of the CNTs stay unchanged.[40] Esra Nur Kaya *et al.* demonstrated that asymmetrically substituted ZnPc (zinc phthalocyanine) bearing one pyrene and six polyoxy groups as side chains linker bind better than symmetrically octasubstitued ZnPc bearing eight polyoxy groups linker. It is shown that SWCNT-pyrene containing ZnPc response towards ammonia vapour was almost 2 times higher than SWCNT without pyrene ZnPc and 6 times higher than pristine SWCNT.[41] Also, Yaqiong Z. *et al.* have shown the high sensing performance of SWCNTs coated with carbazolylethynylene oligomer (Tg-Car) sensor towards nitroaromatic explosive vapors at low concentration (from ppb to ppt levels). Responses are much higher with opposite signal variation compared to pristine SWCNTs.[42]

The covalent functionalization is, as the name suggests, a covalent link between the CNTs wall and the chemical function or molecule grafted. The most employed covalent functionalized CNTs are based on esterification or amidation of the carboxylic groups that are introduced on defect site of the CNTs wall during acid treatment (cf. Chapter II). For example, L. Niu *et al.* demonstrated that MWCNTs functionalized by poly(ethylene glycol) showed remarkable gas

sensing properties toward chloroform detection.[43] H. Mu *et al.* show the superior performance of amino group functionalized MWCNTs for formaldehyde sensing. They could reach high sensitivity (limit of detection of 20 ppb) compared to pristine MWCNTs that remained almost insensitive.[44]

1.4.2. Metal decorated CNT gas sensors

Metals exhibit a broad range of electronic and physico-chemical properties like adsorption capacity, high catalytic activity and efficient charge transfer. Consequently, metal nanoclusters play an important role in the gas sensing pathway in which sensitivity and selectivity can be tuned based on the reactivity of the nanocluster used.[45] Furthermore, metal nanoclusters are mechanically and chemically robust and are able to support high temperature and aggressive environment. Reactivity of metal nanocluster-CNTs upon gas exposure will depend on the metal used and the nature of the charge transfer between the metal nanocluster and the CNT induced by gas adsorption.[46, 32] The general rule of this concept is to use nanoclusters (nanosize for high specific area and maximize effect of the adsorbate on the nanocluster) that donate or accept a significant amount of charge upon adsorption of a volatile molecule resulting in a change of electron transport in the nanotube. For example, I. Sayago *et al.* have demonstrated the good response to hydrogen of Pd-decorated SWCNTs and their excellent sensitivity respected to the tested interfering gases (octane, toluene and ammonia). M. Penza *et al.* have improved NO_2 and NH_3 detection respect to pristine

MWCNTs thanks the Pt and Au nanoparticles used to catalyse the surface of MWCNTs as resistive gas sensor. The sensors had a working temperature in the range of 100-250°C.

1.5. Benzene detection based on CNT composites as gas sensitive interface

In the literature, only few studies have been focused on the detection of benzene vapours using CNTs based sensor at room temperature. Some of them are presented in **Table 2**.

Table 2: CNTs based gas sensor performance towards benzene

CNTs type	Sensor configuration	Gas vector	Detection limit	Ref.
Rh-MWCNTs	Resistor	Air	50 ppb	[47]
Pt/Au-SWCNTs	Resistor	Air	5 ppm	[48]
polyurethane-MWCNTs	Resistor	Air	N/S	[49]
FeTPP-SWCNTs	FET*	Air	500 ppb	[50]
MWCNTs	PCQMB*	Air	95 ppm	[41]
HTBN/MWNTs-OH	Resistor	Air	N/S	[51]

FET = Field Effect Transistor
PCQMB = PiezoelectriC Quartz Crystal Microbalance

Benzene remains difficult to be detected. Some improvements in the sensitivity by Rh-MWCNTs sensitive layer is observed (LOD = 50 ppb). Nevertheless, no studies with carbon nanomaterials based

chemical gas sensors investigated the selectivity towards benzene. Today, the unique way to achieve a partial selectivity is to employ an array of gas sensors and apply an algorithm of pattern recognition [47, 48, 52] (like principal component analysis, linear discriminant analysis and artificial neural networks).

References

[1] E. N. Kaya, S. Tuncel, T. V. Basova, H. Banimuslem, A. Hassan, A. G. Gürek*, et al.*, "Effect of pyrene substitution on the formation and sensor properties of phthalocyanine-single walled carbon nanotube hybrids," *Sensors and Actuators B: Chemical,* vol. 199, pp. 277-283, 2014.

[2] C. Manuela, T. Francesco, C. Tiziana, C. Assunta, S. Lara, N. Nadia*, et al.*, "Environmental and biological monitoring of benzene in traffic policemen, police drivers and rural outdoor male workers," *Journal of environmental monitoring,* vol. 14, pp. 1542-1550, 2012.

[3] S. B. Wilbur, S. Keith, O. Faroon, and D. Wohlers, "Toxicological profile for benzene," *Atlanta, Ga, USA: US Department of Health and Human Services,* 2007.

[4] D. Dougherty, S. Garte, A. Barchowsky, J. Zmuda, and E. Taioli, "NQO1, MPO, CYP2E1, GSTT1 and GSTM1 polymorphisms and biological effects of benzene exposure—a literature review," *Toxicology letters,* vol. 182, pp. 7-17, 2008.

[5] R. E. Hester and R. M. Harrison, *Volatile organic compounds in the atmosphere*: Royal Society of Chemistry, 1995.

[6] A. P. DeCaprio, "The toxicology of hydroquinone-relevance to occupational and environmental exposure," *CRC Critical Reviews in Toxicology,* vol. 29, pp. 283-330, 1999.

[7] (2014, Apr 4, 2011). *The National Institute for Occupational Safety and Health, NIOSH Pocket guide for chemical hazards: Benzene*. Available: www.cdc.gov/niosh/npg/npgd0049.html

[8] (2008, Apr 14, 2008). *Official Journal of the European Union,50/EC of the European Parliament and of the Council of 21 May 2008 on ambient air quality and cleaner air for Europe*. Available: http://ec.europa.eu/environment/air/quality/legislation/existing_leg.htm

[9] J. Sun, F. Guan, D. Cui, X. Chen, L. Zhang, and J. Chen, "An improved photoionization detector with a micro gas chromatography column for portable rapid gas chromatography system," *Sensors and Actuators B: Chemical,* vol. 188, pp. 513-518, 2013.

[10] C. Liaud, N. Nguyen, R. Nasreddine, and S. Le Calvé, "Experimental performances study of a transportable GC-PID and two thermo-desorption based methods coupled to FID and MS detection to assess BTEX exposure at sub-ppb level in air," *Talanta,* vol. 127, pp. 33-42, 2014.

[11] R.-S. Jian, Y.-S. Huang, S.-L. Lai, L.-Y. Sung, and C.-J. Lu, "Compact instrumentation of a μ-GC for real time analysis of sub-ppb VOC mixtures," *Microchemical Journal,* vol. 108, pp. 161-167, 2013.

[12] M. J. Madou and S. R. Morrison, *Chemical sensing with solid state devices*: Elsevier, 2012.

[13] F.-G. Banica, *Chemical sensors and biosensors: fundamentals and applications*: John Wiley & Sons, 2012.

[14] M. Arafat, B. Dinan, S. A. Akbar, and A. Haseeb, "Gas sensors based on one dimensional nanostructured metal-oxides: a review," *Sensors,* vol. 12, pp. 7207-7258, 2012.

[15] H. Lang, R. Berger, F. Battiston, J.-P. Ramseyer, E. Meyer, C. Andreoli*, et al.*, "A chemical sensor based on a micromechanical cantilever array for the identification of gases and vapors," *Applied Physics A: Materials Science & Processing,* vol. 66, pp. S61-S64, 1998.

[16] S. Gun-Joo, C. Sun-Woo, J. Sung-Hyun, K. Akash, and K. Sang Sub, "V-groove SnO 2 nanowire sensors: fabrication and Pt-nanoparticle decoration," *Nanotechnology,* vol. 24, p. 025504, 2013.

[17] M. Bouvet, P. Gaudillat, and J.-M. Suisse, "Phthalocyanine-based hybrid materials for chemosensing," *Journal of Porphyrins and Phthalocyanines,* vol. 17, pp. 913-919, 2013.

[18] Y. Dan, Y. Cao, T. E. Mallouk, A. T. Johnson, and S. Evoy, "Dielectrophoretically assembled polymer nanowires for gas sensing," *Sensors and Actuators B: Chemical,* vol. 125, pp. 55-59, 7/16/ 2007.

[19] E. Llobet, "Gas sensors using carbon nanomaterials: A review," *Sensors and Actuators B: Chemical,* vol. 179, pp. 32-45, 2013.

[20] T. Thundat, R. Warmack, G. Chen, and D. Allison, "Thermal and ambient-induced deflections of scanning force microscope cantilevers," *Applied Physics Letters,* vol. 64, pp. 2894-2896, 1994.

[21] T. Thundat, G. Chen, R. Warmack, D. Allison, and E. Wachter, "Vapor detection using resonating microcantilevers," *Analytical Chemistry,* vol. 67, pp. 519-521, 1995.

[22] R. Raiteri and H.-J. Butt, "Measuring electrochemically induced surface stress with an atomic force microscope," *The Journal of Physical Chemistry,* vol. 99, pp. 15728-15732, 1995.

[23] N. V. Lavrik, M. J. Sepaniak, and P. G. Datskos, "Cantilever transducers as a platform for chemical and biological sensors," *Review of scientific instruments,* vol. 75, pp. 2229-2253, 2004.

[24] G. Meyer and N. M. Amer, "Novel optical approach to atomic force microscopy," *Applied physics letters,* vol. 53, pp. 1045-1047, 1988.

[25] M. Tortonese, H. Yamada, R. C. Barrett, and C. F. Quate, "Atomic force microscopy using a piezoresistive cantilever," in *Solid-State Sensors and Actuators, 1991. Digest of Technical Papers, TRANSDUCERS '91., 1991 International Conference on*, 1991, pp. 448-451.

[26] B. Rogers, L. Manning, M. Jones, T. Sulchek, K. Murray, B. Beneschott*, et al.*, "Mercury vapor detection with a self-sensing, resonating piezoelectric cantilever," *Review of Scientific Instruments,* vol. 74, pp. 4899-4901, 2003.

[27] M. Helm, J. J. Servant, F. Saurenbach, and R. Berger, "Read-out of micromechanical cantilever sensors by phase shifting interferometry," *Applied Physics Letters,* vol. 87, p. 064101, 2005.

[28] D. R. Baselt, B. Fruhberger, E. Klaassen, S. Cemalovic, C. L. Britton Jr, S. V. Patel*, et al.*, "Design and performance of a microcantilever-based hydrogen sensor," *Sensors and Actuators B: Chemical,* vol. 88, pp. 120-131, 1/15/ 2003.

[29] T. W. Kenny, S. B. Waltman, J. K. Reynolds, and W. J. Kaiser, "Micromachined silicon tunnel sensor for motion detection," *Applied Physics Letters,* vol. 58, pp. 100-102, 1991.

[30] H. Debéda, R. Lakhmi, C. Lucat, and I. Dufour, "Use of the longitudinal mode of screen-printed piezoelectric cantilevers coated with PEUT for toluene detection: Comparison with

silicon cantilevers," *Sensors and Actuators B: Chemical,* vol. 187, pp. 198-203, 2013.

[31] S. Iijima, "Helical microtubules of graphitic carbon," *nature,* vol. 354, pp. 56-58, 1991.

[32] D. R. Kauffman, D. C. Sorescu, D. P. Schofield, B. L. Allen, K. D. Jordan, and A. Star, "Understanding the Sensor Response of Metal-Decorated Carbon Nanotubes," *Nano Letters,* vol. 10, pp. 958-963, 2010/03/10 2010.

[33] Y.-Y. Ou and M. H. Huang, "High-density assembly of gold nanoparticles on multiwalled carbon nanotubes using 1-pyrenemethylamine as interlinker," *The Journal of Physical Chemistry B,* vol. 110, pp. 2031-2036, 2006.

[34] I. Sayago, E. Terrado, M. Aleixandre, M. Horrillo, M. Fernández, J. Lozano*, et al.*, "Novel selective sensors based on carbon nanotube films for hydrogen detection," *Sensors and Actuators B: Chemical,* vol. 122, pp. 75-80, 2007.

[35] D. R. Kauffman and A. Star, "Carbon nanotube gas and vapor sensors," *Angewandte Chemie International Edition,* vol. 47, pp. 6550-6570, 2008.

[36] P. Lambin, L. Philippe, J.-C. Charlier, and J.-P. Michenaud, "Electronic band structure of multilayered carbon tubules," *Computational Materials Science,* vol. 2, pp. 350-356, 1994.

[37] Y.-K. Kwon and D. Tománek, "Electronic and structural properties of multiwall carbon nanotubes," *Physical Review B,* vol. 58, pp. R16001-R16004, 12/15/ 1998.

[38] I. Dumitrescu, P. R. Unwin, and J. V. Macpherson, "Electrochemistry at carbon nanotubes: perspective and issues," *Chemical Communications,* pp. 6886-6901, 2009.

[39] M. Monthioux, *Carbon meta-nanotubes: Synthesis, properties and applications*: John Wiley & Sons, 2011.

[40] R. J. Chen, Y. Zhang, D. Wang, and H. Dai, "Noncovalent sidewall functionalization of single-walled carbon nanotubes for protein immobilization," *Journal of the American Chemical Society,* vol. 123, pp. 3838-3839, 2001.

[41] E. S. Mañoso, R. Herrera-Basurto, B. M. Simonet, and M. Valcárcel, "A quartz crystal microbalance modified with carbon nanotubes as a sensor for volatile organic compounds," *Sensors and Actuators B: Chemical,* vol. 186, pp. 811-816, 9// 2013.

[42] Y. Zhang, M. Xu, B. R. Bunes, N. Wu, D. E. Gross, J. S. Moore*, et al.*, "Oligomer-Coated Carbon Nanotube Chemiresistive Sensors for Selective Detection of Nitroaromatic Explosives," *ACS applied materials & interfaces,* vol. 7, pp. 7471-7475, 2015.

[43] L. Niu, Y. Luo, and Z. Li, "A highly selective chemical gas sensor based on functionalization of multi-walled carbon nanotubes with poly (ethylene glycol)," *Sensors and Actuators B: Chemical,* vol. 126, pp. 361-367, 2007.

[44] M. Haichuan, W. Keke, Z. Shicheng, S. Keyi, S. Shaochi, L. Zhi*, et al.*, "Fabrication and Characterization of Amino Group Functionalized Multiwall Carbon Nanotubes (MWCNT) Formaldehyde Gas Sensors," *Sensors Journal, IEEE,* vol. 14, pp. 2362-2368, 2014.

[45] A. Star, V. Joshi, S. Skarupo, D. Thomas, and J.-C. P. Gabriel, "Gas Sensor Array Based on Metal-Decorated Carbon Nanotubes," *The Journal of Physical Chemistry B,* vol. 110, pp. 21014-21020, 2006/10/01 2006.

[46] A. Felten, C. Bittencourt, J.-F. Colomer, G. Van Tendeloo, and J.-J. Pireaux, "Nucleation of metal clusters on plasma treated multi wall carbon nanotubes," *Carbon,* vol. 45, pp. 110-116, 2007.

[47] R. Leghrib, T. Dufour, F. Demoisson, N. Claessens, F. Reniers, and E. Llobet, "Gas sensing properties of multiwall carbon nanotubes decorated with rhodium nanoparticles," *Sensors and Actuators B: Chemical,* vol. 160, pp. 974-980, 2011.

[48] Y. Lu, C. Partridge, M. Meyyappan, and J. Li, "A carbon nanotube sensor array for sensitive gas discrimination using principal component analysis," *Journal of Electroanalytical Chemistry,* vol. 593, pp. 105-110, 2006.

[49] Q. Fan, Z. Qin, T. Villmow, J. Pionteck, P. Pötschke, Y. Wu*, et al.*, "Vapor sensing properties of thermoplastic polyurethane multifilament covered with carbon nanotube networks," *Sensors and Actuators B: Chemical,* vol. 156, pp. 63-70, 2011.

[50] A. D. Rushi, K. P. Datta, P. S. Ghosh, A. Mulchandani, and M. D. Shirsat, "Selective Discrimination among Benzene, Toluene, and Xylene: Probing Metalloporphyrin-Functionalized Single-Walled Carbon Nanotube-Based Field

Effect Transistors," *The Journal of Physical Chemistry C,* vol. 118, pp. 24034-24041, 2014/10/16 2014.

[51] Y.-L. Luo, B.-X. Wang, and F. Xu, "Effect of soft–hard segment structure on vapor responsiveness of polyurethane conducting composite thin films loaded with multi-walled carbon nanotubes," *Sensors and Actuators B: Chemical,* vol. 156, pp. 12-22, 8/10/ 2011.

[52] M. O. Bristeau, R. Glowinski, and J. Periaux, "Numerical methods for the navier-stokes equations. Applications to the simulation of compressible and incompressible viscous flows," *Computer Physics Reports,* vol. 6, pp. 73-187, 8// 1987.

CHAPTER II: Transducers fabrication, CNTs deposition and experimental gas sensing setup

In this chapter, we will describe the fabrications of the transducers used and the experimental steps for the deposition of O-MWCNTs on the different substrates studied. Also, the design and the fabrication of a test chamber for the characterization of gas sensing properties will be discussed.

2.1. Transducer fabrication

2.1.1. Generalities on the screen-printing technique

The screen printing technique has been chosen for the fabrication of the transducers (resistive and cantilever-based) designed for gas sensing application. The "standard" thick layer process allows for the collective fabrication of microchips at very low cost. This process is widely used in hybrid microelectronics for the fabrication of interconnections, passive components and the encapsulation of hybrid circuits. It enables the deposition of patterns with a controlled thickness (from 10 to few tens of microns per coating). The screen-printing technique includes different steps:

- Ink fabrication, which generally consists of mixing a powder giving a final functionality of the layer and an

organic binder assuring the required rheological properties essential for the coating of the layer.

- A screen is made of a piece of stainless steel mesh stretched over a frame. A stencil is formed by blocking off parts of the screen in the negative image of the design to be printed; that is, the open spaces are where the ink will appear on the substrate. To deposit a layer, a screen is located over and just above the substrate. Like this, the deposition can be accurately executed. Then, the mesh of the screen is brought into line contact with the squeegee and scanned across the screen. The mesh should peel away from the surface immediately behind the squeegee, leaving all the ink that was in the mesh deposited onto the printing surface. A print cycle and description of the different elements are represented in **Figure 6.**
- Drying of the screen-printed layer, which allows the removing the solvents present in the ink.
- Firing of the different layers allowing decomposition of the binder giving them functional properties thanks to the sintering.

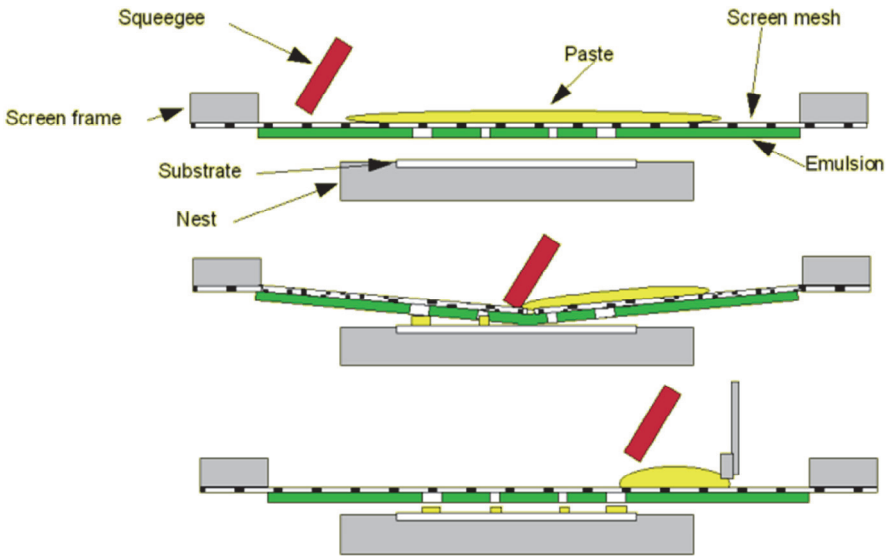

Figure 6 : Print cycle of the screen-printing process.

2.1.2. Fabrication of the resistive transducer

It is important to choose an adequate substrate to carry out the measurement of the gas sensing properties of the active material. It has to be:

- Chemically stable
- Withstand high temperature
- Low cost
- Robust

Commercially available alumina substrates (96% Al_2O_3 10×10×0.635 mm^3) were employed to fabricate the transducer element for resistive gas sensors using the standard screen-printing technique. The transducer element consists of a pair of interdigitated

platinum electrodes (electrode gap is 500 µm) at the front side of the alumina substrate and a platinum heating resistor at the back side. Different screens were used for the two step deposition. First, platinum electrodes were deposited using a 325 meshs screen and a commercial conductive paste (LPA 88/11 S, Heraeus). Once printed, the substrates were left for flattening during 20 min (help in the sintering step during the firing). After, sensor substrate were dried during 15 min at 150°C and fired in a furnace with a ramp of 30°C/min until 1100°C and then during 10 min at this temperature under air atmosphere. Finally, substrates were cooled down until room temperature. After, the heating element was made following the same steps on the backside. The final thickness for the platinum electrodes and heating resistor are approximately 7-8 µm. The alumina substrate is finally bonded on the PCB support with platinum wires (150 µm diameter) using a silver paste.

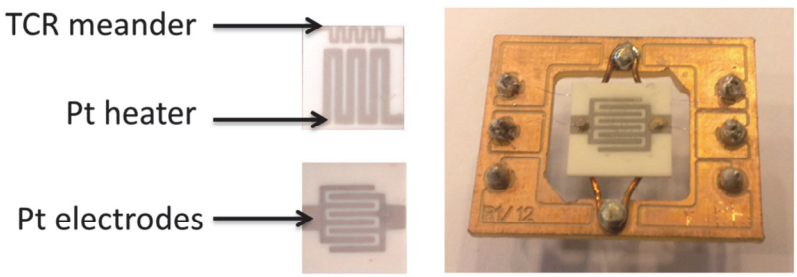

Figure 7: Screen printed alumina substrate with top view showing interdigitated electrodes, bottom view showing the heater both in platinum and wire bonded on PCB support

More details about the fabrication of the substrates can be found in reference [1].

2.1.3. Fabrication of the resonant transducer

Electroded PZT cantilevers (2x8x0.1 mm^3) are fabricated on an alumina substrate (1x1x0.250 $inch^3$) precut in four elements. By associating the screen-printing technique with the sacrificial layer process the fabrication of a movable cantilever is achieved. Details on this process can be found in [2], where the cantilevers are sandwich ones. For this new generation of cantilevers, a Pt resistive heater is integrated on the alumina substrate, and the top electrode has been replaced by interdigitated electrodes. The role of these new electrodes will be explained in chapter IV. The new patterns are given in **Figure 8**.

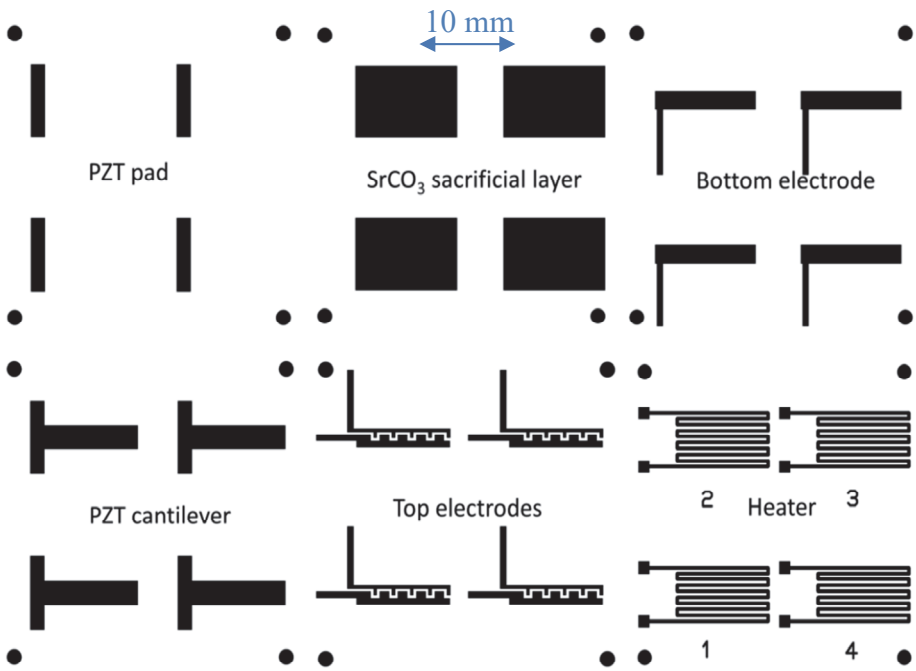

Figure 8: Patterns of the different screen-printed layers

Circles are used for alignment purposes. The fabrication process by screen-printing consists of the successive deposition of each pattern and after each screen-printed layer, the alumina substrate is dried at 120°C during 30 min in an oven. In case of the thick piezoelectric layer, a specific drying is led in order to limit the presence of cracks or holes in the PZT layer: it is dried at 1°C/mn up to 120°C before its maintaining 30min at this temperature.The fabrication steps are detailed in **Figure 9**.

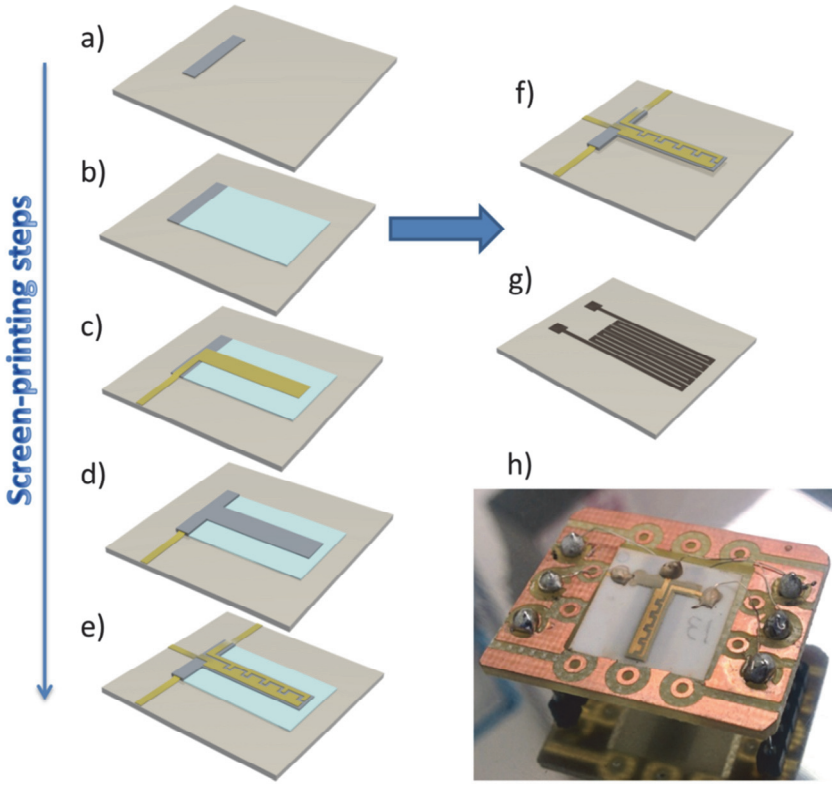

Figure 9: Fabrication steps of the (2x8x0.1 mm^3) PZT cantilever a) screen-printing of the PZT pad, b) screen-printing of the sacrificial layer, c) screen-printing of the bottom gold electrode, d) screen-printing of the PZT cantilever, e) screen-printing of the interdigitated top gold electrodes, f) top view of the cantilever after co-firing at 900°C and sacrificial layer elimination with H_3PO_4 solution at 1M, g) bottom view with the heater, h) device connected on PCB support.

The PZT ($PbZr_{0.52}Ti_{0.48}O_3$) piezoelectric ink is composed of a commercial PZT powder (pz26 PZ26 from Ferroperm) and 3 wt% LBCu as sintering aid. LBCu is composed of 25 wt% Li_2CO_3 (Alfar Aesar), 40 wt% Bi_2O_3(Alfar Aesar) and 35 wt% CuO (Sigma Ald). The piezoelectric powder is first homogenized using a Turbula equipment. Zircone balls (5 mm) and the piezoelectric powder PZT:LBCu (~20g) are rotated in 40 ml methanol during 6 hours in the Turbula. The homogenized powder is afterwards dried under a ventilated hood at ambient temperature. The piezoelectric paste is then prepared, by blending the PZT:LBCu powder with the ESL 400 (ElectroScience Laboratories) organic binder. 86%wt of powder PZT:LBCu are added in the binder to achieve good viscosity. After manual mixing in a mortar, the particles dispersion is optimized during 5 min using a three-roll mill (EXAKT 80S). The sacrificial layer paste is a mixture of 60%wt epoxy CV59 (from ElectroScience Laboratories) and 40%wt strontium carbonate ($SrCO_3$, Carlo Erba), taking into account its printability. The gold ink is commercially available (ESL8836 from ElectroScience Laboratories).

The characteristics of the chosen screens for the different layer printing are summarized in **Table 3**:

Table 3: Screens characteristics

Microheater	325 meshs, 50 µm emulsion
Sacrificial layer	70 meshs, 50 µm emulsion
Piezoelectric pad	70 meshs, 50 µm emulsion
Bottom Au electrode	325 meshs, 15 µm emulsion
Piezoelectric cantilever	150 µm stencil
Top Au electrodes	325 meshs, 15 µm emulsion

A 150 µm thick stencil is used for the piezoelectric cantilever printing to print ~150 µm thick layer at once. Then, to improve the sample densification before the firing step, the dried layers are isostatically pressed at 40 MPa during 4 min at 65°C. 3D profile analysis has been carried out with the Altisurf 500 after the densification step (before firing) and presented in **Figure 10.** This device allows running contactless measurements thanks to a polychromatic white beam whose reflection wavelengths depend on surface's relief.

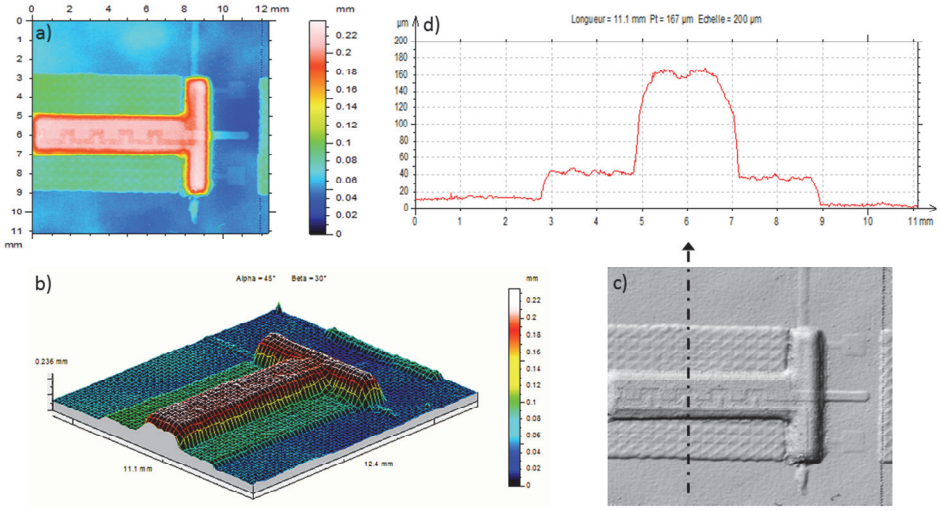

Figure 10 : 3D profile of the ID microcantilever with a) top view of z axis topography, b) 3D thickness profile, c) top view with grey contrast showing the cross-section axis analysis of d).

A homogenous deposition of each consecutive screen-printing layer is observed with the thickness profile of the microcantilever. Nevertheless, mesh patterns are visible on the sacrificial layer surface due to the printing technology. The surface remains flat through the cantilever length. A cross-section measurement shows that the thickness of the sacrificial layer and the cantilever are 35 and 120 µm, respectively.

The samples are afterwards co-fired at 900°C. The temperature profile has been optimized regarding the organic binder elimination (30<T(°C)<350), carbonate decomposition (450<T(°C)<650), LBCu eutectic fusion (T~600°C) and the PbO evaporation (onset at T~920°C). Using an heating rate of 1°C/min for 30<T(°C)<400 and 20°C/mn for 400<T(°C)<900, the samples are fired 2 hours at 900°C and cooled down to room temperature in air with a ramp of

20°C/min. They are collected at the end of the firing before reaching 50°C and immersed in ethanol (to prevent the breakage of the microcantilever due to humidity adsorption). The cantilever is finally partially released from the alumina substrate by dissolving the sacrificial layer in 1M of H_3PO_4 with ultrasonic.

Before poling and testing the piezoelectric cantilevers (chapter IV), silver wires (diameter 300µm) are glued on the gold contacts using an epoxy based paste (ESL1901 from Electroscience) cured 30 min at 120°C.

2.1.4. Microstructural characterization

A SEM analysis has been carried out on a cross section of the cantilever after the firing step. The cantilever has been embedded in a thermosetting resin and then cut following an axis as shown in **Figure 11**.

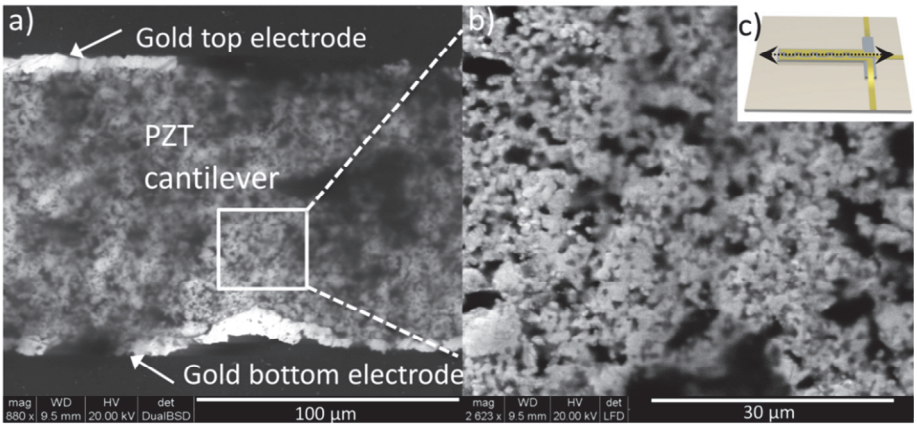

Figure 11: SEM image of a) the cross section of the cantilever and b) a zoom-in of the PZT cantilever and c) the axis of the cross section analyzed.

The thickness of the cantilever and gold electrodes are 94 µm and 5 µm, respectively. EDX analysis revealed the atomic composition of the PZT cantilever in **Table 4.** It is in accordance with the phase diagram of the commercial powder of $Pb(Zr_x,Ti_{1-x})O_3$ with x ~ 0.5, which corresponds to the mix of the quadratic and rhombohedra crystalline structure for achieving better piezoelectric properties.

Table 4: EDX analysis of the PZT cantilever

Element	Weight%	Atomic%
C K	45.46	76.22
O K	13.97	17.59
Al K	0.91	0.68
Ti K	2.84	1.19
Zr L	5.64	1.24
Au M	9.23	0.94
Pb M	21.94	2.13
Totals	100.00	

2.2. O-MWCNTs deposition method

2.2.1. On the resistive transducer

The functionalized carbon nanotubes (O-MWCNTs) were dispersed in an organic vehicle (ethanol or DMF), ultrasonically stirred during 20 min at room temperature and subsequently air-brushed onto alumina of resistive sensor substrates while controlling the resistance of the resulting film during the deposition. Details on their functionalization can be found in Chapter III. Controlling film

resistance during deposition enables us to obtain sensors with reproducible baseline values.[3]

To achieve the air brushing deposition, a homemade holder and shadow mask (with an open windows size of 5x5 mm^2) have been designed and fabricated to be used during the coating of the electrode area with active films. The holder consists of a PCB support where the sensor can be electrically connected. This allows us to heat the sensor and measure the resistance of the nanomaterial during the deposition. The suspension is introduced inside the container connected to the spraying nozzle at 5 cm from the substrate. A nitrogen gas flow is used at 10 $mL.min^{-1}$ to overcome the contamination of samples (oxidation). A fine spray from the suspension is generated. Since the airbrush deposition cone is significantly wider than the opening of the shadow mask, the deposited films show high uniformity. During deposition, substrates were kept at 100°C [4] by applying a suitable voltage to the Pt heating resistor from the holder. It ensured a fast evaporation of the solvent and very good adhesion of carbon nanotubes to the substrate. This set-up is shown in **Figure 12**.

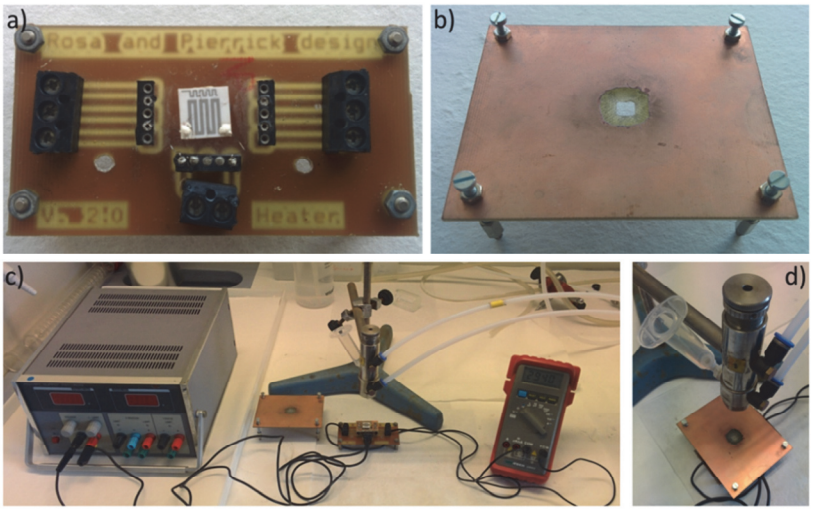

Figure 12 : Homemade system allowing resistance measurement and heating during the air brushing process with a) the holder, b) the shadow mask ($5\times5mm^2$), c) the overall system and d) the fixation of shadow mask up to the holder.

100°C is a temperature that ensures the complete evaporation of the solvent in which O-MWCNTs are dispersed when these reach the heated substrate. Lower temperatures would result in the solvent wetting the substrate during the deposition and higher temperatures would result in the solvent being totally evaporated before nanotubes actually reach the substrate. These two situations are undesirable since the former leads to a non-uniform deposition and the latter to poor adhesion of the films. After encapsulation and wire bonding, the sensors were introduced in the test chamber at 150°C during 10 min in dry air. This operation allows a 'cleaning' of the sensors without affecting the nanotube morphology, thanks to humidity and gas contamination desorption. The cleaning temperature of 150°C was set by applying a suitable voltage to the Pt heating resistor included in the sensor substrate.

2.2.2. On the cantilever transducer

A similar procedure is led for the deposition of the CNTs on the surface of the piezoelectric cantilever, with a new shadow mask window (2x8 mm^2). Again, thanks to the top gold interdigitated electrodes, the film resistance is controlled during the deposition to achieve the desired value. The cantilever is also placed at 100°C during the CNTs deposition using the Pt resistor heater from the holder.

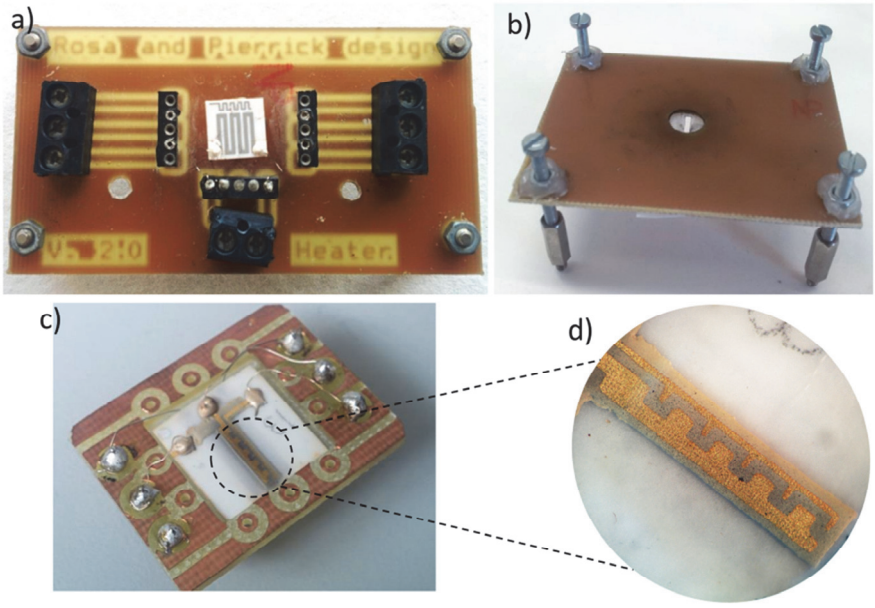

Figure 13: Homemade system allowing resistance measurement and heating during the air brushing process with a) the holder, b) the shadow mask (2×8mm^2), c) O-MWCNTs coated cantilever and d) a zoom-in of c)

2.3. Gas sensing test setup

2.3.1. Sensor test chamber design and fabrication

2.3.1.1. COMSOL simulation

Most of the times, the importance of having a correct design of the sensor test chamber is overlooked when studying the gas sensing properties of active films. In fact, it is a crucial point because the dynamic sensor response will depend on how quick and effective the injection of test gases or the cleaning process is carried out.[5] For this reason it is advantageous to use a low volume chamber and to work under laminar flow conditions. Therefore, the behavior of the gas flow in a sensor test chamber was studied employing a multiphysics approach. In order to generate an optimized geometry, simulations were carried out employing the COMSOL Multiphysics software (version 5.0). The optimized structure was then fabricated in our workshop.

The Navier-Stokes equation is used in laminar flow and is simplified for an incompressible flow approximation.[6]

$$\rho \frac{\partial \boldsymbol{u}}{\partial t} + \rho(\boldsymbol{u} \cdot \nabla)\boldsymbol{u} + \nabla p - \eta \nabla^2 \boldsymbol{u} = \boldsymbol{g}$$

With $\nabla \cdot \boldsymbol{u} = 0$

Equation 1

Where ρ is the fluid density, $\boldsymbol{u}$ is the flow velocity, η is the dynamic fluid viscosity, p is the pressure and $\boldsymbol{g}$ represents body accelerations acting on the continuum from various origins (like for example gravity). The Reynolds number calculated at the entrance of the sensor test chamber for a flow of 200 mL.min^{-1} and 4 mm inner tube diameter is 105, which corresponds to a laminar flow. The test chamber has been designed to host 4 sensors while having the lower possible number of smash-ups and keeping cavity volume as small as possible. Some additional details for the dimensions are presented in the Annex. The geometry employed in simulations is presented in **Figure 14.**

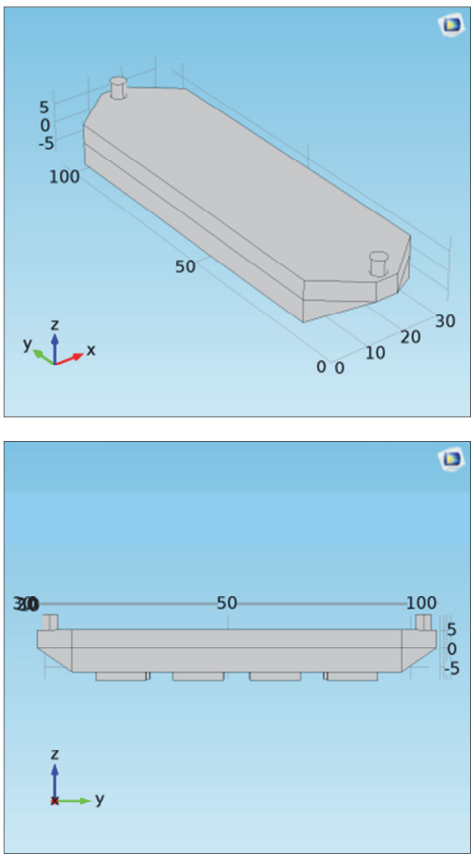

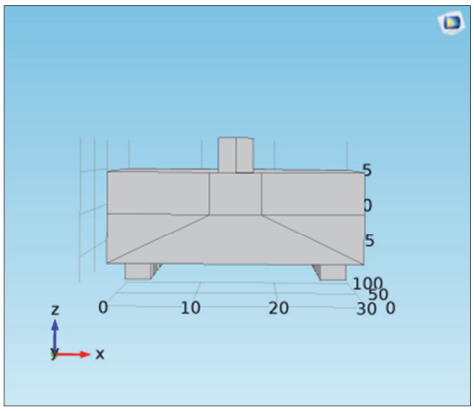

Figure 14 : Scheme design of the room sensor in a) general view, b) side view and c) front view. Dimensions are in mm.

The inlet flow enters perpendicularly from the top of the sensor chamber. Then a 45° inclination is used to orientate and lead in the flow through the chamber. Space is provided at the bottom of the chamber for the electrical connections of sensors. Results of these simulations are presented in **Figure 15.**

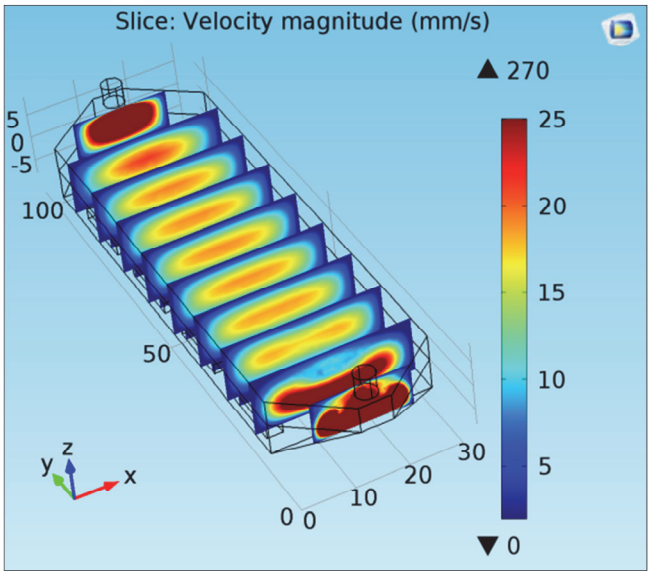

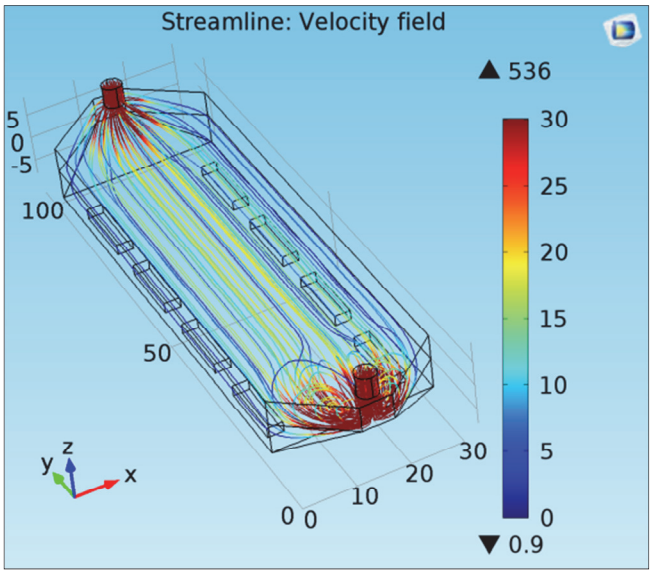

Figure 15 : Velocity magnitude and velocity field of a 200 mL.min^{-1} air flow through the room sensor. The inlet flow is at the bottom and the outlet at the top.

We observe that the variation in velocity magnitude remains small enough within a wide section at the center of the chamber, where the sensors will be plugged. The velocity field allows us to see that low turbulence is observed at the entrance of the sensor chamber and then the flow remains laminar until it reaches the outlet. It is important to notice that no turbulence is observed at the chamber corners resulting in an efficient (i.e. fast) change in the chemical environment of the chamber both if a step change in gas concentration or a cleaning phase are implemented.

2.3.1.2. Chamber fabrication

COMSOL allowed us to determine a suitable geometry for the sensor test chamber. Before fabrication, the chamber was drawn employing

the CAD Orcad software (version 9.2). This is shown in the Annex. Teflon material has been chosen for the body of the test chamber since it is an inert material (to prevent contamination from oxidative gases). Then, the top cover was made of stainless steel for allowing suitable connections with tubes and also to provide good sealing of the whole system when assembling both parts (i.e., the chamber is airtight). Pictures of the final test chamber are presented in **Figure 16.**

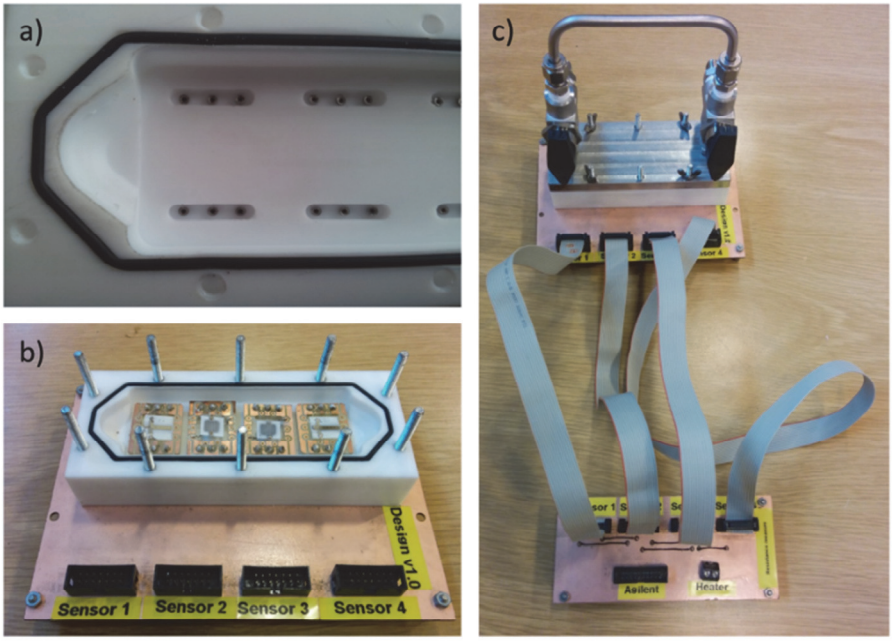

Figure 16 : Different pictures of the room sensor with a) the sensor PCB connection, b) the four sensors plugged inside the chamber and c) the whole system with the stainless steel top and electrical connections

A PCB was designed in order to have suitable connections between the four sensors and the Agilent equipment as shown in **Figure 16.** Then, heaters are connected and can be used by applying a voltage at the heater port. A by-pass valve has been implemented on the top of

the lid to facilitate purging of the gas line when a calibrated gas bottle has to be changed.

2.3.2. Setup for gas sensing characterization

2.3.2.1. First setup

To characterize sensor performance towards different hazardous species a gas line system was assembled in order to deliver different concentrations of these species in a reproducible way. The gas sensing properties of the sensors were measured using the 35 mL volume, Teflon test chamber described above. Computer-controlled mass flow (FIC=Flow Indictor and Controlled) meters (Bronkhorst hi-tech 7.03.241) and calibrated gas bottles were used (NO_2, CO, ethanol, benzene, toluene, all diluted in pure air from Praxair) with pure air from Air Products. Such a system allows for obtaining different concentrations of the species tested. A temperature sensor was included after the test chamber (TI=Temperature Indicator). The general scheme of the measurement setup is presented in **Figure 17.**

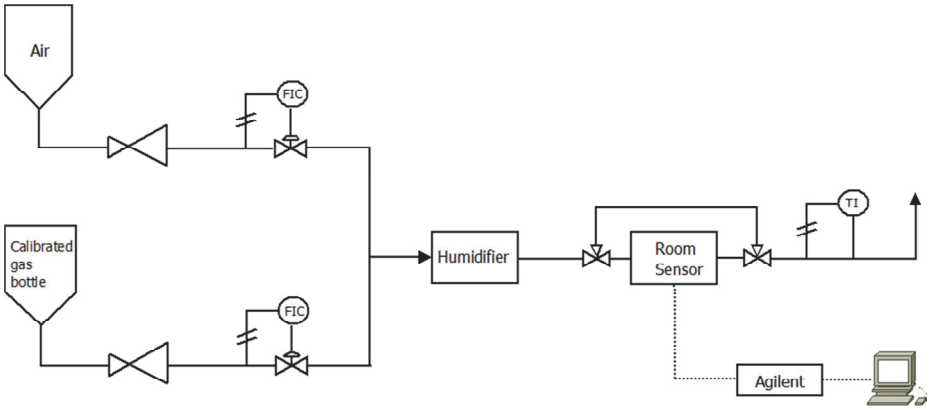

Figure 17 : Scheme of the first experimental setup

A continuous flow (100, 200 or 400 mL/min) was used throughout measurements. The flow was humidified to 10%, 25% and 60% R.H. (Relative Humidity) by employing an Environics Series 4000 gas mixing system (Environics Inc., Tolland, CT, USA). Once sensors were placed inside the test chamber, they were connected to a multimeter or impedance meter interface, which allowed the real-time reading. Given the low concentration levels tested, the measurement rig was checked to rule out the presence of contaminants in mass-flows and tubing by performing a set of control GC/MS tests (run before, during and after gas measurements).

2.3.2.2. Second setup

The second setup is quite similar to the first one but it differs in the generation of volatile contaminants. Two manual flow meters with a capacity of 200 mL/min are connected to a pure air bottle. The

first flow meter indicates the flow of contaminant and the second one is used for the dilution as shown in **Figure 18.**

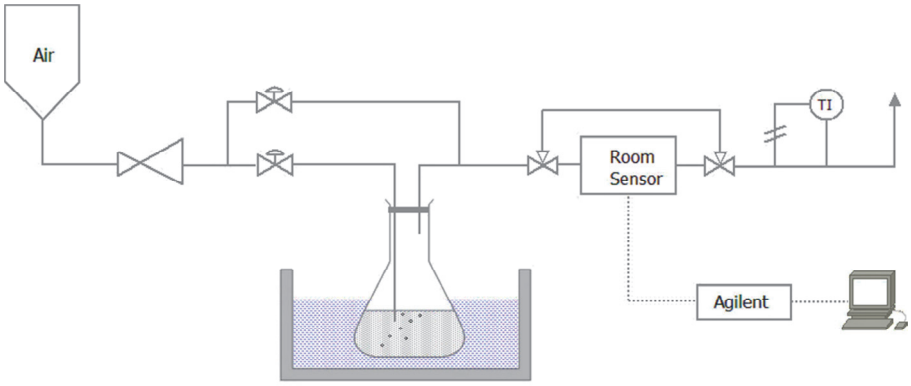

Figure 18: Scheme of the second experimental setup

Vapors are generated by bubbling dry air through the contaminant in the liquid phase. The concentration of saturated vapors is controlled by immersion in a thermostatic bath (as shown in Fig. 10). The concentration of the vapor follows the Raoult's law which gives an approximation to the vapor pressure of mixtures of liquids as shows the following equation:

$$p_{tot} = \sum_i p_i \chi_i$$

Equation 2

Where p_{tot} is the atmospheric pressure, i is one of the component of the liquid, χ_i is the mole fraction and $p_i\chi_i$ is the partial pressure of the component i in the mixture (here χ_i=1 since there is only one component) at a constant temperature. The liquids (benzene, toluene, ethanol, methanol and acetone) are maintained at a constant

temperature in order to generate the same concentration of vapor. They are provided from Sigma Aldrich with a purity of 99.8%. For each new liquid, the concentration of the vapor generated is calibrated by HPLC (high pressure liquid chromatography).

2.4. Conclusion

In this chapter, sensor transducers have been made by screen-printing technique. It allows fast and low cost fabrication of the devices. The maximum resolution reached with our method is 200 µm. Then, the air-brushing has been the method of choice to deposit the O-MWCNTs on each device. The possibility to measure the resistance while depositing the absorbent film is suitable for ensuring good device to device reproducibility. The design and the fabrication of an adapted test chamber for successfully characterizing the gas sensing performance of our resonant/ resistive sensors has been described as well. The final configuration chosen allows a fast, laminar flow of the gases tested, which minimizes the time needed for completing the different measurement phases such as contaminant injection and cleaning (i.e. baseline recovery). Furthermore, the use of mass flow control units has enabled us to fully automate the whole measurement process.

References

[1] P. Ivanov, E. Llobet, X. Vilanova, J. Brezmes, J. Hubalek, and X. Correig, "Development of high sensitivity ethanol gas sensors based on Pt-doped SnO 2 surfaces," *Sensors and Actuators B: Chemical,* vol. 99, pp. 201-206, 2004.

[2] R. Lakhmi, "Étude de micropoutres sérigraphiées pour des applications capteurs," Université Sciences et Technologies-Bordeaux I, 2011.

[3] Y. Zilberman, U. Tisch, G. Shuster, W. Pisula, X. Feng, K. Müllen*, et al.*, "Carbon Nanotube/Hexa-peri-hexabenzocoronene Bilayers for Discrimination Between Nonpolar Volatile Organic Compounds of Cancer and Humid Atmospheres," *Advanced Materials,* vol. 22, pp. 4317-4320, 2010.

[4] G. Mittal, V. Dhand, K. Y. Rhee, S.-J. Park, and W. R. Lee, "A review on carbon nanotubes and graphene as fillers in reinforced polymer nanocomposites," *Journal of Industrial and Engineering Chemistry,* vol. 21, pp. 11-25, 2015.

[5] F. Ménil, M. Susbielles, H. Debéda, C. Lucat, and P. Tardy, "Evidence of a correlation between the non-linearity of chemical sensors and the asymmetry of their response and recovery curves," *Sensors and Actuators B: Chemical,* vol. 106, pp. 407-423, 2005.

[6] M. O. Bristeau, R. Glowinski, and J. Periaux, "Numerical methods for the navier-stokes equations. Applications to the simulation of compressible and incompressible viscous flows," *Computer Physics Reports,* vol. 6, pp. 73-187, 8// 1987.

CHAPTER III: Benchmark study of oxygen functionalized MWCNTs as gas sensing interface

In this chapter, the gas sensing properties of oxygen functionalized multiwall carbon nanotubes (O-MWCNTs) are studied since this nanomaterial will be used as a building block undergoing further modifications. Here we will focus on the fabrication, the structure and electronic properties of such a system and finally, the gas sensing characterization results towards different volatile contaminants will be shown and discussed.

3.1. Overview

Like hydrocarbon compounds, MWCNTs are hydrophobic and inert in standard conditions and tend to aggregate resulting in poor solubility in most of solvents, which is not favorable for gas sensing application. Also, after the fabrication process, some impurities such as amorphous graphite or residual metal catalyst remain on the surface of as-grown MWCNTs [1] and can seriously affect the sensing potential of this material. To improve their solubility and purity level, MWCNTs can be cleaned, sorted (e.g. separate semiconducting from metallic nanotubes) and functionalized employing different methods. Hence, the most common way to functionalize them is the modification of their surface chemistry by the attachment of oxygen-containing groups (e.g. hydroxyl, peroxide,

ketone, and carboxylic groups) mainly on tube ends and side-walls. Furthermore, such functionalization can serve for the creation of anchoring sites for further chemical functionalization and processing [2].

3.1.1. Oxygen functionalization methods

Various methods for the oxidation of CNTs have been reported and can be identified in tree types: Liquid phase, gas phase, and plasma treatment.

The liquid phase method consists in the use of wet chemical techniques using different oxidizing agents and acids (e.g. HNO_3, H_2SO_4, HCl, $KMnO_4$, H_2O_2) [3-5]. It is a continuous process that can eliminate impurities at large scale and leads to surface modification that preferentially takes place on CNTs sidewalls. The main drawback of such method is the occurrence of CNT fragmentation (shortening) and damage CNTs walls altering their electronic properties [6]. Also, filtering and washing steps are needed in order to clean CNTs from oxidizing agents. The gas phase method involves the use of oxidative atmosphere at temperatures of few hundred degrees. The commonly used oxidants include air, ozone, a mixture of Ar-O_2 and H_2O, a mixture of Cl_2-H_2O and HCl. It is a simple method for removing carbonaceous impurities without vigorously introducing sidewall defects. Nevertheless, this method does not allow for the removal of the metal catalyst and toxic gases are used at high temperature. Finally, plasma treatment appears to be an efficient method to functionalize the surfaces of CNTs with the advantages of

shorter reaction time, nonpolluting and simple experimental process. The plasma is generated under Ar or He in presence of an oxygen specie like O_2 or H_2O [7-9]. CNTs can be functionalized depending on the parameters of the plasma and its composition without damaging CNTs walls due to milder treatment conditions. For all those advantages, we have chosen plasma treatment in this thesis to functionalize our MWNCTs.

3.1.2. Structural and electronic properties changing

Functionalization of CNTs sidewalls not only allows better interactions with gas species, but also leads to drastic changes in the electronic states near the Fermi level of carbon nanotubes. Indeed, CNTs present more sp^3 rehybridization (**Figure 19**) of the carbon atom at the functional site which act as a strong scattering center inducing a localized impurity state near the Fermi level.[10]

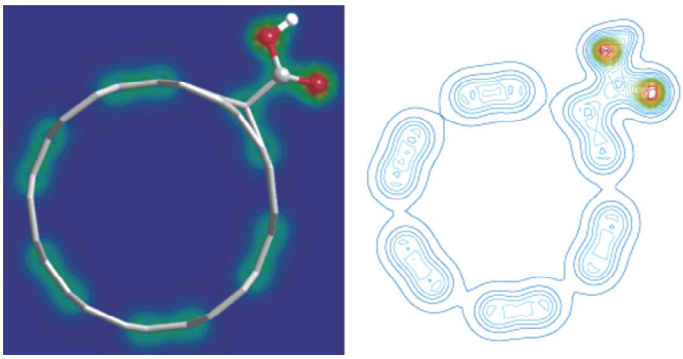

Figure 19 : Atomic structure (left) of COOH-attached to a (6,6) SWNT and contour plot of electron density (right) on the slice passing through the COOH group. Red, yellow, green, and blue colors on the contour plot indicate electron density from higher density to lower density. The structural distortion on the nanotube is found to confine to the nearest neighbors of the bonding site [11] .

Such functionalization gives a better semiconducting behaviour by the formation of impurity states near the Fermi level [12]. DFT calculations indicated that the presence of oxygen atoms at the functionalized site reduces the HOMO–LUMO (Highest Occuppied Molecular Orbitals–Lowest Unoccupied Molecular Orbitals) gap to 0.82 eV [13]. This reduction can be explained by the higher density of states near the Fermi level, arising from the overlap of the 2p electrons of the O atoms and the p electron system of the nanotube.

3.1.3. Gas sensing interaction mechanism

This oxygen functionalization step gives rise to few advantages for the use of CNTs in gas sensing applications. Indeed, it has been shown that functionalization enhances electronic properties by creating additional states near the Fermi level, but also oxygen polar species present on CNTs wall can generate electrostatic interactions with the target gas. R. Ionescu et al. have used an oxygen plasma functionalized MWCNTs for the detection of NO_2 and NH_3 at concentration as low as 500 ppb and 200 ppm respectively at ambient temperature [14]. Higher responsiveness is observed when there is a higher presence of oxygen at the surface of the nanotube. Sin et al. have studied the response of chemically functionalized MWCNTs to alcohol detection [15]. The proposed mechanism of ethanol detection (**Figure 20**) shows that –COOH groups tend to form hydrogen bonding with the ethanol molecule at room temperature.

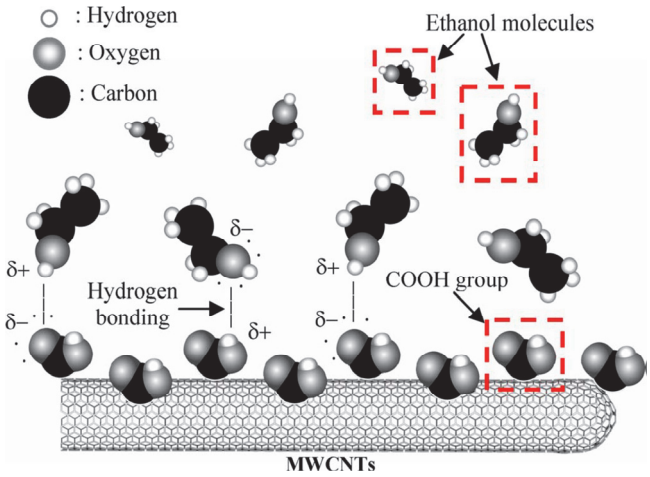

Figure 20 : Interaction COOH groups of the CNTs wall and ethanol molecules [15]

They were able to detect as low as 1 ppm of ethanol. C. Lu et al. chemically functionalized MWCNTs as sensitive layer for BTEX detection [16]. They showed that adsorption mechanism of BTEX via CNTs is mainly due to π-π interaction between the aromatic ring of BTEX and the surface carboxylic group of the CNTs as shown in **Figure 21.**

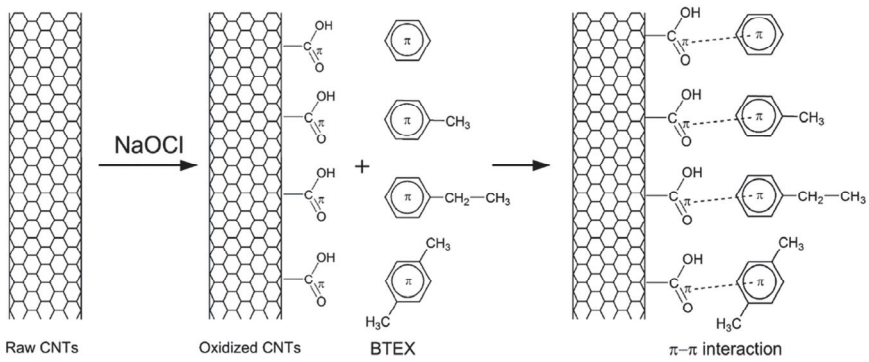

Figure 21 : Mechanism of the adsorbed BTEX on oxidized CNTs [16] .

The oxygen functionalization of CNTs results in significant improvements in their gas sensing properties. In the following sub-sections, we report on the use of O_2-Ar plasma treated MWNTs and discuss their gas sensing properties following this clean and easy process experiment.

3.2. Gas sensor fabrication

3.2.1. MWCNTs synthesis and functionalization

The MWCNTs used in the experiment were obtained from Nanocyl, S.A. (Belgium). They were synthesized by chemical vapor deposition and their purity was higher than 95%. The nanotubes were up to 50 µm in length and their outer and inner diameters ranged from 3 to 15 nm and 3 to 7 nm, respectively. A uniform functionalization with oxygen was applied to the as provided carbon nanotubes in order to improve their dispersion and surface reactivity. For this activation step, the MWCNTs were placed inside a glass vessel and a magnet, externally controlled from the plasma chamber, was used to stir the nanotubes powder during the plasma treatment. Inductively coupled plasma at a RF frequency of 13.56 MHz was used during the process [14]. Once the MWCNTs powder was placed inside the plasma glow discharge, the treatment was performed at a pressure of 0.1 Torr, using a power of 15 W, while the processing time was adjusted to 1 min. A controlled flow of oxygen was introduced inside the chamber, which gave rise to functional oxygen species attached to the carbon

nanotubes sidewalls (i.e., oxygenated vacancies consisting of hydroxyl, carbonyl and carboxyl groups). It is possible to determine and quantify these functional oxygen species thanks to XPS (X-photon spectroscopy) analysis.

Then, O-MWCNTs were deposited by air-brushing method presented in Chapter II. The morphology of the as deposited O-MWCNTs was studied by means of transmission electron microscopy (TEM) carried out using a JEOL model 1011 instrument operated at 100 kV. In order to reduce potential knock-on radiation damage caused by the 100 keV electron beam, the electron dose was significantly decreased such that during the entire electron-beam exposure no changes in the nanotubes were observable. Morphology of the as-prepared films was also investigated by means of scanning electron microscopy (SEM). SEM measurements were performed using an ESEM-FEI Quanta 600 equipment, with a resolution of 15 nm. Accelerating voltages of 25 or 30 kV were employed. The system allows for sample rotation (360°) and sample inclination (90°).

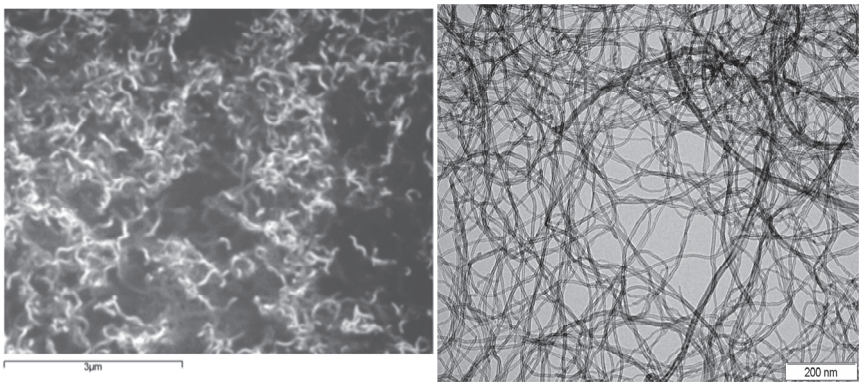

Figure 22 : SEM (left) and TEM (right) pictures of plasma treated multiwall carbon nanotubes.

The morphology of the airbrushed O-MWCNTs films investigated by SEM and TEM is shown in **Figure 22.** This figure shows that O-MWCNTs deposited on interdigitated Pt electrodes consists of porous films with two-dimensional arrays of nanopores with different sizes and with homogenous distribution. The inner diameter of typical O-MWCNTs was found equal to 3.53 nm and the outer diameter equal to 16.50 nm. The composition of O-MWCNT films had been studied in detail by X-ray photoelectron spectroscopy (XPS) techniques and results were reported in [17]. The C1s core level spectrum of the oxygen-plasma-treated nanotubes was analyzed. This spectrum can be decomposed into five components. The main peak is centered at 284.6 eV and corresponds to the graphite signal, assuming a pure nanotube similar to a graphite layer. The second peak is centered at 285.1 ± 0.2 eV and is attributed to the sp^3 carbon atoms. And the components centered at 286.2 ± 0.2 eV, 287.2 ± 0.2 eV, and 288.9 ± 0.2 eV correspond to hydroxyl, carbonyl, and carboxyl groups, respectively. After quantitative analysis, the relative distribution of the last three peaks is found to be 5%, 12%, and 2%. These numbers should be treated with care due to the fact that the XPS signal of the O-MWCNT is referenced to the graphite signal and due to inherent uncertainties in the peak fitting. However, it is clear that the majority of the functions added to the nanotube surface are carbonyl groups. Also, the atomic composition was examined by energy-dispersive X-ray spectroscopy (EDX). To perform this analysis O-MWCNTs were deposited on onto silicon substrate in which gold layer had been previously evaporated by sputtering. Results are summarized in **Table 5.**

Table 5 : Atomic composition of O-MWCNTs

Spectrum label	C	O	Au	Total
Composition (%)	72.61	10.46	16.93	100

3.2.2. Impedance spectroscopy characterization

The electrical characterization under vapor environment was performed by impedance spectroscopy (IS). This technique has emerged as a useful analytical tool for the development of sensor devices in a wide variety of configurations. The HP 4192A impedance analyzer was used to obtain impedance spectra. It provided the AC voltage signals that were applied to sensors. Perturbation amplitude of ±10 mV (peak to peak) was chosen and the frequency was varied in the range of 5–10^6 Hz. The impedance of O-MWCNT films was derived from the measurements of Bode's diagrams with the equivalent electrical circuit in **Figure 23**.

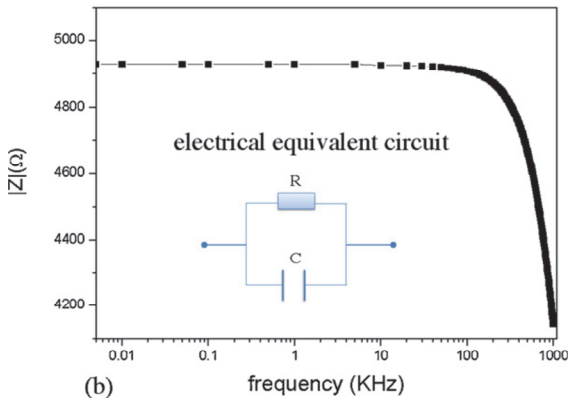

Figure 23 : Typical impedance spectrum taken between 5 and 10^6 Hz at room temperature for oxygen plasma treated MWCNT mat film deposited onto interdigitated electrodes. The inset shows the electric equivalent circuit.

The proposed equivalent electrical circuit includes the following two elements: the O-MWCNTs film resistance and capacitance. The figure clearly shows that sensors remain resistive impedance up to 100 kHz. From 100 kHz onwards, sensors show the effect of a capacitance. In order to maintain a pure resistive behavior, electrical measurements are carried out at 1 kHz.

3.3. Gas sensing properties of O-MWCNTs

3.3.1. VOCs detection

Different concentrations of VOCs (i.e., benzene, toluene, acetone, methanol and ethanol) were measured using the second experimental set-up shown in Chapter II**.** All measurements under the presence of different concentrations of volatile organic compounds were performed using the impedance analyzer operated at fixed frequency of 1 kHz. Sensor response was defined as the normalized resistance change with $SR=(R_{gas}-R_{air})/R_{air}\times100$. Considering at first the measurements of benzene and toluene vapours, **Figure 24** shows the experimental response and recovery curves to increasing concentrations of these vapors.

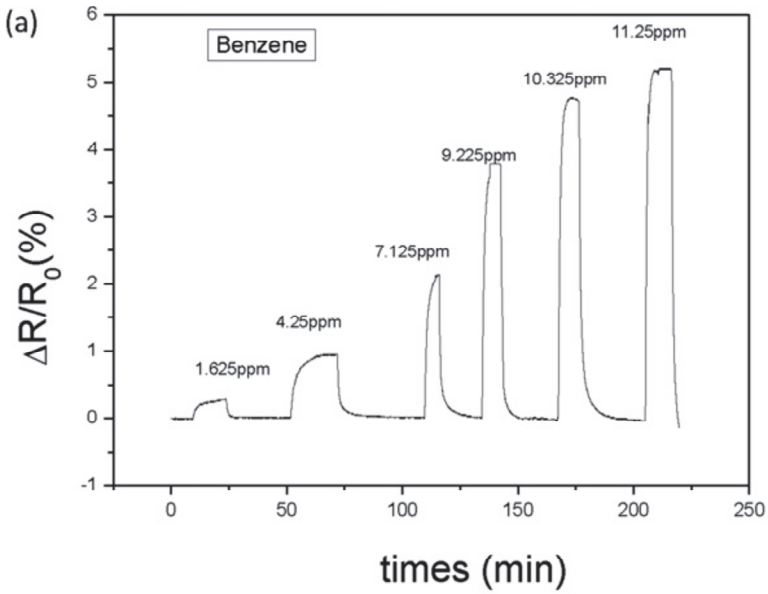

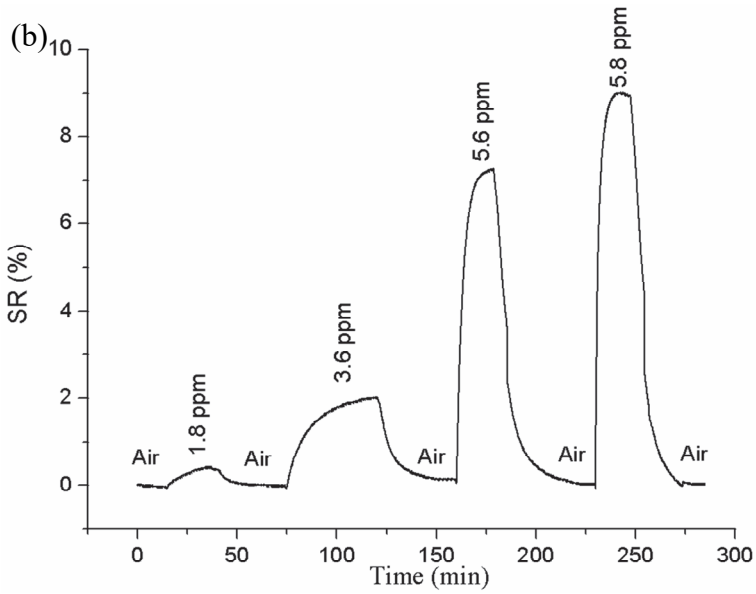

Figure 24 : Typical response to increasing concentrations of benzene vapors (top) and toluene vapors (bottom) of an oxygen plasma treated MWCNT sensor operated at room temperature.

The sensor response versus time increases as a consequence of exposure to benzene and toluene vapors. The adsorption of these two analytes within the multiwall carbon nanotube layers was able to induce a significant increase in the resistance of the films. The lower concentrations measured were 1.62 and 1.8 ppm for benzene and toluene, respectively (these lower concentrations are determined by the dilution set-up employed). The experimental data clearly reveal the capability to detect very low concentrations of the tested pollutants. Additionally, when the analyte is removed by flowing clean air, sensors do recover their initial baseline signal, showing that the complete desorption of analyte molecules occurs at room temperature. Therefore, sensors exhibit a complete reversibility in their response toward benzene and toluene vapors. However, sensor response and recovery dynamics are significantly faster for benzene than for toluene. These results are of great importance for vapor sensing applications in which portability is required, since they show that such sensors could be easily and quickly reused after a given measurement, avoiding the use of cleaning procedures (such as heating or UV-irradiating) that are costly, power-demanding and time-consuming. For benzene, the noise level in the response is about 0.01% and if we consider that the limit of detection (LOD) is reached when the signal to noise ratio becomes equal to 3, then the LOD for benzene is below 100 ppb (assuming a linear interpolation of sensor response for the low concentrations of benzene). **Figure 25** shows the calibration curves of sensor response at room temperature toward benzene and toluene vapors. Oxygen plasma treated MWCNT sensors are more sensitive to toluene than to benzene vapors. In view of the

non-linear behavior of the calibration curve shown in Fig. 5, the assumption of a linear interpolation for estimating the LOD discussed above might be somewhat crude.

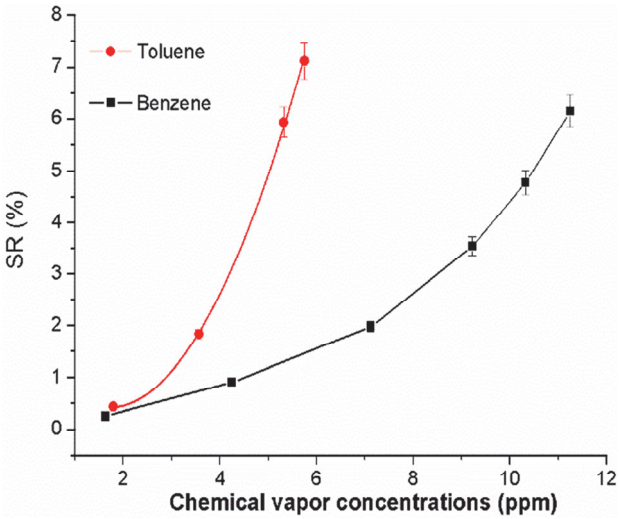

Figure 25 : Room-temperature sensor response calibration curves for benzene and toluene vapors. Error bars have been added to show the repeatability of the results.

In the second step, the room-temperature responses of the MWCNTs sensor to acetone, methanol and ethanol vapors was investigated and compared against the responses to benzene and toluene vapors. **Figure 26** shows the sensor response and recovery curves for increasing methanol, ethanol and acetone concentrations. The baseline drift occurs after exposure to these analytes. Baseline recovery both from benzene and toluene responses is better than from alcohols and acetone. The occurrence of a more significant baseline drift for alcohols and acetone than for benzene or toluene reveals a stronger interaction between O-MWCNTs and methanol, ethanol or acetone molecules than that of benzene or toluene molecules. It is

likely that applying mild heating would help completely desorbing analytes from MWCNT sidewalls leading to a complete baseline recovery.

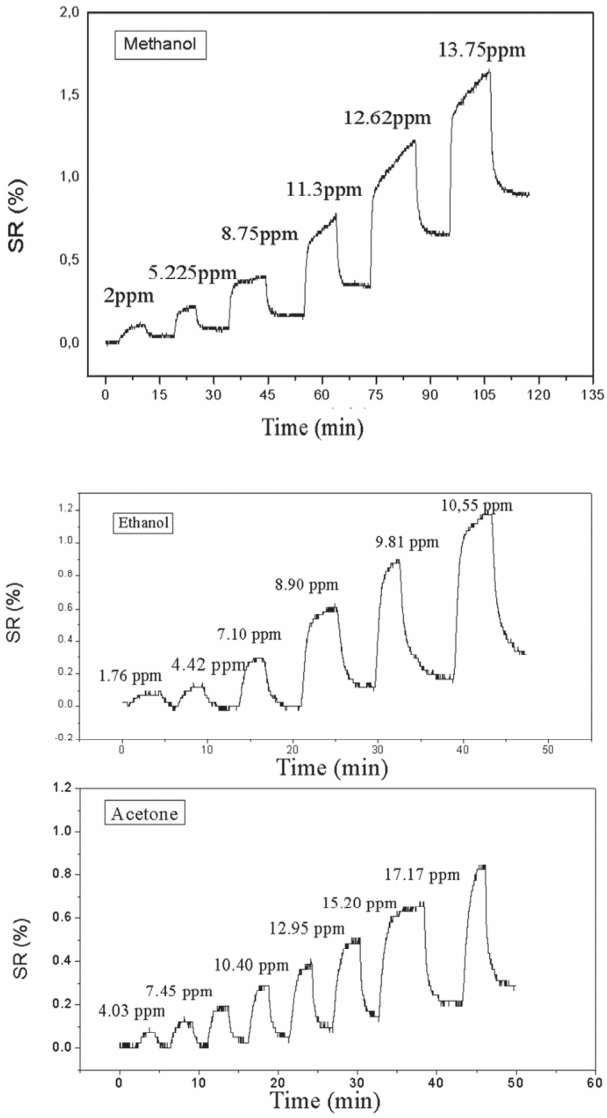

Figure 26 : Typical response to increasing concentrations of methanol (top), ethanol (middle) and acetone (bottom) vapors of an oxygen plasma treated MWCNT sensor operated at room temperature.

3.3.2. Discussion

The interaction between carbon nanotubes and the vapor molecules is generally weak (van der Waals interactions) [18]. The adsorption of vapor molecules can induce a change in the dielectric constant and electrical properties of O-MWCNTs [19]. Both physisorption and chemisorption phenomena have been reported in the study of the interaction between CNTs and gas/vapor molecules [20]. In particular, theoretical studies have shown that a strong interaction occurs between methyl groups and carbon nanotubes [21, 22]. Based on our experimental results, the kinetics of the interaction between alcohols and acetone vapors with multiwall carbon nanotubes might be based on chemisorption where a rapid covalent bonding occurs. This covalent bonding cannot be broken easily and this is why drift in the baseline signal is observed (see **Figure 26.**) On the other hand, for aromatic VOCs such as toluene or benzene, the interaction might be mainly based on physisorption. This is a slow phenomenon where adsorbed molecules can be easily removed from the surface of nanotubes (e.g. by flowing the sensors with clean air), and this is why no significant baseline drift can be observed (see **Figure 25.**). Sensitivities of the different analytes tested are summarized in **Figure 27.**

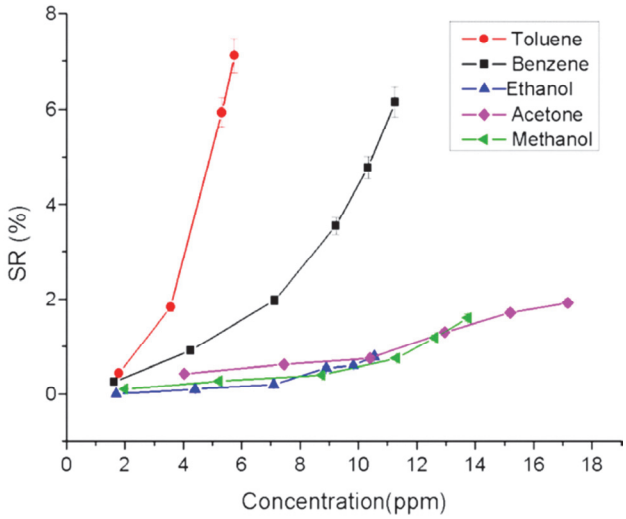

Figure 27 : Room-temperature sensor response calibration curves for the different volatile organic compounds studied.

The difference in sensitivity for the room-temperature detection of the two aromatic VOCs tested can be due to their differences in dipole moment and dielectric constant (**Table 6**) and, particularly, the stronger response to toluene than to benzene vapours could be attributed to the presence of a methyl group in the former molecule.

Table 7 : Dielectric constant and dipolar moment for the different analyte studied

Solvent	Dielectric constant	Dipole moment (Debye)
Benzene	2.3	0
Toluene	2.38	0.360
Methanol	32.6	1.66
Ethanol	24.3	1.68
Acetone	20.7	2.88

The higher dipole moment of toluene induces higher dipole–dipole interactions which facilitate the physisorption mechanism. Moreover, the higher dielectric constant of toluene can induce a higher conductivity variation of carbon nanotubes. This result is of importance, since it suggests that an array of plasma treated MWCNT sensors could be designed with tailored sensitivities (e.g. by having their sidewalls decorated with nano-clusters of different metals) to discriminate benzene from toluene and xylenes (while the former lacks of methyl groups, the latter two have methyl groups attached to a benzene ring). Moreover, from the analysis of the mean response time (the mean response time was defined as the time needed to reach 90% of the final steady value of the sensor resistance after the injection of a given VOC), it turned out that the MWCNTs-based sensors provided a faster response to alcohol and acetone vapors (see **Figure 28.**). The average response time was equal to 2.30 min, 2.28 min and 1.85 min for ethanol, acetone and methanol, respectively. On the other hand, this response time was 6.63 min and 7.62 min for benzene and toluene, respectively. This means that the oxygen plasma treated multiwall carbon nanotube layers lead to significant differences in the adsorption dynamics of the different analytes studied, revealing the existence of different interaction mechanisms. These results show that the alcohols and acetone vapors could be easily discriminated from aromatic VOCs according to the differences in response times.

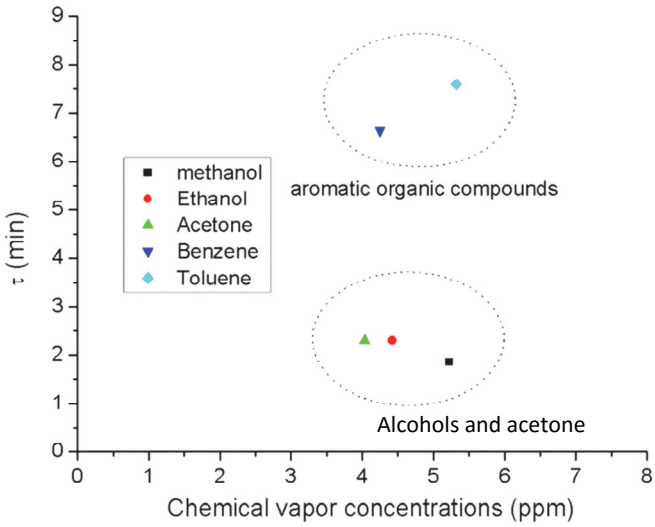

Figure 28 : Response time of an O-MWCNT sensor operated at room temperature exposed to aromatic compounds, alcohols and acetone vapors.

This could be exploited as a method to increase sensor selectivity for detecting aromatic VOCs in environments where alcohols or acetone may be present. Ambient moisture is an important interfering species in the detection of VOCs in the environment. The oxygen plasma treatment of carbon nanotubes turns them less hydrophobic. While this helps to unbundle CNTs, ameliorates their solubility and allows for obtaining good dispersions that can be drop coated or air-brushed onto transducer substrates, the treatment also makes nanotubes more prone to respond to changes in ambient moisture.[14] However, moisture interference can be compensated for by processing the response of oxygen plasma treated MWCNT arrays or minimized by conducting treatments (e.g. fluorination) for enhancing the hydrophobicity of carbon nanotubes.[23]

3.4. Conclusion

Oxygen plasma functionalized multiwall carbon nanotubes have been used for the detection of volatile organic compounds (VOCs) at room temperature. Alumina substrates with interdigitated Pt electrodes were employed as transducers and the air-brushing method was used to coat them with carbon nanotubes film. The electrical properties of the carbon nanotube sensors were studied by impedance spectroscopy in the presence of benzene, toluene, methanol, ethanol and acetone vapors. The resistance of the prepared MWCNTs films increased with the concentration of the different vapors tested. The sensors showed high sensitivity and excellent baseline recovery in the presence of benzene or toluene vapors compared to the others tested VOCs. The limits of detection for benzene and toluene are in the high ppb range. Responses were repeatable and sensors were reproducible. The significantly faster kinetic response together with the difficulty for fully recovering the baseline resistance at room temperature experienced with methanol, ethanol and acetone seems to suggest that, for these vapors, the main mechanism of interaction with carbon nanotubes is chemisorption. On the other hand, slower response kinetics and fully recovery of the baseline suggest that benzene and toluene are physisorbed onto carbon nanotubes. MWCNT sensors were more responsive to toluene than to benzene vapors. This could be due to the presence of a methyl group in the toluene molecule. Methyl groups are known to better interact with carbon nanotube sidewalls than the benzene ring. This result brings about the possibility of selectively detecting benzene in the presence of toluene or xylenes by employing arrays of plasma

treated MWCNT chemoresistors in which nanotubes are functionalized (e.g. with nanoparticles of different metals, or with different functional groups). The results presented in this chapter have been published in [24].

References

[1] P.-X. Hou, C. Liu, and H.-M. Cheng, "Purification of carbon nanotubes," *Carbon,* vol. 46, pp. 2003-2025, 2008.

[2] H. Peng, L. B. Alemany, J. L. Margrave, and V. N. Khabashesku, "Sidewall carboxylic acid functionalization of single-walled carbon nanotubes," *Journal of the American Chemical Society,* vol. 125, pp. 15174-15182, 2003.

[3] V. Likodimos, T. A. Steriotis, S. K. Papageorgiou, G. E. Romanos, R. R. Marques, R. P. Rocha*, et al.*, "Controlled surface functionalization of multiwall carbon nanotubes by HNO 3 hydrothermal oxidation," *Carbon,* vol. 69, pp. 311-326, 2014.

[4] K. A. Wepasnick, B. A. Smith, K. E. Schrote, H. K. Wilson, S. R. Diegelmann, and D. H. Fairbrother, "Surface and structural characterization of multi-walled carbon nanotubes following different oxidative treatments," *Carbon,* vol. 49, pp. 24-36, 2011.

[5] V. Datsyuk, M. Kalyva, K. Papagelis, J. Parthenios, D. Tasis, A. Siokou*, et al.*, "Chemical oxidation of multiwalled carbon nanotubes," *Carbon,* vol. 46, pp. 833-840, 2008.

[6] F. Avilés, J. Cauich-Rodríguez, L. Moo-Tah, A. May-Pat, and R. Vargas-Coronado, "Evaluation of mild acid oxidation treatments for MWCNT functionalization," *Carbon,* vol. 47, pp. 2970-2975, 2009.

[7] H. Yu, D. Cheng, T. S. Williams, J. Severino, I. M. De Rosa, L. Carlson*, et al.*, "Rapid oxidative activation of carbon nanotube yarn and sheet by a radio frequency, atmospheric pressure, helium and oxygen plasma," *Carbon,* vol. 57, pp. 11-21, 2013.

[8] J.-F. Colomer, B. Ruelle, N. Moreau, S. Lucas, R. Snyders, T. Godfroid*, et al.*, "Vertically aligned carbon nanotubes: Synthesis and atomic oxygen functionalization," *Surface and Coatings Technology,* vol. 205, pp. S592-S596, 2011.

[9] C. Chen, A. Ogino, X. Wang, and M. Nagatsu, "Oxygen functionalization of multiwall carbon nanotubes by Ar/H 2 O plasma treatment," *Diamond and Related Materials,* vol. 20, pp. 153-156, 2011.

[10] H. Park, J. Zhao, and J. P. Lu, "Effects of sidewall functionalization on conducting properties of single wall carbon nanotubes," *Nano letters,* vol. 6, pp. 916-919, 2006.

[11] J. Zhao, H. Park, J. Han, and J. P. Lu, "Electronic properties of carbon nanotubes with covalent sidewall functionalization," *The Journal of Physical Chemistry B,* vol. 108, pp. 4227-4230, 2004.

[12] H. Ago, T. Kugler, F. Cacialli, W. R. Salaneck, M. S. Shaffer, A. H. Windle*, et al.*, "Work functions and surface functional groups of multiwall carbon nanotubes," *The Journal of Physical Chemistry B,* vol. 103, pp. 8116-8121, 1999.

[13] T. Prasomsri, D. Shi, and D. E. Resasco, "Anchoring Pd nanoclusters onto pristine and functionalized single-wall carbon nanotubes: A combined DFT and experimental study," *Chemical Physics Letters,* vol. 497, pp. 103-107, 9/10/ 2010.

[14] R. Ionescu, E. Espinosa, E. Sotter, E. Llobet, X. Vilanova, X. Correig*, et al.*, "Oxygen functionalisation of MWNT and their use as gas sensitive thick-film layers," *Sensors and Actuators B: Chemical,* vol. 113, pp. 36-46, 2006.

[15] M. L. Sin, G. Chun Tak Chow, G. M. Wong, W. Li, P. Leong, and K. W. Wong, "Ultralow-power alcohol vapor sensors using chemically functionalized multiwalled carbon nanotubes," *Nanotechnology, IEEE Transactions on,* vol. 6, pp. 571-577, 2007.

[16] C. Lu, F. Su, and S. Hu, "Surface modification of carbon nanotubes for enhancing BTEX adsorption from aqueous solutions," *Applied Surface Science,* vol. 254, pp. 7035-7041, 2008.

[17] A. Felten, C. Bittencourt, J.-J. Pireaux, G. Van Lier, and J.-C. Charlier, "Radio-frequency plasma functionalization of carbon nanotubes surface O2, NH3, and CF4 treatments," *Journal of Applied Physics,* vol. 98, p. 074308, 2005.

[18] J. Zhao, A. Buldum, J. Han, and J. P. Lu, "Gas molecule adsorption in carbon nanotubes and nanotube bundles," *Nanotechnology,* vol. 13, p. 195, 2002.

[19] M. Grujicic, G. Cao, and W. Roy, "A computational analysis of the carbon-nanotube-based resonant-circuit sensors," *Applied surface science,* vol. 229, pp. 316-323, 2004.

[20] Z. Zanolli, R. Leghrib, A. Felten, J.-J. Pireaux, E. Llobet, and J.-C. Charlier, "Gas Sensing with Au-Decorated Carbon

Nanotubes," *ACS Nano,* vol. 5, pp. 4592-4599, 2011/06/28 2011.

[21] S.-p. Du, W.-h. Zhao, and L.-f. Yuan, "Absorption and structural property of ethanol/water mixture with carbon nanotubes," *Chinese Journal of Chemical Physics,* vol. 25, pp. 487-493, 2012.

[22] W.-H. Zhao, B. Shang, S.-P. Du, L.-F. Yuan, J. Yang, and X. C. Zeng, "Highly selective adsorption of methanol in carbon nanotubes immersed in methanol-water solution," *The Journal of chemical physics,* vol. 137, p. 034501, 2012.

[23] Y. C. Hong and H. S. Uhm, "Superhydrophobicity of a material made from multiwalled carbon nanotubes," *Applied physics letters,* vol. 88, pp. 244101-244101-3, 2006.

[24] I. Hafaiedh, W. Elleuch, P. Clement, E. Llobet, and A. Abdelghani, "Multi-walled carbon nanotubes for volatile organic compound detection," *Sensors and Actuators B: Chemical,* vol. 182, pp. 344-350, 6// 2013.

CHAPTER IV: Piezoelectric resonant cantilever gas sensor with double transduction

Traditionally, microcantilever sensors have been operated in out-of-plane resonance modes. They generally suffer strong damping forces and hence higher vibration energy losses. Previous studies have shown that PZT microcantilevers resonating in in-plane-modes tended to undergo shear rather than compressing phenomena. In this way, higher quality factors (Q) are expected when the cantilever would be used in the 31-longitudinal vibration mode, which would result in higher sensitivity. For gas sensing application, such vibration mode may be suitable because at low contaminant concentrations, small resonance frequency shifts are expected, hence the need of reaching high resolution.

In this chapter, a piezoelectric cantilever with an in plane resonating mode has been used. Enhancement of sensitivity and selectivity is proposed by measuring both the resonance frequency shift of a CNTs-coated piezoelectric cantilever and the resistance change of the CNTs film upon the absorption of gas species. To implement this double transduction, the top electrode, which normally covers the full surface of the piezoelectric cantilever (called “norm-cant”), has been replaced here by two interdigitated electrodes (called “ID-cant” with ID=InterDigitated). This new configuration will be presented in the first part. The electromechanical characterization of this new electroded piezoelectric cantilever compared with a theoretical

simulation will be afterwards detailed. Finally, to demonstrate the advantages of this combination, 3 types of toxic gases carefully chosen will be detected. First C_6H_6 and CO, which are known to interact with O-MWCNTs as reducing species then, NO_2 is known to interact strongly with O-MWCNTs as oxidizing species. Humidity effect will be studied since it's a parameter that can alter gas sensing in real operating condition.

4.1. Electromechanical characterization of the microcantilever

The fabrication steps of the piezoelectric microcantilevers used here are detailed in Chapter II.

4.1.1. Configuration of electrical connections

4.1.1.1. "Norm-cant": sandwich conformation

The initial piezoelectric micro-cantilever realized by screen-printing process associated to a sacrificial layer is composed of a PZT layer with printed Au electrodes on each side (**Figure 29**). This symmetrical structure allows an in-plane longitudinal vibration mode: thanks to the voltage applied between the two sandwich electrodes, the cantilever is actuated using the inverse piezoelectric effect; the vibration is parallel to the alumina substrate surface, with an elongation of the cantilever along the x axis. The resonance frequency, image of the gas concentration is then measured by following the resonance spectrum of the cantilever.

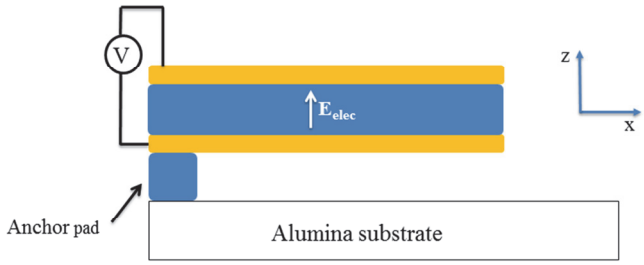

Figure 29: Sandwich configuration of "Norm-cant" with two gold electrodes at the top and the bottom of the PZT cantilever and applying voltage in z axis.

4.1.1.2. "ID-cant": interdigitated electrodes

The top full electrode is here replaced by two interdigitated electrodes for the simultaneous resonance and resistive measurements. For all the electro-mechanical characterizations and the gas sensing tests performed, the configuration of electrical connections is shown **Figure 30**. The actuation and the resonance frequency measurement are carried out between electrodes e_1 and e_2. The electrode e_2 is designed wider than e_1 in order to actuate in a similar way as in the case of the 'norm-cant' cantilever. But the e_3 electrode will be inactive in respect to actuation.

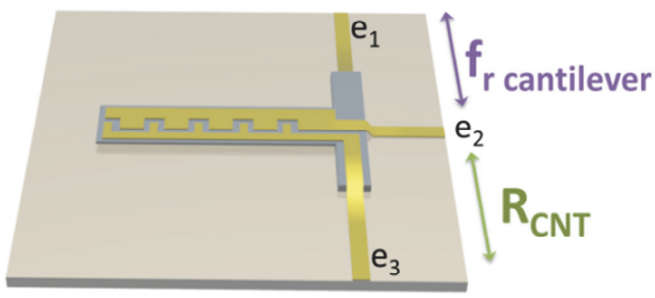

Figure 30: Picture showing the double transduction method where the bottom electrode is e_2 and the interdigitated electrodes are e_1 and e_3.

Then, alternatively, the resistance of the CNTs film is measured between electrodes e_2 and e_3 in static mode (without cantilever vibration). The measurement is led at 1 kHz since the CNTs show a resistive behavior at this frequency (as shown in chapter III).

4.1.2. Polarization step

After the fabrication of the cantilever, the PZT cantilever is poled in order to reach the piezoelectric behaviour. The two top electrodes e_1 and e_2 are short circuited for this purpose to reach a homogeneous polarization in the PZT microceramic parallel to the z axis. Then, the substrate is introduced into the polarization chamber where atmosphere and temperature are controlled.

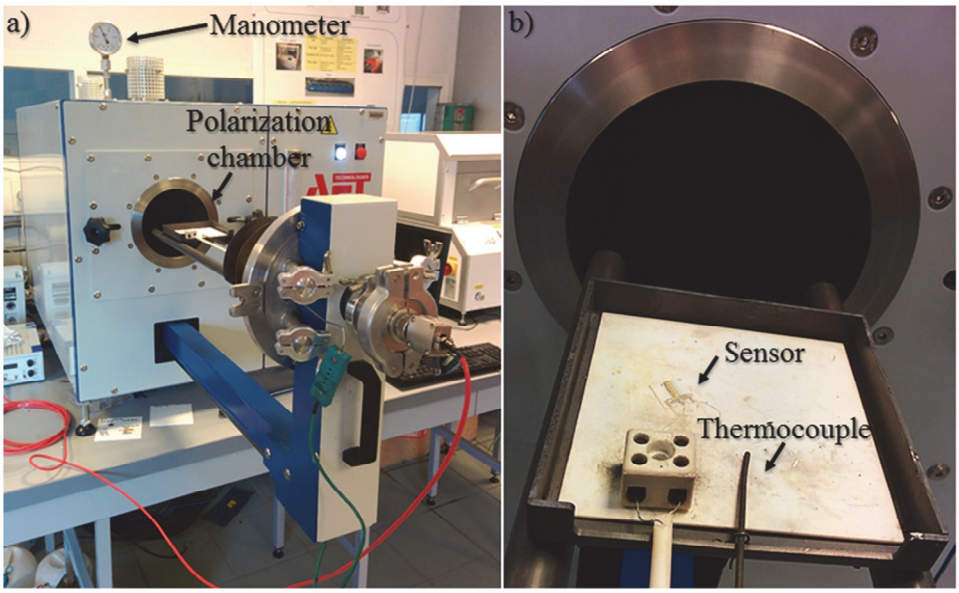

Figure 31: a) Overall view of the polarization chamber and b) view of the transfer rod

At first, vacuum is generated inside the room where a primary pump allows reaching a pressure of under 0.1 mbar. At the same time, this step enables the removal of ambient humidity and prevents the occurrence electric arc discharges at high voltages (due to higher conductivity of the ambient). Then, the polarization room is filled with dry nitrogen which is an inert gas (avoiding material spoilage). To exhibit piezoelectric properties, the cantilever is progressively polarized between the bottom electrode e_3 and the top short-circuited electrodes (e_1, e_2). A maximum electric field of 55 $kV \cdot cm^{-1}$ (value before dielectric breakdown) is increasingly applied under nitrogen atmosphere while the leakage current intensity is monitored to ensure it remains below 5 µA. The temperature is set at 280°C, just below the Curie temperature (284°C) of PZT (**Figure 32**)

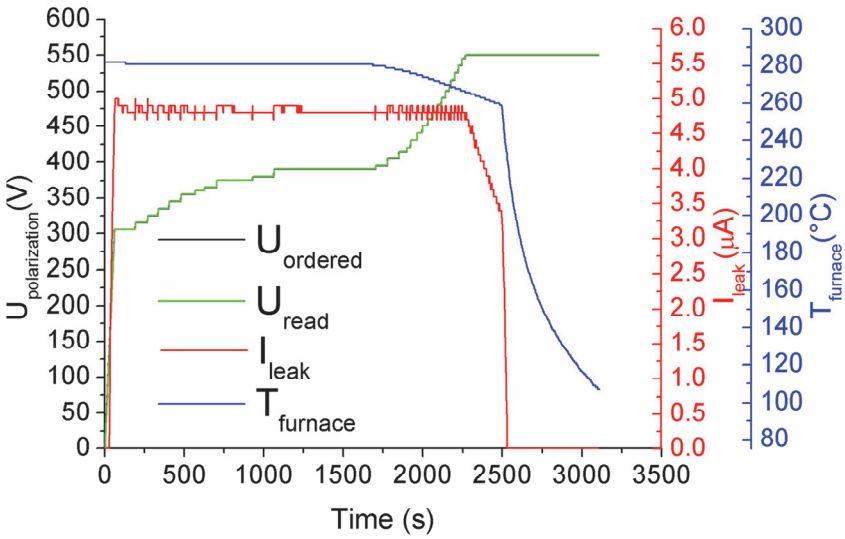

Figure 32: Different parameters of the polarization step

Then the system is cooled down while reaching and keeping constant the maximum electric field. Afterwards, the samples are collected and

the alumina substrate is wire bonded on the PCB support via Sn-Ag-Cu soldering.

4.1.3. Electro-mechanical characterization

The x, y and z named axis are equivalents to 1,2 and 3 axis, respectively. This notation is used to define the different piezoelectric parameters.

4.1.3.1. 31-longitudinal vibration mode

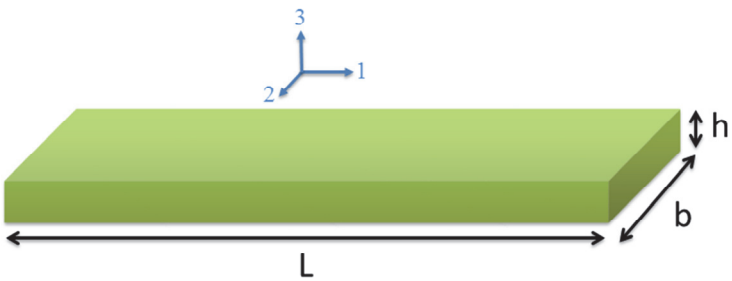

Figure 33 : Length parameters of the microcantilever

In the case of a parallelepiped (**Figure 33**) with length *L*, width *b*, and thickness *h*, the 31-longitudinal wave's propagation velocity (υ_{31}) and their frequency f_{31} along the structure are written as follows:

$$v_{31}^{E} = \frac{1}{\sqrt{\rho_{cantilever} s_{11}^{E}}}$$

Equation 3

$$f_{31}^{(n)} = \frac{\lambda_{31}^{(n)}}{2\pi}\sqrt{\frac{k}{m}}$$

Equation 4

With $k = \frac{Ebh}{L}$

Where m is the cantilever mass, k the stiffness constant and ρ its density and s^E_{11} the elastic compliance constant. The Eigen values $\lambda^{(n)}_{31}$ depend on the vibration mode and are expressed by the following law:

$$\lambda_{31}^{(n)} = \frac{2n-1}{2}\pi \qquad with\, n \in \mathbb{N}$$

Equation 5

Finally, by associating **Equation 3** and **Equation 4** the resonance frequency for the 31-longitudinal vibration mode can be deduced and is proportional to the inverse of the cantilever's length:

$$f_{31}^{(n)} = \frac{2n-1}{4L}\frac{1}{\sqrt{\rho_{cantilever} s_{11}^{E}}}$$

Equation 6

In this hypothesis of low damping, the quality factor Q for a (n) mode of vibration can be approximated to:

$$Q = \frac{f_r}{\Delta f}$$

Equation 7

Where f_r is the resonance frequency and Δf is the bandwidth at -3dB. The resonance vibration modes of the excited cantilever can be observed electrically by following the impedance Z or the admittance Y (real or imaginary parts) of the piezoelectric microceramic as a function of the frequency. When oscillating, the piezoelectric ceramic can be replaced by an electrical equivalent circuit diagram and resonance peaks can be thus detected.[1] **Figure 34** shows the conductance G(f) (real part of the admittance Y) of the first in-plane 31-longitudinal vibration modes of a normal cantilever recorded with an impedancemeter (Agilent E5061B). The first three resonance frequencies are measured at approximately 70, 225 and 360 kHz. The quality factor is significantly higher for the first mode, which is promising for gas sensing application.[2, 3] Therefore, we will work in a range near 70 kHz in the study of the piezoelectric properties of the 'norm-cant' and the 'ID-cant' devices.

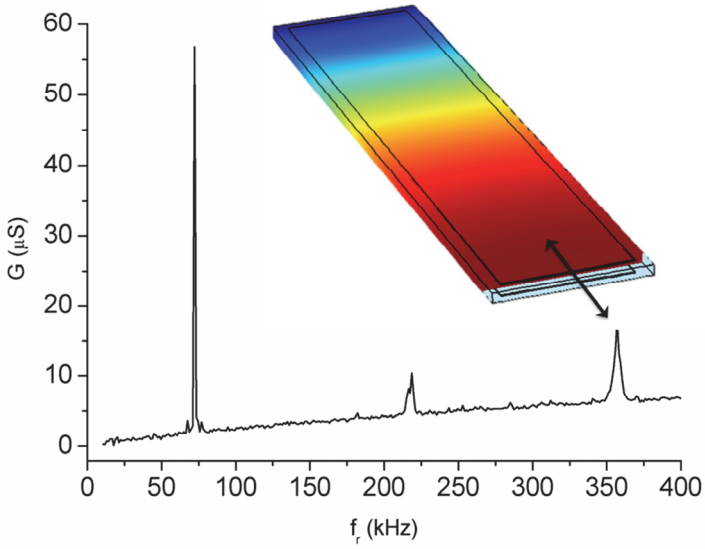

Figure 34 : Electric signature of the in plane 31-longitudinal vibration modes of the 8x2x0.1 norm-cant

4.1.3.2. Piezoelectric d_{31} constant calculation

Thanks to the microcantilever electric signature at the fundamental mode (n=1), it is possible to extract dielectric and electromechanical parameters such as:

- the piezoelectric charge coefficient d_{31} in $V.m^{-1}$ or in $C.m^{-1}$ (also called piezoelectric deformation coefficient or piezo modulus): it is the ratio of induced electric charge to mechanical stress or of achievable mechanical stress to electric field applied. The 31 indexes indicate respectively the electric field and mechanical stress directions.
- the electromechanical coupling factor k_{31}: it is a measure of the extent of the piezoelectric effect which describes the ability of a piezoelectric material to convert electrical energy into mechanical energy and vice versa. The coupling factor is

determined by the square root of the ratio of stored mechanical energy to the total energy absorbed. The indexes 31 refer to the vibration mode.

- the relative dielectric constant ε_{33}^{T} is the ratio of the absolute permittivity of the ceramic PZT material and the permittivity in vacuum, where the absolute permittivity is a measure of the polarizability in the electrical field. The indexes 33^{T} indicate the polarization direction (3) when the electric field is applied in the direction of polarization (direction 3) at a constant mechanical stress (T=0).

This study is realized on the 'norm-cant' and 'ID-cant' cantilevers. The resonance frequency $f^{(1)}_{31,R}$ is determined for the maximum of the admittance module |Y| and the anti-resonance frequency $f^{(1)}_{31,A}$ for the minimum of the admittance module.

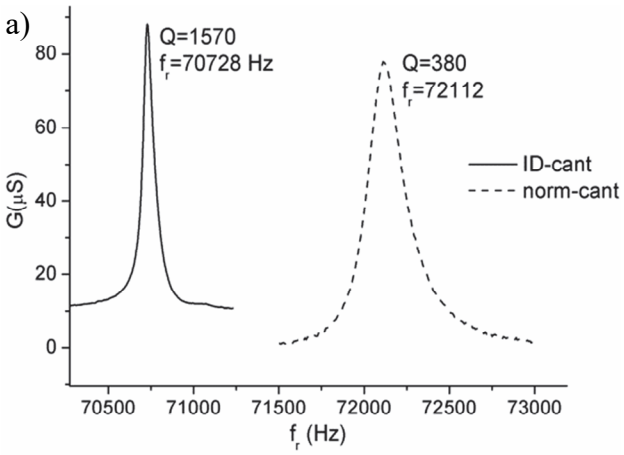

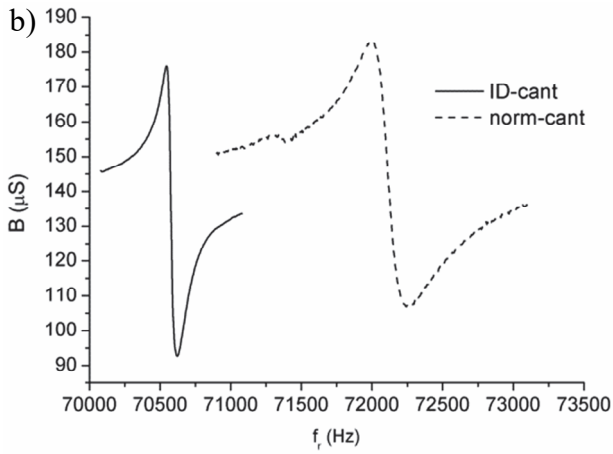

Figure 35 : Electrical signature for the fundamental mode (n=1) of the 31-longitudinal vibration for a) the conductance and b) the susceptance of the "ID-cant" and the "norm-cant"

The real and imaginary parts of the admittance Y (respectively conductance G and susceptance B) as a function of the frequency are presented in **Figure 35**. We note that the resonance frequency of the "ID-cant" is similar as the "norm-cant" since the geometry of the microcantilever remains largely unchanged. Moreover, a notable improvement (almost 3 times higher) of the quality factor from the "ID-cant" compared to the "norm-cant" is observed. This can be explained by the fact that the top electrode changed in two interdigitated electrodes allows a better sintering of the whole device and also by the improvement of the PZT ink preparation. For the calculation of the different piezoelectric constants, we make the hypothesis that the microcantilevers are simple "planar parallelepiped" structures polarized in the direction 3 of the thickness, without 'bound' part. This configuration allows the determination of the relative permittivity ε^{T}_{33} the piezoelectric charge coefficient d_{31}

and the electromechanical coupling factor k_{31} by IEEE standard on piezoelectricity.[1]

$$\frac{k_{31}^2}{1-k_{31}^2} = \frac{\pi}{2}\frac{f_{31,AR}^{(1)}}{f_{31,R}^{(1)}}\tan\left[\frac{\pi}{2}\left(\frac{f_{31,AR}^{(1)}}{f_{31,R}^{(1)}}-1\right)\right]$$

Equation 8

$$\varepsilon_{33}^T = \frac{h_{PZT}}{bL(1-k_{31}^2)}C_0$$

Equation 9

C_0 is the capacity measured at 1kHz far from the resonance frequency.

$$v_{31}^E = 4Lf_{31,R}^{(1)}$$

Equation 10

$$s_{11}^E = \frac{1}{\rho_{cantilever}(v_{31}^E)^2}$$

Equation 11

$$d_{31} = k_{31}\sqrt{\varepsilon_{33}^T S_{11}^E}$$

Equation 12

Table 8 : Piezoelectric, electric and elastic characteristics related to the 31-longitudinal mode of the "norm-cant" and the "ID-cant".

	Q	υ^E_{31} ($m.s^{-1}$)	s^E_{11} ($.10^{-12}$)	k_{31}	ε^T_{31}	$-d_{31}$ ($pC.N^{-1}$)
norm-cant	380	2221	33.7	6.9%	234	18.16
ID-cant	1500	2173	35.27	4.7%	294	14.21

In **Table 8**, parameters are quite homogenous for the two microcantilever structures. This means that the piezoelectric properties of microcantilevers are not altered with the modification of the top electrode in the new design. The resonance frequency of the "ID-cant" is comparable to that of "norm-cant" since geometry is similar. The higher ε^T_{33} for the "ID-cant" should be due to the better sintering of the PZT layer increasing its compacity. The d_{31} parameter is similar to the "ID-cant", which translates a similar electromechanical performance. However, this parameter is not a priority when the device is used in resonant mode as a sensor. Indeed, it is more important to have a high quality factor even at the expense of slightly worsening the piezoelectric properties. Here, the "ID-cant" has a Q factor that is three times higher than the 'norm-cant' what will be advantageous for our gas sensing application

4.1.4. Theory correlation of experimental observation

From the different experimental results obtained previously, theoretical correlations have been carried out. Beginning with the

constitutive equation for piezoelectric materials it is established the relation between electrical and mechanical properties according to the **Equation 13** and **Equation 14**.

$$D = \varepsilon^T E + dT$$

Equation 13

$$S = dE + s^E T$$

Equation 14

Where D, E, S and T are the electric displacement, the electric field, the mechanical strain and the mechanical stress, respectively. Thanks to the symmetry of the cantilever in the 1 axis, it is possible to establish a general invariance relation of the piezoelectric constants and permittivity:

$$d = \begin{bmatrix} 0 & 0 & 0 & 0 & d_{15} & 0 \\ 0 & 0 & 0 & d_{15} & 0 & 0 \\ d_{31} & d_{31} & d_{33} & 0 & 0 & 0 \end{bmatrix}$$

Equation 15

$$\varepsilon = \begin{bmatrix} \varepsilon_{11} & 0 & 0 \\ 0 & \varepsilon_{11} & 0 \\ 0 & 0 & \varepsilon_{33} \end{bmatrix}$$

Equation 16

A previous study [4] following the same fabrication process and compounds used for the elaboration of a piezoelectric microcantilever has been chosen as a reference for the different parameter to use in the simulation as shown in **Table 9**.

Table 9: Values of mechanical and piezoelectric parameters used

Parameter	Value	Unit
s_{11}	$4.14\ 10^{-11}$	$m^2.N^{-1}$
s_{12}	$-1.242\ 10^{-11}$	$m^2.N^{-1}$
s_{13}	$-2.07\ 10^{-11}$	$m^2.N^{-1}$
s_{33}	$5.18\ 10^{-11}$	$m^2.N^{-1}$
s_{44}	$10.76\ 10^{-11}$	$m^2.N^{-1}$
d_{15}	$30.0\ 10^{-12}$	$m.V^{-1}$
d_{31}	$-10.0\ 10^{-12}$	$m.V^{-1}$
d_{33}	$20.0\ 10^{-12}$	$m.V^{-1}$
ε_{11}	200.0	$F.m^{-1}$
ε_{33}	250.0	$F.m^{-1}$

To model the electromechanical behaviour of the microcantilever, a system of masses and springs is used with hexahedra as basics elements [5, 6] (**Figure 36**).

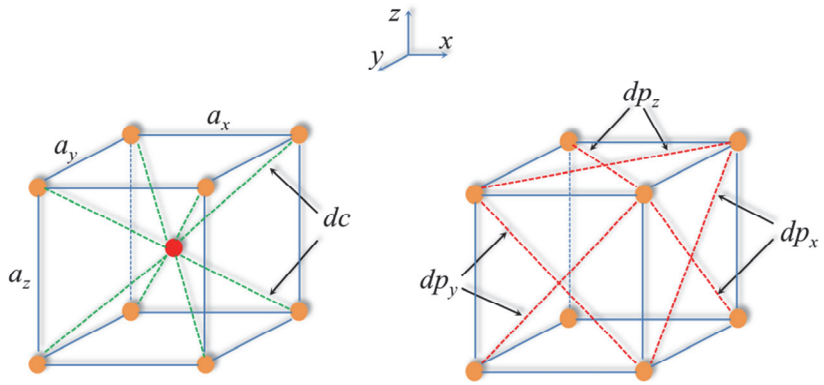

Figure 36: Two views of springs in the hexahedron and their description with on the left, springs in ridges (a_x, a_y, a_z), springs in vertex and the central node (*dc*). On the right, springs in ridges and springs in diagonal of a same plane (dp_x, dp_y, dp_z). For clarity, springs of union between central nodes and neighboring hexahedra hare not presented.

In each vertex and in the mass center of the hexahedron are located punctual masses (nodes) which concentrate the distributed mass in the space of its domain. Nodes are interconnected to springs in four different ways: springs located in ridges (a_x, a_y, a_z), springs of union between the central node and vertexes (*dc*), springs in diagonal of union between vertexes in a same face (dp_x, dp_y, dp_z) and finally, springs of union between central nodes and neighbouring hexahedra (*uc*).

From the parameters of the **Table 9**, it is possible to reproduce the dynamic behaviour of the cantilever using the second law of Newton:

$$m_i \ddot{\boldsymbol{p}}_i + a_i \dot{\boldsymbol{p}}_i = \boldsymbol{F}s_i + \boldsymbol{F}e_i$$

Equation 17

Where m_i is the mass associated of the node i, a_i is the damping factor on the node i, $\ddot{\boldsymbol{p}}_i$ and $\dot{\boldsymbol{p}}_i$ are acceleration and velocity of the node i, respectively. $\boldsymbol{Fs}_i$ is the elastic strength exerted for all of springs united at the node and $\boldsymbol{Fe}_i$ is the external strength actuating on the node i. In the same time, the elastic strength is given by:

$$\boldsymbol{Fs}_i = b_{ij}\left(\left\|\boldsymbol{p}_j - \boldsymbol{p}_i\right\| - l_{ij}^0\right)\frac{\boldsymbol{p}_j - \boldsymbol{p}_i}{\left\|\boldsymbol{p}_j - \boldsymbol{p}_i\right\|}$$

Equation 18

Where b_{ij} is the elastic coefficient associated to the spring located between the nodes j and i. j is referred to each neighbouring nodes with whom that a node i share a spring. The external strength is a consequence of the piezoelectric effect and is applied on the nodes located on the surfaces submitted to the action of the electric field. From the **Equation 13** and the **Equation 14** and the unique excitation of E_3, it results the **Equation 19.**

$$T_3 = E_3 \frac{d_{31}}{s_{13}}$$

Equation 19

The **Table 10** shows values of the elastic constant of springs that adjust cursives values of the **Table 9** for 64x16x1 hexahedra. The damping factor a_i used is 10^{-6} N.s.m^{-1}and a specimen density of 5.2. The semi-implicit type integrator of Euler is used with a sample time of 35 ns.

Table 10: Results of calculated elastic constants

Type of spring	Elastic constant ($kN.m^{-1}$)
(a_x)	370
(a_y)	350
(a_z)	720
(dp_x)	1400
(dp_y)	1400
(dp_z)	290
(dc)	1400
(uc_x)	370
(uc_y)	350
(uc_z)	720

Results show a resonance frequency of 67485 kHz, in agreement with the **Equation 4** and a quality factor of 1400 which are similar values from the experimental (~70 kHz). For a sinusoidal excitation of 4025 Pa (see **Figure 37**), peaks magnitude in resonance is 710 nm in *x* axis for the norm-cant and 287 nm for the ID-cant is observed.

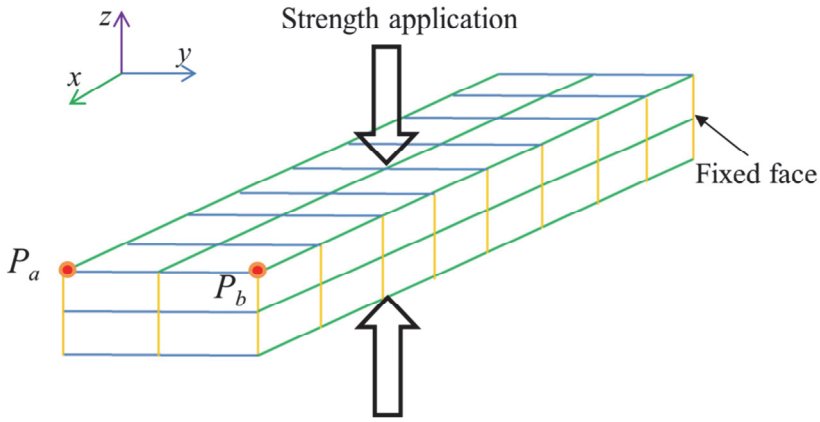

Figure 37: Scheme of the theoretical approach of the cantilever displacement with the strength application face and the displacement studies of the nodes P_a and P_b

It is noticed that the reduction in the magnitude of the vibration between the "ID-cant" and the "norm-cant" is similar to the reduction of the surface covered by electrodes (60%).

For the "norm-cant", the movement in the center of the free face $(P_a+P_b)/2$ of the cantilever (opposite of the fixed face) is zero. However, it appears a small displacement (<1nm) in the direction *y* three magnitude order lower than the movement in direction *x* as shown in **Figure 38**. It is shown that the ID-cant has an asymmetric oscillation in *y*.

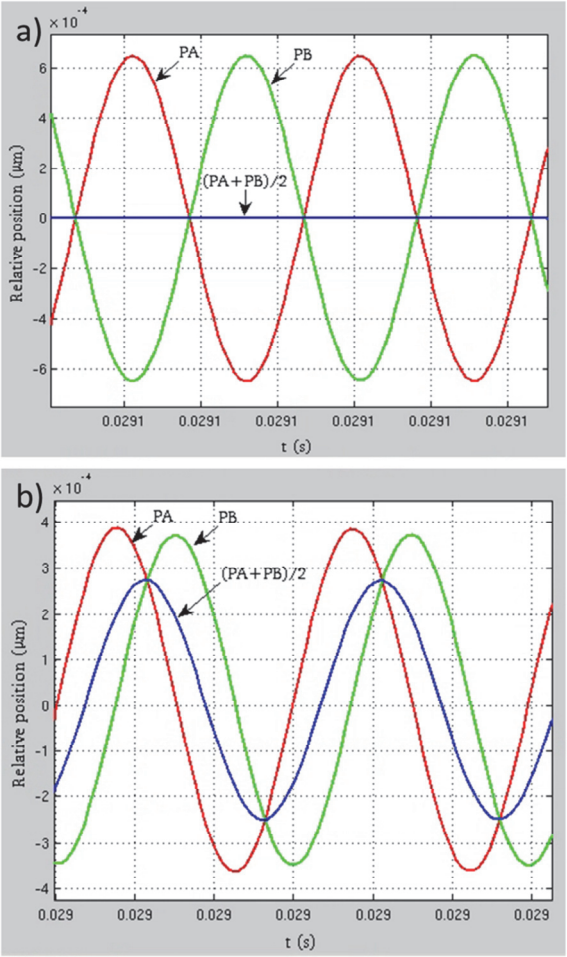

Figure 38: Cantilever displacement in *y* direction of a) the norm-cant and b) the ID-cant

By neglecting the viscosity and density effects and assuming that the gas and the cantilever are at the same temperature, the resonance frequency shift of the 31-longitudinal vibration mode related to molecules adsorption is:

$$\Delta f_{31,R} = \frac{f_{31,R}}{2}\left(\frac{\Delta k}{k} - \frac{\Delta m}{m}\right)$$

where the frequency variation ($\Delta f_{r,31}$), is proportional to the resonance frequency ($f_{r,31}$) and linked to the mass m and the stiffness k of the cantilever. To simulate the sensitivity of the cantilever in mass changing, the mass magnitude associated to the nodes in the plan *12* (with axis *3* constant) is altered. To simulate the sensitivity in stiffness changing, the elastic constants associated to the springs in the same plan are also altered. For the both cases, we confirm the validation of the **Equation 20** in the relative changing range of ±0.25% as shown in **Figure 39**.

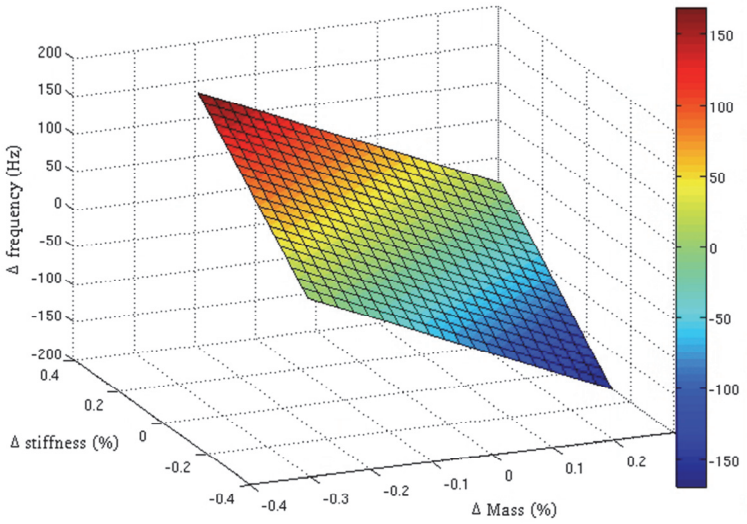

Figure 39: Simulation of the resonance frequency variation in function of the relative stiffness and mass changing

It is noted that a shift of the resonance frequency is driven by a competition between stress (positive shift) and mass (negative shift) effect.

4.2. Microcantilever preparation for gas sensing tests

4.2.1. Effect of CNTs deposition

After the CNTs deposition on the "ID-cant" cantilever (following the procedure detailed chapter II), a negative resonance frequency shift of few hundreds Hertz is observed because of the predominant cantilever mass effect. The quality factor is not affected as shown in **Figure 40.**

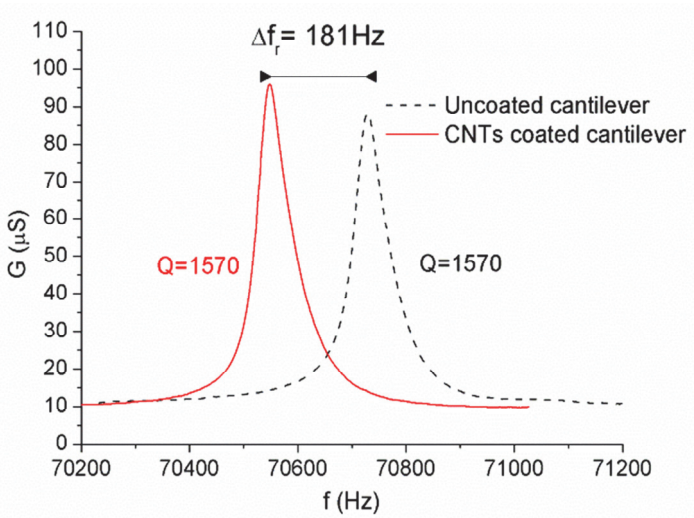

Figure 40: Conductance of the PZT cantilever at the resonance frequency before and after CNTs deposition.

The fact that quality factor remains unchanged is explained by the small amount of O-MWCNTs deposited.[7]

4.2.2. Electrical measurement processing

The characterization of the sensing performance towards different hazardous species were performed following the same conditions as explained in chapter II. Once sensors were placed inside the test chamber, they were connected to the impedancemeter. To allow the real-time reading of the resistance and the resonance frequency, a Labview interface is created. First the resonance frequency f_{r0} is determined by measuring 10 times (each two seconds) the maximum value of the conductance $G(f_{r0})$ and calculating the average. Then, a susceptance value S_0 is determined from the f_{r0} on the susceptance B(f) curve near the resonance frequency. This value is always the same near the resonance frequency. Finally, a scan of the resonance frequency f_r (t) is deduced from S_0 each 8 seconds.

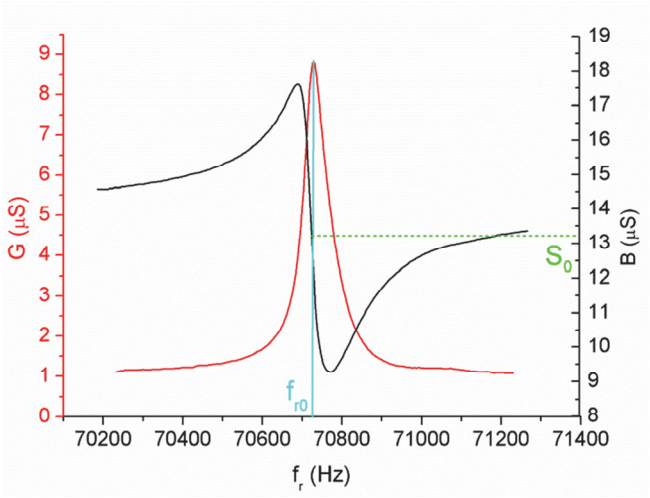

Figure 41: Resonance frequency scan measurement protocol

This method is preferred from direct read of the maximum (conductance curve) since less noise is generated and consequently higher accuracy in resonance frequency measurement is observed.

4.3. Results and discussion

All the results presented in the next paragraphs concern the 'ID-cant' cantilever.

4.3.1. Temperature effect

The resonance frequency of the cantilever has been studied varying the temperature of the cantilever. Thanks to the heater screen-printed at the back of the alumina substrate, it is possible to apply a voltage corresponding to the temperature since the resistance R of the heater is linked to the temperature by the formula:

$$R = R_o(1 + \alpha(T - T_0))$$

Equation 21

Where R_0 is the resistance of the heater at room temperature, α is the temperature coefficient of the material (here platinum based thick film α ~3200ppm), T the temperature of the heater and T_0 the room temperature. The sensor is introduced in the chamber under a dry air flow and the conductance is measured near the resonance frequency as shown in **Figure 42.**

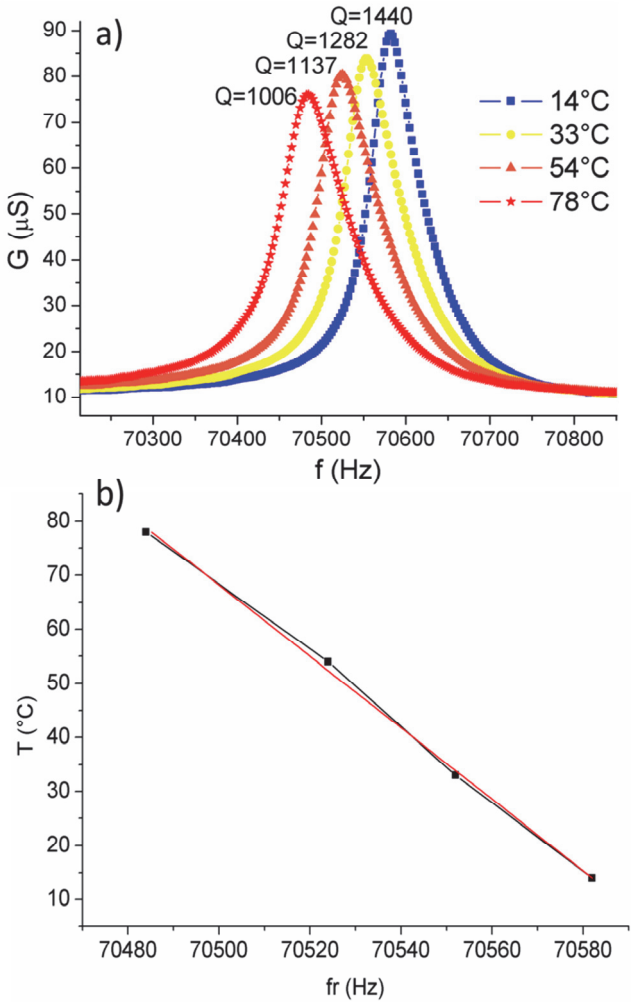

Figure 42: a) Conductance as function of the frequency at different temperatures and b) temperature as function of resonance frequency

We observe that the resonance frequency of the cantilever decreases inversely with the temperature in a linear behaviour (-1.51±0.5 Hz.K^{-1}). This variation is due, in part, to the modification of the temperature that changes the dimensions of the cantilever under temperature variation. Thermal dilatations are not majority responsible but the Young's modulus changing is the principal reason

as explained in [8]. Furthermore, it is important to notice that the quality factor significantly diminishes when the temperature of the heater is increased. Since the quality factor traduce general losses like inner and viscous losses, its decreasing reveals the increasing of these losses with the temperature. As the resonance frequency linearly varies with the temperature in a reversible way, it is possible to previously calibrate the sensor in order to compensate the temperature fluctuation effect in real measurement conditions.

4.3.2. Detection of volatile compounds at room temperature

Different concentrations of NO_2, benzene and CO were generated and the sensor responses were studied. CNTs resistance and resonance frequency measurements were performed at room temperature with the impedance analyser.

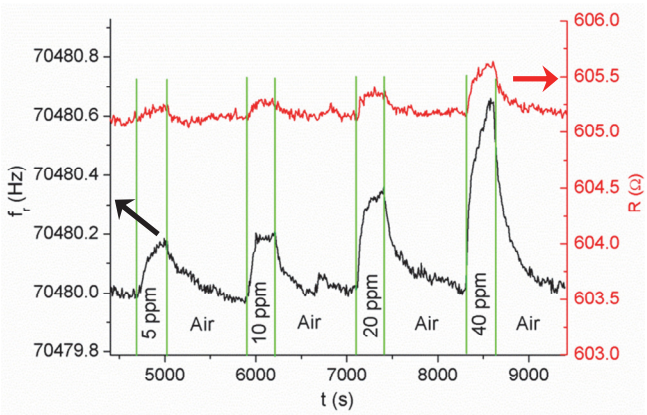

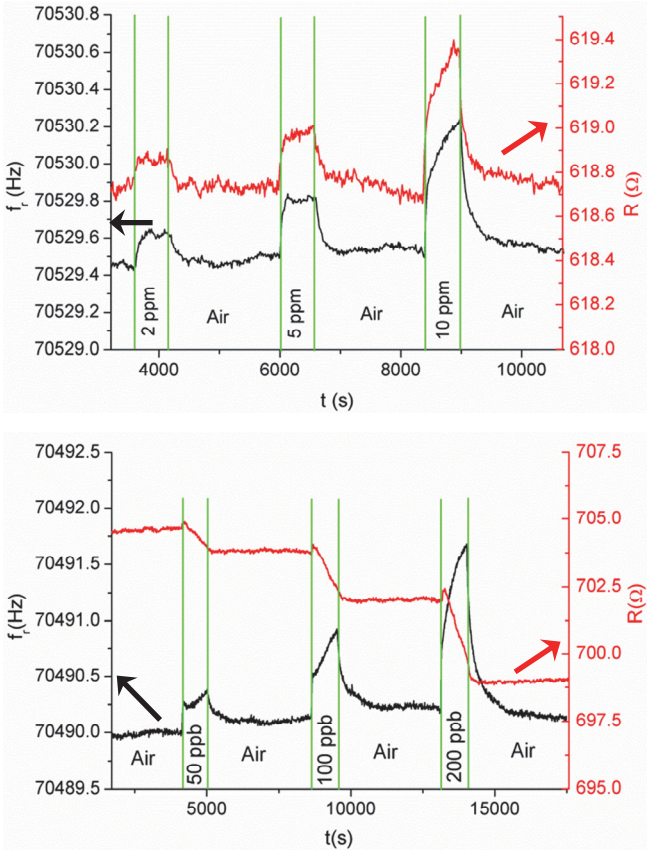

Figure 43: a) Response under CO b) under benzene and c) under NO_2 of O-MWCNTs coated PZT cantilever at room temperature (RT).

Figure 43 shows the experimental responses and recovery curves of the double transduction to increasing concentration of these volatiles. The resonance frequency versus time increased as a consequence of exposure to benzene, CO and NO_2. Such positive resonance frequency shifts, already observed in previous works [9-11], result from surface stress modification on the cantilever occurring during vapors/gas sorption and inducing either positive or negative frequency shifts depending on interactions between the coating and the volatile. At such low concentrations, stress effect is predominant

and hence a positive resonance frequency shift is observed. Thanks to a high quality factor (Q>1500), measurements present low noise level. Also, significant variations of the resonance frequency are observed with a complete recovery of the baseline at room temperature. As in a *p*-type semiconductor, the resistance of O-MWCNT films increased with the concentration of benzene and CO. Conversely, resistance shift was negative when NO_2 concentration was increased. We observed that baseline recovery is reached for benzene and CO but not for NO_2 detection. This is due to the very low dynamic desorption of nitrogen dioxide since these species strongly interacts with O-MWCNTs. The lower concentrations measured were 2 ppm, 5 ppm and 50 ppb for benzene, CO and NO_2, respectively. The interest of the double transduction is already demonstrated for the detection of CO. Resistance changes of O-MWCNTs films do not allow CO detection below 40 ppm, whereas the signal of the resonance frequency shift is already significant at 5 ppm. Furthermore, thanks to the sign of the shifts experienced by the resistance of O-MWCNTs films it is possible to discriminate an oxidizing from a reducing contaminant (provided that these are considered separately). In order to better understand the detection mechanisms and, in particular, the opposed effects of stress and mass in the sensing performance of the cantilever, additional measurements of benzene at higher concentrations have been investigated (**Figure 44**.)

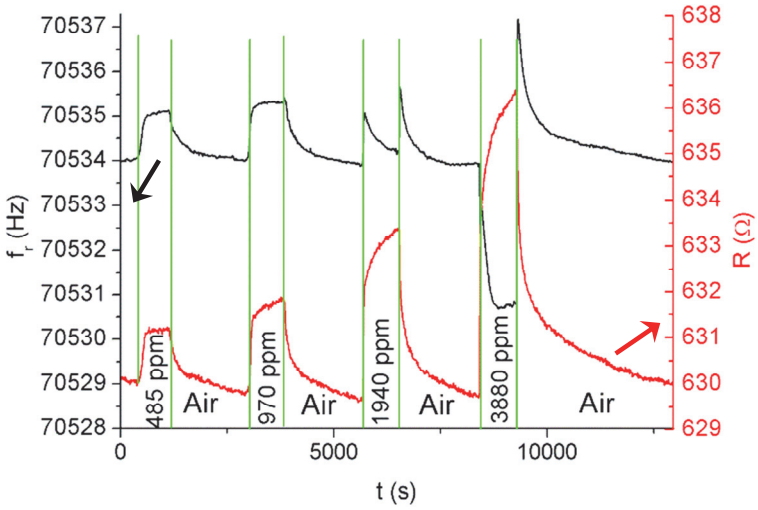

Figure 44: Response under high concentrations of benzene at RT.

We progressively see that stress and mass effects nearly compensate at around 2000 ppm of benzene. The mass effect becomes then the dominant phenomenon at higher benzene concentrations and results in negative shifts of the resonant frequency. During this process, the resistance of the O-MWCNTs films monotonically increases with benzene concentration. Sensor responses of the tests performed are reported in **Figure 45.**

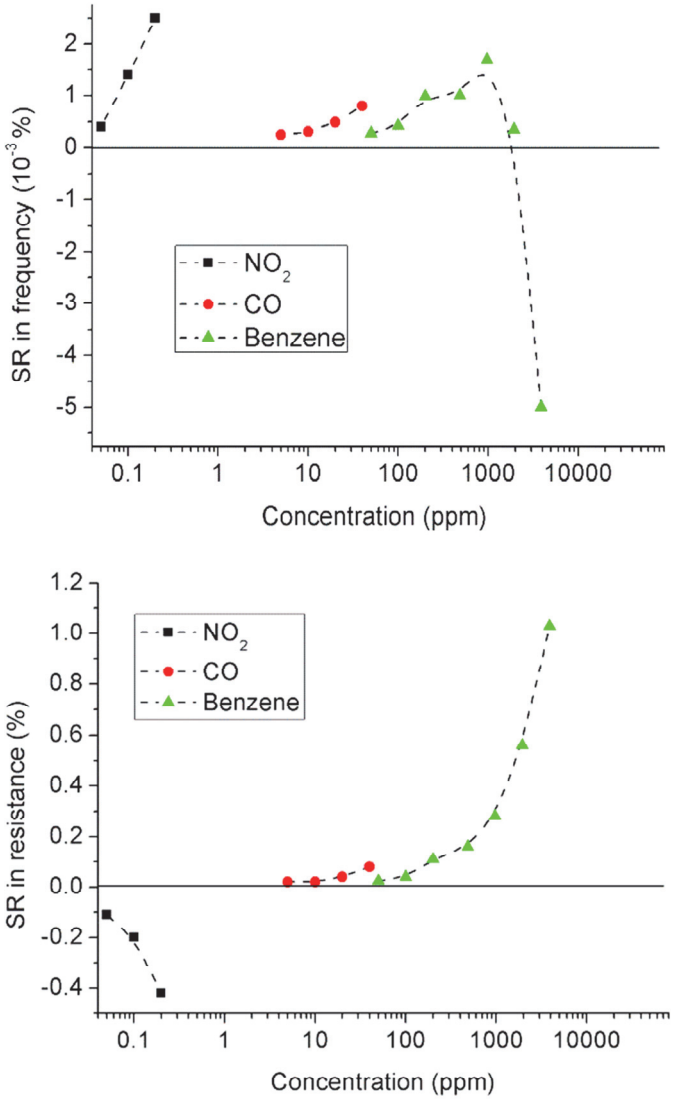

Figure 45: Sensor response SR in a) frequency and b) resistance toward different gases with SR=$\Delta x/x_{air}$ (where Δx is the resonance frequency or resistance difference under air and contaminants).

4.3.3. Effect of humidity

The effect of humidity changes has been also investigated. The measurements were conducted under 10±1% to 90±2% of R.H. (corresponding to 2,630 and 24,161, respectively at 1 atm and 22°C). Here, as for high concentrations of benzene, negative shifts of the resonance frequency are already observed at RH of 25% due to the fact that a wide change in the relative humidity content has been studied. Humidity presence is significant from RH of 75% with a negative shift of the O-MWCNTs resistance.

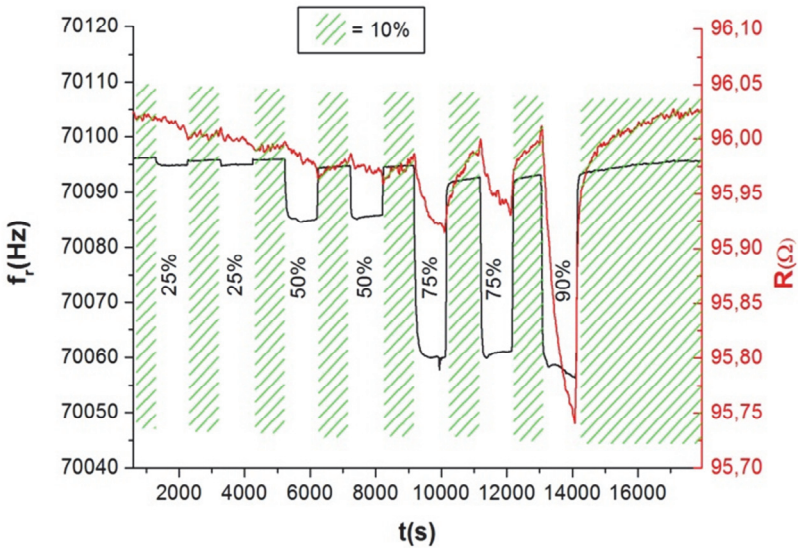

Figure 46: Response under different humidity ratios

4.4. Conclusion

In this chapter, it has been shown that the 'ID-cant' cantilever possess similar electromechanical properties than the 'norm-cant' cantilever. Furthermore, an improvement in the fabrication of the PZT cantilever (paste preparation and thermal treatment) has allowed

the increase of the quality factor. Theoretical studies have shown that ‘’ID-cant’ vibrates in an asymmetric oscillation compared to the ‘norm-cant’. But this not a problem for gas sensing application since the movement in direction *1* is three magnitudes order higher than in direction *y*. The double transduction has been very useful in gas sensing tests. The lower concentrations measured are 2 ppm, 5 ppm and 50 ppb for benzene, CO and NO_2, respectively. The interest of the double transduction is shown first for the detection of CO. Resistance changes of O-MWCNTs films do not allow CO detection below 40 ppm, whereas the signal of the resonance frequency shift is already significant at 5 ppm. In second, thanks to the sign of the shifts experienced by the resistance of O-MWCNTs films it is possible to discriminate separately an oxidizing from a reducing contaminant. The major drawback of such system is the humidity effect. Even at low RH (25%), a mass effect is observed and the stiffness effect due to low amount adsorption of volatiles cannot be read.

References

[1] B. Jaffe and W. Cook, "Jr and H. Jaffe, Piezoelectric ceramics," ed: Academic Press, New York, 1971.

[2] H. Debéda, R. Lakhmi, C. Lucat, and I. Dufour, "Use of the longitudinal mode of screen-printed piezoelectric cantilevers coated with PEUT for toluene detection: Comparison with silicon cantilevers," *Sensors and Actuators B: Chemical,* vol. 187, pp. 198-203, 2013.

[3] I. Dufour, F. Josse, S. M. Heinrich, C. Lucat, C. Ayela, F. Ménil*, et al.*, "Unconventional uses of microcantilevers as chemical sensors in gas and liquid media," *Sensors and Actuators B: Chemical,* vol. 170, pp. 115-121, 7/31/ 2012.

[4] C. Castille, "Etude de MEMS piézoélectriques libérés et microstructurés par sérigraphie. Application à la détection en milieu gazeux et en milieu liquide," Université Sciences et Technologies-Bordeaux I, 2010.

[5] S. F. Gibson and B. Mirtich, "A survey of deformable modeling in computer graphics," Citeseer1997.

[6] V. Baudet, M. Beuve, F. Jaillet, B. Shariat, and F. Zara, "Integrating tensile parameters in hexahedral mass-spring system for simulation," 2009.

[7] Z. Qian, F. Liu, Y. Hui, S. Kar, and M. Rinaldi, "Graphene as a Massless Electrode for Ultra-high-frequency Piezoelectric Nano Electro Mechanical Systems," *Nano letters,* 2015.

[8] A. D. Rushi, K. P. Datta, P. S. Ghosh, A. Mulchandani, and M. D. Shirsat, "Selective Discrimination among Benzene, Toluene, and Xylene: Probing Metalloporphyrin-Functionalized Single-Walled Carbon Nanotube-Based Field Effect Transistors," *The Journal of Physical Chemistry C,* vol. 118, pp. 24034-24041, 2014/10/16 2014.

[9] T. Thundat, G. Chen, R. Warmack, D. Allison, and E. Wachter, "Vapor detection using resonating microcantilevers," *Analytical Chemistry,* vol. 67, pp. 519-521, 1995.

[10] A. BOISEN, "Stress formation during self-assembly of alkanethiols on differently pre-treated gold surfaces," 2001.

[11] G. Chen, T. Thundat, E. Wachter, and R. Warmack, "Adsorption-induced surface stress and its effects on resonance frequency of microcantilevers," *Journal of Applied Physics,* vol. 77, pp. 3618-3622, 1995

CHAPTER V: Cavitand functionalized MWCNTs for sensitive benzene detection

In previous chapters, we have seen that benzene detection at low concentration remains difficult. In this chapter, we propose a different approach to increase the interaction between benzene and the sensitive layer, which is based on the host-guest molecular recognition.

5.1. Motivation

For a few decades, many studies have been focused on the use of weak and reversible interactions for the development of receptors for the selective complexation of aromatic compounds via "host-guest" strategy. Cram *et al.* pioneered host-guest studies using deep cavitands derived from resorcin[4]arene scaffolds.[1] The shallow aromatic cavity present in the resorcin[4]arene parent compound was further elaborated by installing bridging groups at the upper rim. Quinoxaline-bridged resorcin[4]arene cavitands are known to bind aromatic guests (e.g. benzene, toluene, fluorobenzene), not only in the liquid, but also in the gas phase.[2, 3] The attractive CH-π and π-π interactions established between the receptor and the included aromatic compound constitute the main driving forces responsible for the formation of inclusion complexes. Thoden *et al.* modified the alkyl substituents at the lower rim of the cavitands with thioether functions in order to anchor the receptors on a gold surface.[4-6] The improvements achieved in the synthesis of the cavitands together with

the possibility to deposit them as self-assembled monolayers on different solid substrates led to the emergence of new strategies in the design of sensors devices.[7-9] Consequently, several approaches for the detection of aromatic compounds both in liquid and gas phases have been reported. The recognition event (formation of a host-guest complex) was transduced in changes on optical properties (surface plasmon resonance,[10-15] fluorescence spectroscopy[16]) or in mass changes in the case of resonant devices (quartz crystal micro balance sensor,[17-21] or a PZT piezoelectric device[22]). For these devices, the reported LOD for BTEX ranges from 50 to hundreds of ppm. Resorcin[4]arene cavitands have also been used as absorbent materials in pre-concentrator devices coupled to a μ-GC column for analyte separation. Furthermore, the detection of analytes was performed by a metal oxide gas sensor or mass spectrometer.[23, 24] In these examples the detection limit for BTEX was found to be in the ppb range.[25-28] Recently, resorcin[4]arene cavitands were covalently attached to carbon nanotubes (CNTs) that acted as transducers[29-31] for conductance measurement in the solid-liquid sensor interphase. CNTs have attracted considerable interest as nanomaterial for sensing in solid-gas interphase.[32] They are particularly sensitive to local chemical environment of the gas phase.[33] The functionalization of CNTs with metal-NPs has been exploited to enhance the sensitivity of the material for benzene sensing, reaching an LOD of about 50 ppb in dry air.[34, 35] The metal-NP-CNT system acts as the transduction unit of the adsorbed event in a resistive gas sensor. Indeed, the interaction of the material with molecules of benzene in the gas phase results in an electronic

charge transfer process between the organic molecule and the metal-NP-CNT nanomaterial. This affects the position of the Fermi energy and, hence, the conductivity of the detection unit. The different used metals show different response towards a variety of gas or vapor molecules, which can be used to improve the selectivity.[36] However, the decoration of CNTs with metal nanoparticles for improving the device's selectivity has been implemented with limited success because these nanomaterials show similar sensitivity to variety of aromatic compounds and heating is needed to recover the sensor baseline.[34]

Here we describe a simple experimental procedure to prepare an unprecedented type of resistive gas sensing device that employs gold nanoparticle (Au-NP) decorated oxygen-functionalized multiwall carbon nanotubes (O-MWCNTs). The Au-NPs are functionalized after deposition on the O-MWCNTs with quinoxaline-walled thioether-legged cavitand **4** (**Figure 47**) leading to highly sensitive molecular recognition of benzene vapors. Additionally, we explored the sensitivity of the sensor towards others air pollutants such as toluene, *o*-xylene, carbon monoxide, nitrogen dioxide and ethanol vapors in order to evaluate cross sensitivity. The gas sensing mechanism is discussed on the basis of the experimental findings and the mechanism of inclusion complex (benzene⊂**4**) formation in the light of reported, structurally related systems in solutions.

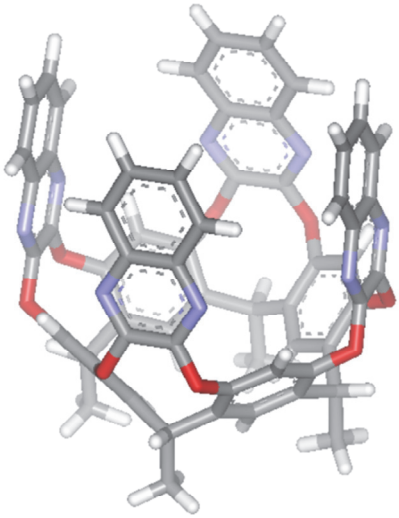

Figure 47. Energy-minimized (MM3 as implemented in Scigress v3.0) structure of cavitand 4 in vase conformation. Included molecule is omitted and cavitand legs -$(CH_2)_9$-S-$(CH_2)_9$-CH_3 are presented as methyl groups for clarity.

5.2. Anchoring of the cavitand on MWCNTs

5.2.1. Experimental section

The gas sensitive, hybrid nanomaterial was prepared by employing a three-step approach. In the first step MWCNTs were obtained from Nanocyl^{TM} (3101 grade). They were grown by chemical vapor deposition with purity higher than 95%. Carbon nanotubes were up to 1.5 μm long and 9.5 nm in outer diameter. They underwent an oxygen plasma treatment to clean them from amorphous carbon, to promote their dispersion in an appropriate solvent and to create reactive sites (i.e. oxygenated vacancies, O-MWCNTs) quoted in literature as VO_2 (oxygenated vacancies) and

V_2O_2 (oxygenated double-vacancies) in which metal nanoparticles can nucleate. O-MWCNTs were suspended in chloroform (0.5% w/w) and sonicated during 30 min to uniformly disperse them in the solution, which led to a reproducible CNT density. The prepared suspension was air-brushed on an alumina substrate that comprised of 10x10 mm screen-printed, Pt-interdigitated electrodes with gap of 500 μm between electrodes. During the airbrushing, the substrate was kept at 100°C for achieving fast evaporation of the solvent coupled with the resistance monitoring of the device until it reached the defined value of 5 kΩ. This strategy, which is very similar to the one reported by Zilberman et al.,[37] enables us to control both the density of the CNT coating and the amount of O-MWCNTs deposited, ensuring device to device reproducibility. To ensure the complete removal of the solvent and promote adhesion of the MWCNT mat to the substrate, sensors were heated at 150 °C for 2 h. The final resistance of thermally-treated sensors was a few hundred of ohms. The next step was decoration of O-MWCNTs with Au-NPs achieving by RF sputtering process conducted at 13.56 MHz with a power of 30 W under Ar plasma at room temperature, under 0.1 Torr, for 10 s. For the formation of the self-assembled monolayer of the deep cavitand, sensor substrates were immersed in a solution (20 mL) of the cavitand (0.5 mM). The SAM process was conducted at 60°C for a period of maximum 24 h. These conditions allowed a reversible adsorption in order to have well-ordered assembly of the quinoxaline-walled cavitand (**4**).[4] Finally, the sensor substrates were cooled to room temperature, rinsed with pure chloroform and dried at 50°C during 30 min. These steps are illustrated in **Figure 48.**

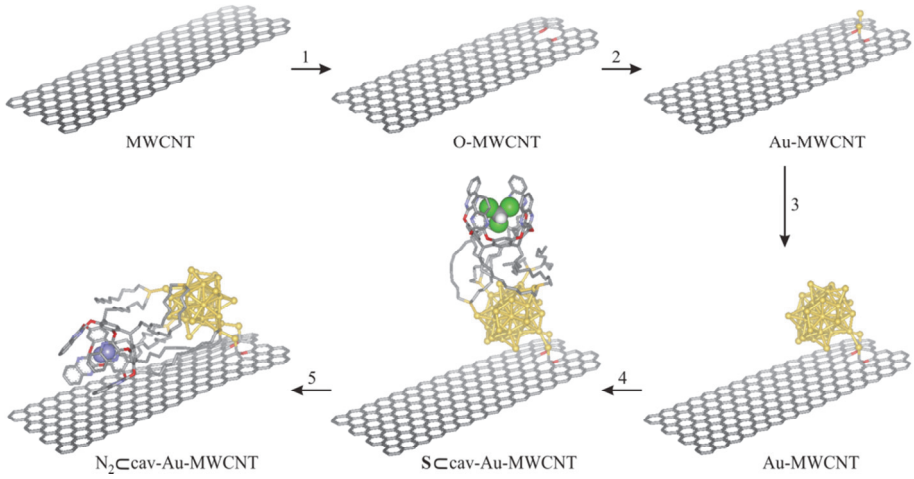

Figure 48. Schematic representation of the preparation of the cav-Au-MWCNT material: (1) oxygen plasma treatment; (2) Au-RF-sputtering (formation of Au-nucleus); (3) Au-RF-sputtering (growth of Au-nucleus and formation of Au-NP); (4) self-assembly of the cavitand 4 monolayer on the Au-NP surface by dipping the material in a chloroform (S) solution of the cavitand 4; (5) solvent removal (an air molecule, e.g. nitrogen, replaces chloroform (S) molecule from the cavitand interior).[38] Nitrogen and chloroform molecules are presented as CPK models. Hydrogen atoms are omitted for clarity. Symbol ⊂ stands for "included in". Note: we hypothesize that upon chloroform removal, the cavitand legs are no longer solvated and the molecule collapses on the Au-MWCNT surface.

The sensing properties of the cav-Au-MWCNTs when operated at room temperature were studied by exposing them to different chemical environments (benzene, toluene, *o*-xylene, carbon monoxide, ethanol and nitrogen dioxide) at different concentrations. For comparison, the results obtained in the gas-sensing measurements performed on Au-MWCNT sensors are also reported. The chemical compositions of O-MWCNT, Au-MWCNT, and cav-Au-MWCNT samples were analyzed using X-ray photoelectron spectroscopy (XPS), VERSAPROBE PHI 5000 from Physical Electronics,

equipped with a Monochromatic Al Kα X-Ray. The energy resolution was 0.7 eV. For the compensation of built up charge on the sample surface during the measurements, a dual beam charge neutralization composed of an electron gun (~1 eV) and the Argon Ion gun (≤10 eV) was used.

5.2.2. Step by step characterization

The morphology and chemical composition of the active layers were characterized using transmission electron microscopy (TEM, Figure 49. and **Figure 50**) and X-ray photoelectron spectroscopy (XPS, **Figure 51**). The homogeneous dispersion of Au nanoparticles (average diameter ~ 2 nm) on MWCNTs is illustrated in **Figure 49** **Figure 50a** and **Figure 50b** show that SAM procedure, implemented for Au-MWCNTs functionalization with the cavitand **4**, promoted aggregation of the previously deposited Au-NPs (with cluster diameters ranging from 10 to 15 nm). The immersion of Au-MWCNTs in a chloroform solution of the cavitand **4** (0.5 mM) under mild heating (60°C), as required by the SAM technique,[32] favored both the cavitand assembly on the Au-NPs and their aggregation on the MWCNTs. We performed XPS analyses for O-MWCNT, Au-MWCNT, cav-Au-MWCNT and cavitand **4** samples.

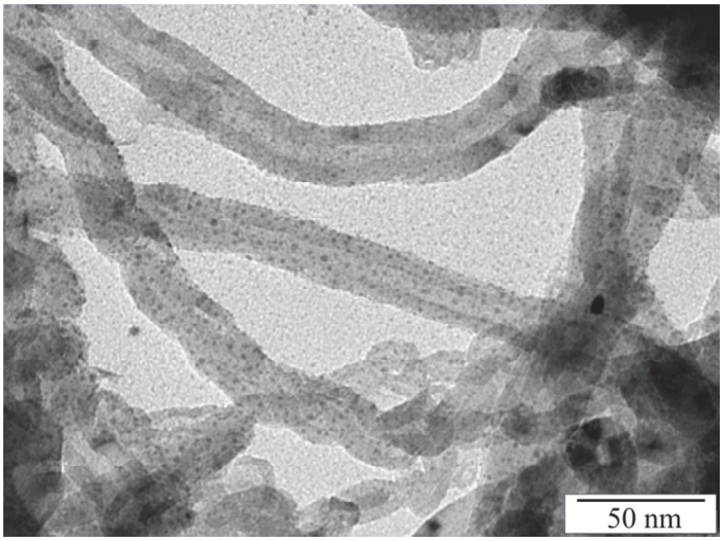

Figure 49. Typical TEM image of Au-MWCNTs.

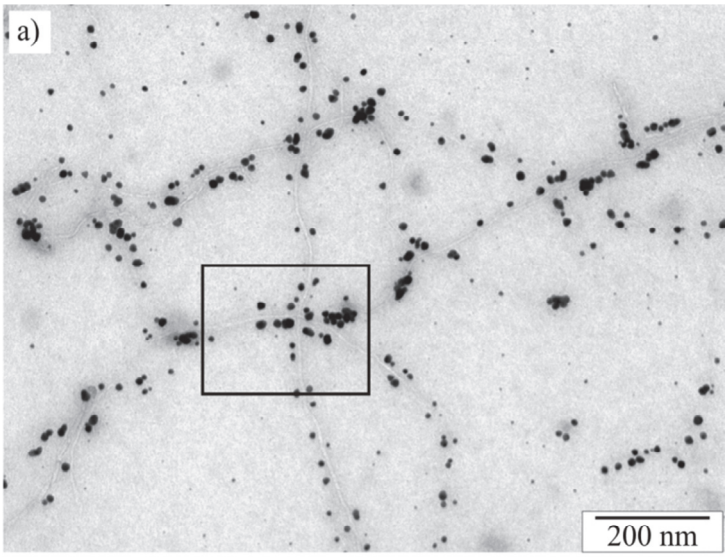

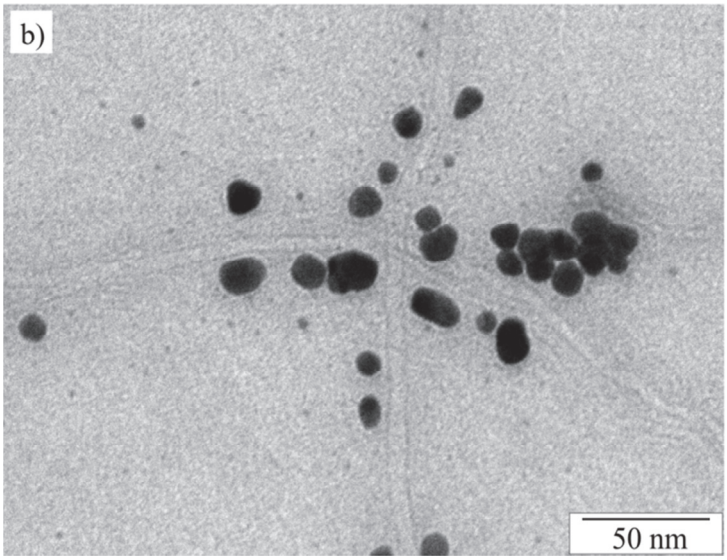

Figure 50. Typical TEM image of: a) cav-Au-MWCNTs and b) zoom-in of the selected area.

In **Figure 51a** we show the XPS spectra acquired for (1) O_2 plasma treated MWCNTs, (2) gold decorated O-MWCNTs and (3-4) cav-Au-MWCNTs samples. The XPS spectra for the cavitand **4** alone (5) is included to assist in the identification of important features in the XPS spectra of cav-Au-MWCNTs samples differing in the time used for the construction of the SAM: 13h (3) and 24h (4). All samples contained the oxygen peak corresponding to O_{1s} (**Figure 51a**) due to the oxygen plasma treatment experienced by the MWCNTs. All Au-decorated samples showed the characteristic Au_{4d} and Au_{4f} doublets. The presence of the cavitand **4** on cav-Au-MWCNT samples, and therefore, the success of the functionalization protocol, was confirmed by the observation of the N_{1s} peak located at 399 eV. This peak is diagnostic of the presence of organic nitrogen and appears only in the spectra of the cavitand and cav-Au-MWCNT samples (**Figure 51b**). We obtained similar values of relative atomic

concentrations ([N]=3% and 2% at. conc.) for the samples treated in the SAM process for 13 and 24 h, curves (3) and (4) respectively, indicating that 13 h are sufficient to fully functionalize the Au-MWCNTs with cavitand **4**.

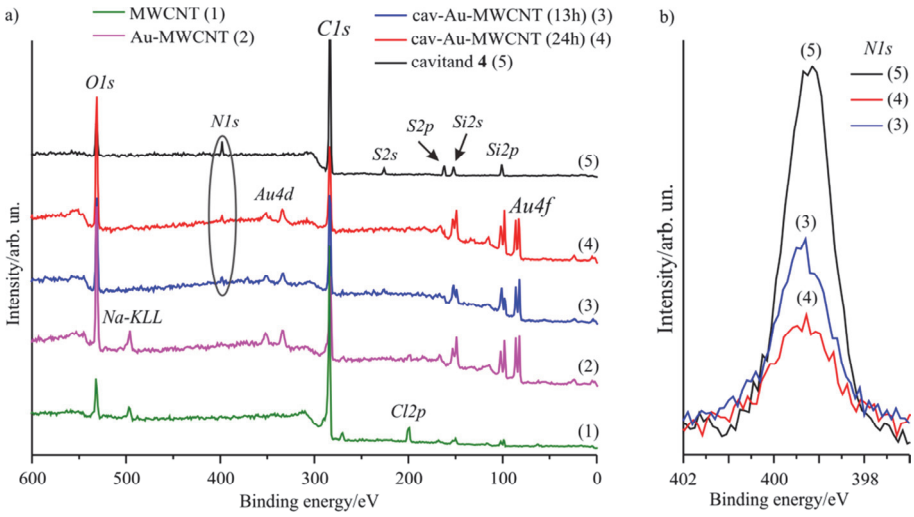

Figure 51. a) Survey spectra acquired for each step of the MWCNTs modification (1-4) and for the cavitand 4 (5). b) a zoom-in of N_{1s} core level spectra are plotted as acquired from cavitand 4 (5) and cav-Au-MWCNT samples (3 and 4).

The resistive sensor consist of a hybrid nanomaterial, which comprises both recognition and transducer elements, embedded in a standard electronic device. With a cavity depth in the order of 8.3 Å, a quinoxaline-bridged cavitand **4** can completely include one BTEX molecule and form a 1:1 host-guest complex mainly stabilized by **π-π** and CH-**π** interactions.[39] The Au-MWCNTs are selected as an integral part of the resistive sensor. They provide sites where the thioether groups of the cavitand **4** can be anchored. The oxygen

plasma treatment resulted in the presence of oxygenated defects on the outer wall of MWCNTs. Such defects help gripping, nucleating and stabilizing Au-NPs. Conversely, pristine carbon nanotubes shows very weak interactions with the Au-NPs by establishing interactions with the p-orbitals of the sp^2 carbons of the network.[40] Theoretical studies have shown that Au atoms get trapped at VO_2 defects (oxygenated vacancies), which are the most abundant in oxygen plasma treated MWCNTs compared to V_2O_2 defects (oxygenated di-vacancies), with a binding energy that is 0.55 eV higher than the binding energy of Au decorated pristine MWCNT.[41] As already discussed in Chapter III, DFT calculations indicated that the presence of oxygen atoms at the functionalized site reduces the HOMO–LUMO gap to 0.82 eV. This reduction can be explained by the higher density of states near the Fermi level, arising from the overlap of the 2p electrons of the O atoms and the p electron system of the nanotube.[42] MWCNTs can either be metallic or semiconducting depending on the axial chirality of the individual shells and depending on the intershell interaction. A detailed description of their conductance is rather complex, but the main contribution to charge conduction near the Fermi energy level is given by the outer tube. Mats of MWCNTs, such as those employed in the present experiment, consist of a mixture of metallic and semiconducting tubes. Macroscopically, these mats behave as mild *p*-type semiconductors since their conductance increases or decreases upon adsorption of electron-accepting or donating molecules, respectively.[35, 41] Furthermore, according to DFT calculations, the decoration with Au-NPs slightly perturbs the band structure of

MWCNTs causing a small shift of the Fermi level energy toward lower energies, which is equivalent to a *p*-doping of the tubes (i.e. there is a small electronic charge transfer from the tube to the Au-NP).[43] Finally, since the MWCNT mat consists of defective nanotubes,[44] its resistance is mostly influenced by the resistance of individual nanotubes and not by the inter-nanotube or the electrode-nanotube junctions.[45] Upon formation of the host-guest complex, BTEX⊂cavitand **4** (molecular recognition event), and by assuming the existence of a close proximity between the walls of the cavitand **4** and the surface of the MWCNT, we are prone to speculate that the overall resistance of the MWCNT mat will be influenced (transducer function).

5.2.3. Stability study of thioether-Au bond with temperature

In order to establish a temperature limit in the use of the sensor, a study based on TGA (thermogravimetric analysis) was performed. To perform this analysis, a minimum of material amount (cavitand anchored on gold nanoparticle) is needed. Since, the experimental way to fabricate sensors do not allow us to cumulate enough material, an alternative way is proposed to synthesize gold nanoparticles via wet chemistry. Indeed, gold nanoparticles can be synthesized via reduction of a gold salt in chloroform. Then they are functionalized by SAM with the cavitand via the same experimental process that was employed in the sensor fabrication. Finally, MWCNTs are added in

order to simulate the same hybrid material of the sensitive layer. More detail on the general synthesis can be found in Annex III.

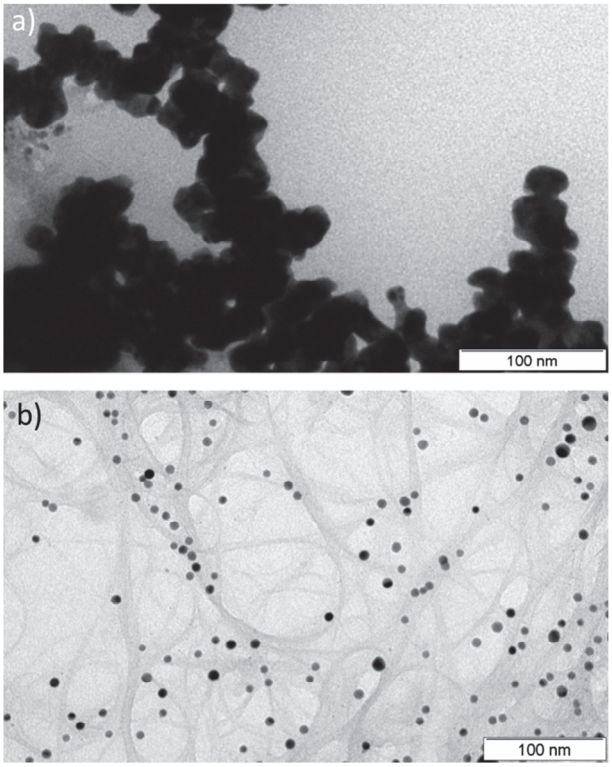

Figure 52. TEM picture of gold growing of a) without cavitand and b) with cavitand

The TEM pictures in **Figure 52** clearly indicate the role of the cavitand as stabilizer of the gold nanoparticles by stopping the growing. Then, all the material in suspension is dropped in TGA vial and dried under vacuum. This operation is repeated until reaching a mass near 2 mg. The vial is introduced in the TGA analyzer and kept 30 min at 60°C in order to evaporate humidity or/and residual solvent. Finally, the sample is warmed from 60°C to 500°C with a ramp of 1°C/min and an air flow of 50 mL/min as shown in

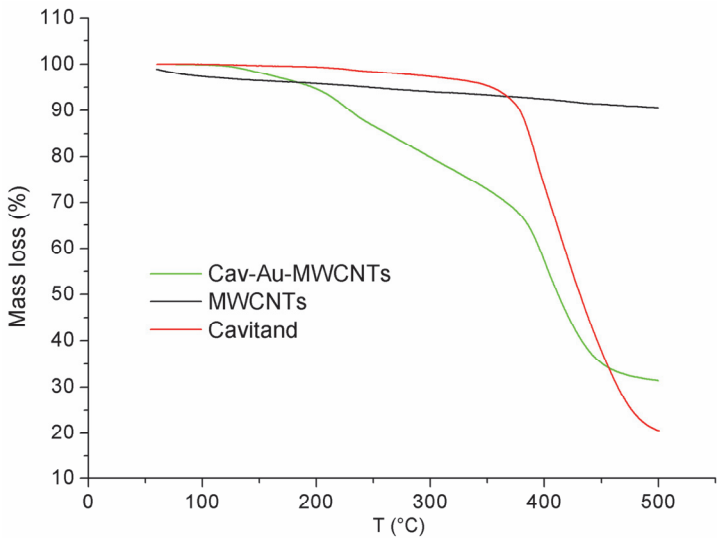

Figure 53. TGA analysis of the cavitand, MWCNTs and cav-Au-MWCNTs

TGA (Thermogravimetric) analysis in **Figure 53** revealed the thermal stability of the MWCNTs until 500°C with more of 95% of the initial mass. The cavitand is also thermally stable with a degradation reached at temperature of 380°C. Finally, for the cav-Au-MWCNTs, it is observed a loss of mass starting from 120°C in accordance with the literature with the break of the thioether-gold bond.

5.3. Gas sensing properties

5.3.1. High sensitivity to benzene

Four cav-Au-MWCNT sensors and two Au-MWCNT sensors were employed for the study of the gas sensing capabilities according the first experimental setup presented in Chapter II. Au-MWCNT sensors were fabricated employing the same conditions to those used

for cav-Au-MWCNT sensors, but the last step (i.e. the functionalization with cavitand **4** via SAM) was performed just with pure chloroform to induce the aggregation of the Au-NPs to the same level. Each measurement was repeated at least three times. The typical response and recovery cycles of a cav-Au-MWCNT sensor towards increasing concentrations of benzene in dry air are shown in **Figure 54a**. The signal to noise ratio for the sensor response was high. The response and recovery cycles were recorded while the sensor was operated at room temperature and the sensing process was demonstrated to be reversible. During the recovery phase, pure dry air was flown resulting in full baseline resistance recovery. The measurement period lasted for about six months in which not significant changes in the baseline resistance nor in sensitivity were observed. In short, the sensor response is reversible and not affected by low-term drift. The typical calibration curves for the cav-Au-MWCNT sensor exposed to benzene, toluene, *o*-xylene, ethanol and carbon monoxide are depicted in **Figure 54b**. This sensor showed significantly higher sensitivity to benzene than to the other tested pollutants. At 100 ppb level of benzene, the sensor is seven and thirty times more responsive than to toluene or *o*-xylene, respectively. Furthermore, the slope of the calibration curve (*i.e.* sensitivity) was calculated for the two lowest tested concentrations and was found to be much higher in the case of benzene (4.2×10^{-3} % ppb^{-1}) than for toluene (1.1×10^{-4} % ppb^{-1}) and o-xylene (3.3×10^{-5} % ppb^{-1}). Therefore, the sensor should be able to detect with high sensitivity traces of benzene in the presence of toluene and/or *o*-xylene. The responses to ethanol and carbon monoxide were significantly lower.

In summary, the sensor is partially selective toward benzene and a possible strategy for further enhancing selectivity (beyond the scope of this paper) would be to use an array of sensors with different sensitive layers together with a pattern recognition engine.[46, 47] Taken together, these results demonstrated an unprecedented high sensitivity of the cav-Au-MWCNT sensor for benzene. The different species whose sensing is reported in **Figure 54b** are electron donors. The overall resistance of the cav-Au-MWCNT mat increased when exposed to any of these species. Macroscopically, this implies that our hybrid nanomaterial retains the *p*-type semiconductor observed for bare or Au-MWCNT mats.

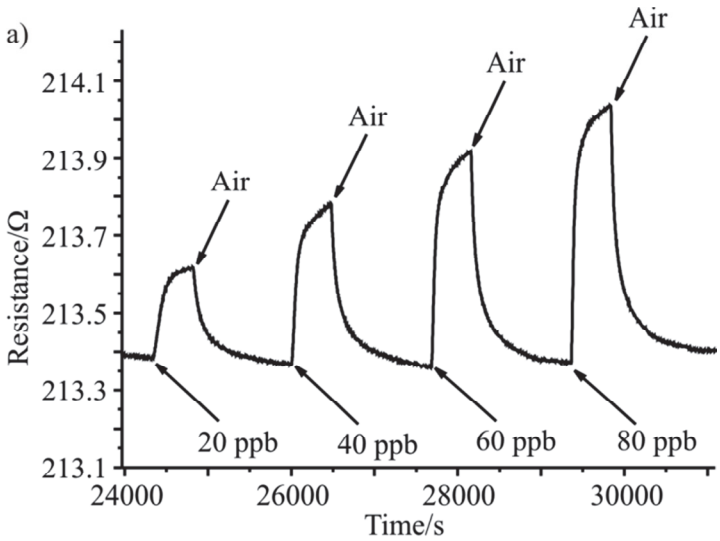

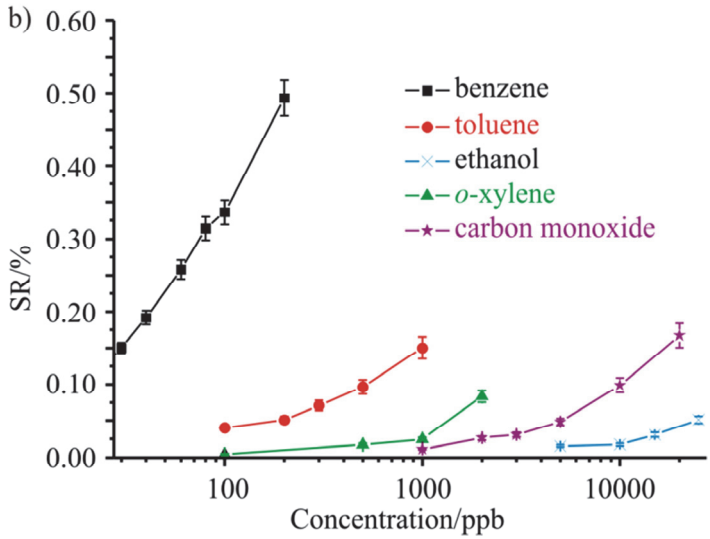

Figure 54. a) A typical cav-Au-MWCNT sensor resistance response in function of benzene concentration in air; b) The relative sensor response for different gas contaminants. In all experiments, we employed a gas flow of 200 mL min^{-1}.

As often encountered in gas sensors, sensitivity and dynamics of response can be further enhanced by increasing the gas flow rate (**Figure 55a**). When the flow is increased, layer gradient that defines a profile of laminar flow attenuated in the boundary layer at the sensor surface. This allowed a better diffusion of benzene towards the sensing layer, and results in an increase of the concentration of the inclusion complexes BTEX⊂cavitand **4** on the surface of MWCNTs mats and therefore a higher sensor response was observed.[48] Up to 2.5 ppb of benzene in air can easily be detected at 400 mL min^{-1} (**Figure 55b**). To the best of our knowledge, this is the first system that can detect such a low level of benzene in the gas phase by employing a CNT-based material.

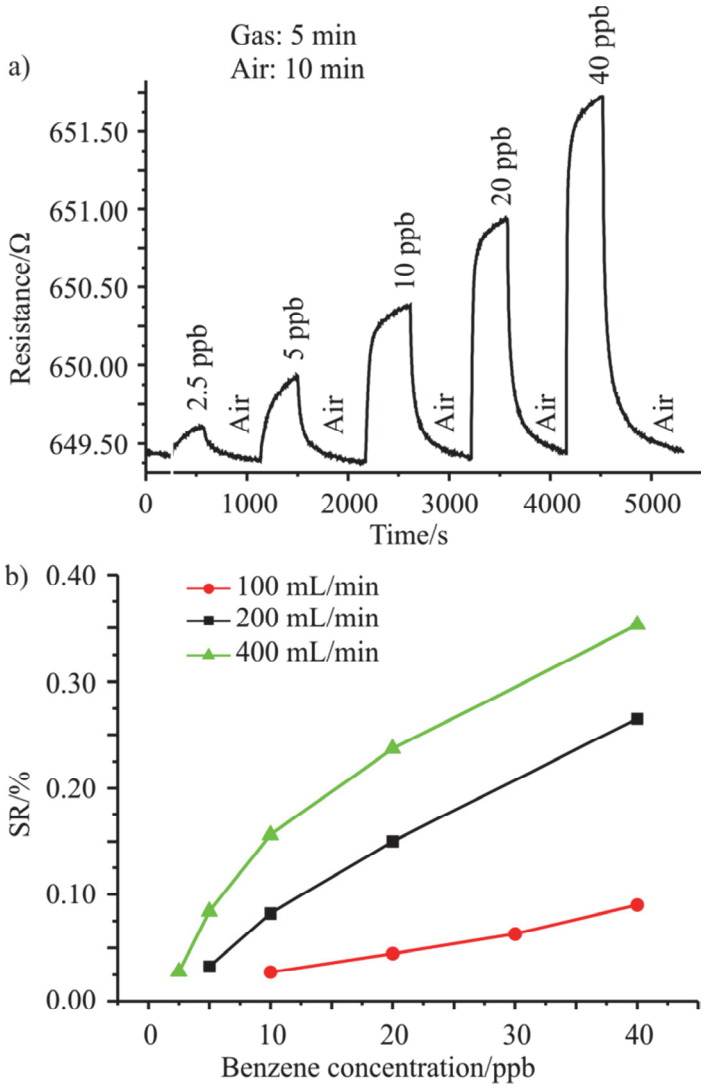

Figure 55. a) cav-Au-MWCNT sensor resistance response in function of benzene concentration in air at 400 mL min^{-1}, and b) the relative sensor response for benzene at different gas flows.

Even at very low benzene levels, the response of the sensor was highly reproducible (**Figure 56**). Thanks to the low levels of noise in the response signals, the theoretical LOD for the sensors was calculated to be 600 ppt, which corresponds to a sensor response

three times higher than the level of the noise.[49] The responses to benzene provided by the Au-MWCNT sensor were tested for comparison. The Au-MWCNT sensor was not responsive to benzene levels under 60 ppb in dry conditions. Even at this concentration (60 ppb), the response was low. This observation is in good agreement with theoretical findings that predict a very weak binding energy and the lack of charge transfer between the benzene molecule and the Au-MWCNTs system. These results supported the idea that cavitand **4**, in junction with Au-NPs and MWCNTs, were necessary for the high sensitivity measured for benzene.

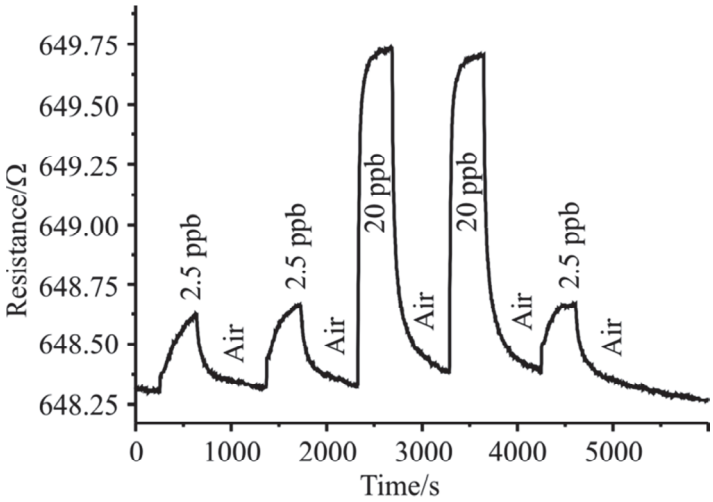

Figure 56. The cav-Au-MWCNT sensor resistance response in function of two benzene concentrations (2.5 and 20 ppb) exposed to sensor in a random order.

5.3.2. Gas sensing mechanism

In **Figure 57**, we portray a simplified scheme of the plausible mechanisms for benzene sensing and recovery. We propose that the

interior of cavitand **4**, anchored to the surface of cav-Au-MWCNT, is initially occupied by an air molecule (*e.g.* nitrogen). This status of the system is referred to as N_2⊂cav-Au-MWCNT. The inclusion of guest in the cavity of **4** is a dynamic process allowing a constant chemical exchange, between free and included air molecules. When the N_2⊂cav-Au-MWCNT system is exposed to air contaminated with benzene vapors, some of the cavitands bind a benzene molecule. Cavitand **4** shows higher affinity for benzene than nitrogen owing to the establishment of additional interactions (CH-***π*** and ***π*-*π***) between the benzene and the walls of the cavitand. In solution, the exchange process is referred to as "hostage-exchange mechanism" and occurs via significant conformation changes involving moving from the vase to the kite conformation of the cavitand, a process with an energy barrier of 11.6 kcal mol^{-1}.[50-52] The kite conformation of the N_2⊂cav-Au-MWCNT allows an easy access of a guest molecule (benzene) to the shallow cavity of the cavitand and substitution of the previously bound guest molecule (N_2).[51] Upon guest-exchange, the cavitand's walls fold back to vase conformation producing a new host-guest inclusion complex (referred to as benzene⊂cav-Au-MWCNT). In this way, two inclusion complexes are present on the surface of cav-Au-MWCNT, one with an included nitrogen molecule and the other with a benzene molecule (Figure 57, marked with *).

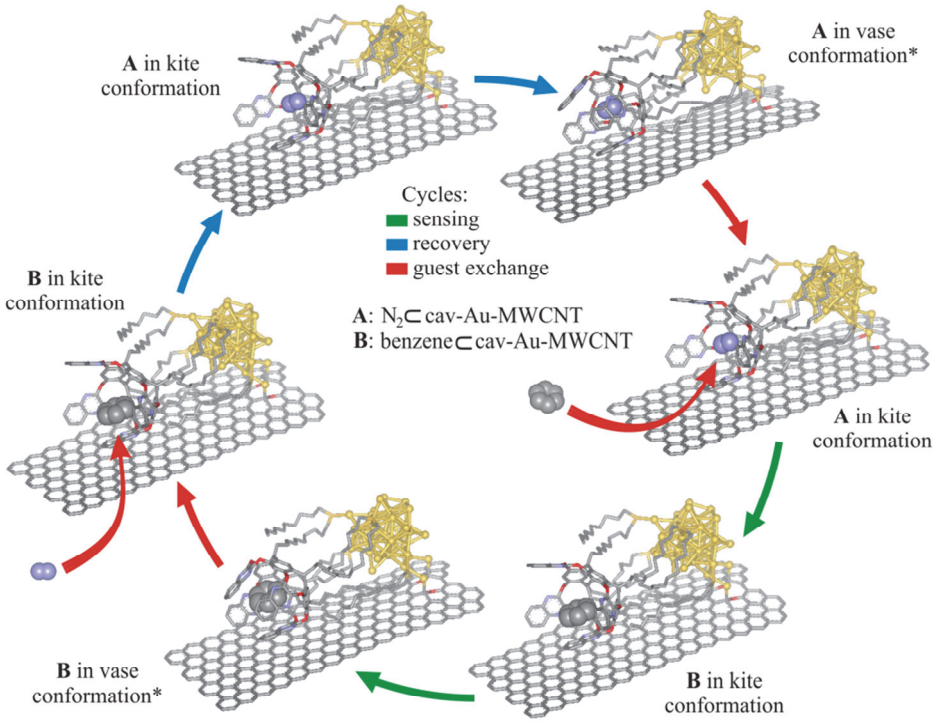

Figure 57. Proposed benzene sensing and recovery mechanism. Benzene and nitrogen molecules are shown as CPK models. Hydrogen atoms are omitted for clarity. Notes: * - crucial structures in the sensing process.

To explain the transduction mechanism we hypothesized two plausible types of communication between the cavitand and the MWCNT **(Figure 58.**). The first type of communication would involve gold mediation between the π-electron cloud(s) of the quinoxaline wall(s) from the cavitand and the **π**-electron clouds of MWCNT (referred to as **π**-Au-**π** communication). The second type of communication would exclude gold mediation and would occur between cavitand molecules located on the edge of Au-NPs whose quinoxaline wall(s) are in direct contact with the MWCNT surface allowing **π**-**π** stacking interaction (referred to as **π**-**π** communication). In both cases, the **π**-electron density of the quinoxaline walls of the

cavitand must be affected by the nature of the included guest molecule (benzene or air molecule). Upon inclusion of a benzene molecule, which also possesses delocalized **π**-electrons, additional **π**-**π** interactions can be established between benzene and the cavitand wall. As a consequence, the π-electron density of the cavitand walls is modified. This electron density changes are translated onto the **π**-electron clouds of the MWCNT through a charge-transfer/electron-transfer mechanisms. This results in hole depletion and decrease in the conductance of MWCNT, experimentally measured as an increase in sensor resistance. Conversely, the stream of pure air modifies the equilibria between benzene⊂cav-Au-MWCNT and N_2⊂cav-Au-MWCNT. The formation of the latter inclusion complex recovers the initial state of the sensor and therefore the baseline resistance of the sensor.

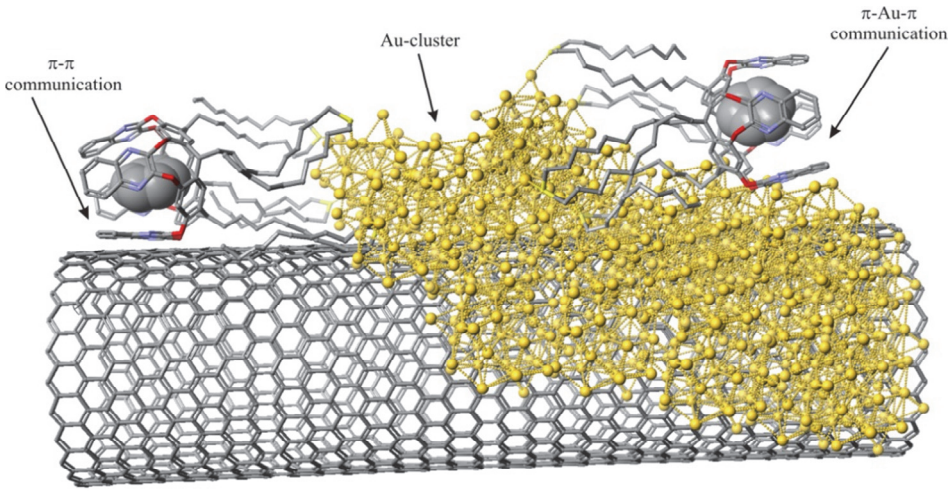

Figure 58. Representation of two proposed types of communication between the cavitand 4 and the Au-MWCNT. Benzene molecules are presented as CPK models. Hydrogen atoms are omitted for clarity.

The lower response displayed by the sensor (reduced increase of resistance) towards the more electron-rich toluene and *o*-xylene molecules, which based on the sensing mechanism proposed above, must imply a reduction of the electron-donating capabilities of their inclusion complexes with the cavitand **4**, is not clear to us. On the one hand, published binding experiments demonstrated that toluene and *o*-xylene, in fact, bind more strongly than benzene inside the cavitand **4**, both in the liquid and gas phase.[25, 39] On the other hand, the dipole moments of benzene, toluene and o-xylene are 0, 0.36 and 0.64 D, respectively. We speculate that the lack of dipole moment exhibited by benzene could be somehow responsible of the different electron donating properties assigned to its host-guest complex (benzene⊂cav-Au-MWCNT). Clearly, the verification of this hypothesis must await the results of further experimental and theoretical studies that are beyond the scope of the present work.

5.3.3. Humidity effect

The measurements of benzene were conducted under 10±1% to 60±2% of relative humidity (corresponding to 2,630 and 15,980, respectively at 1 atm and 22°C). Sensor responses are shown in **Figure 59.**

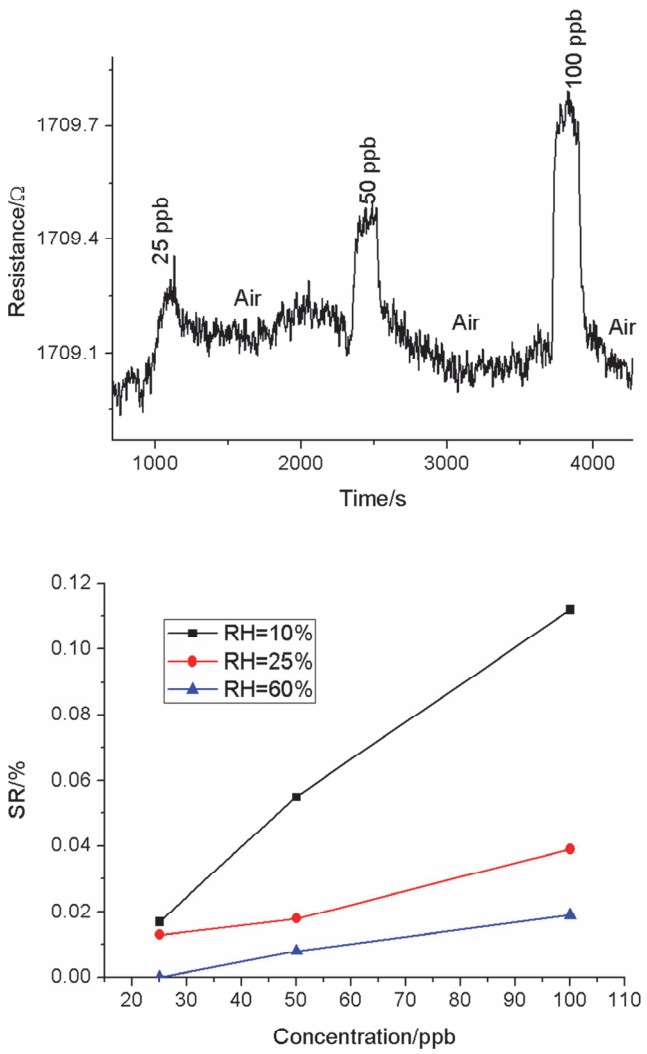

Figure 59. a) cav-Au-MWCNT sensor resistance response as a function of benzene concentration in air at 200 mL min^{-1} with a R.H. of 25% in the background, and b) relative sensor response for benzene concentrations at different R.Hs.

Ambient moisture plays an important role in the response of chemiresistors. [53] Therefore, a new set of measurements was performed in which trace concentrations of benzene, toluene or *o*-xylene in a flow of dry synthetic air were humidified to 10%, 25%

and 60% of relative humidity (R.H.) Taking into account that the pressure was 1 atm and the temperature 22 ºC, the relative humidity tested corresponds to levels that ranged between 2,630 and 15,980 ppm of water, *i.e.* 3 to 5 orders of magnitude higher than the concentrations of the aromatic VOCs present in the mixtures. The presence of moisture affected the sensitivity of the cavitand-Au-MWCNT sensor toward VOCs. According to our results, the sensitivity of the sensor toward benzene (i.e. slope of the calibration curve) is 4.20 % ppm^{-1} under dry conditions and changed to 1.41 % ppm^{-1} @ 10% R.H., 0.48 % ppm^{-1} @ 25% R.H and 0.45 % ppm^{-1} @ 60% R.H. Taken together, these results indicated that the presence of moisture affected significantly the limit of detection (LOD) of the sensor for benzene. While the benzene LOD remains below 20 ppb for R.H. up to 25%, it rises to about 50 ppb at 60% R.H. In case of toluene or *o*-xylene, the presence of moisture resulted in the cav-Au-MWCNT sensor not displaying any measurable response for both aromatic VOCs up to at concentrations of 5,000 ppb (i.e., the partial selectivity is not destroyed by the presence of humidity). Two possible strategies can be exploited to overcome the loss in benzene sensitivity caused by ambient moisture. The first option would involve dehumidification by employing inexpensive filters containing polymers such as polyacrylate, polypyrrole or sodium polyacrylate salts, which selectively absorb polar compounds (i.e. water) from the input gas flow leaving non-polar compounds such as benzene unaffected. This strategy has been implemented in solid-phase micro-extraction for quantitative gas or liquid chromatography analysis of environmental samples [54] or in hand-held photo-ionization gas.[55]

The second option would involve sensor redesign taking into consideration that the oxygen plasma treatment of MWCNTs used to generate defects at their surface for anchoring Au nanoparticles makes CNTs more hydrophilic. Even if the employed cavitand has a hydrophobic character, oxygenated defects present on the surface of carbon nanotubes can be responsible for sensor moisture cross-sensitivity. Alternative methods for achieving Au decoration of CNT sidewalls have been reported, which accounts on the hydrophobic nature of pristine, non-defective CNTs [56] what could be taken into advantage for reducing effect of ambient moisture to the sensor's response.[57]

5.3.4. Case of NO_2

Nitrogen dioxide gas, belongs to the so-called NO_x and is a toxic gas released from combustion facilities and automobiles.[58] Thus, it is present in atmosphere and its effect has to be studied on our sensors. The adsorption of NO_2 was reported to occur either over Au-NP or over oxygenated defects and exhibits strong response.[43, 59] The first-principle modelling of gas adsorption on Au-MWCNT revealed that NO_2, a polar molecule with partial positive charge localized on the nitrogen atom and partial negative charge divided among oxygen atoms, is attracted to Au-NPs by its nitrogen atom. The computed binding energies and bond lengths showed that NO_2 strongly interacts with Au-NPs and that the molecule accepted a significant amount of electronic charge from the Au-MWCNT system. This hypothesis is consistent with the well-known electron

accepting nature of this molecule.[43] Quantum electron transport calculations revealed that the adsorption of a single NO_2 molecule on the surface of the Au-NP resulted in a remarkable decrease of the Fermi energy level of the Au-MWCNT system.[43] This is consistent with the decrease in resistance that we observed for Au-MWCNT mats in the presence of NO_2.

The response of both cav-Au-MWCNT and Au-MWCNT sensors to different concentrations of NO_2 was also studied. The calibration curve of NO_2 detection for a cav-Au-MWCNT and Au-MWCNT sensors operated at room temperature. The simultaneous presence of benzene and nitrogen dioxide in the ambient would make difficult for a cav-Au-MWCNT sensor to correctly measure benzene concentration. This can be overcome by combining the responses of a cav-Au-MWCNT and a Au-MWCNT sensor array.

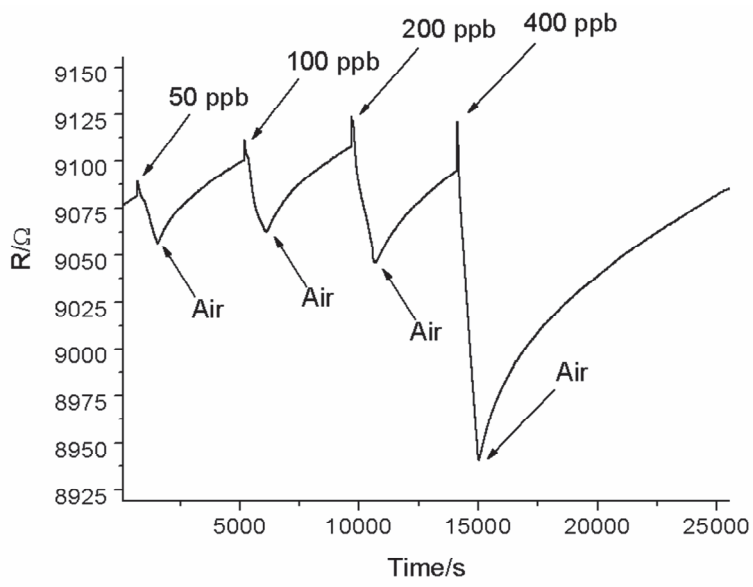

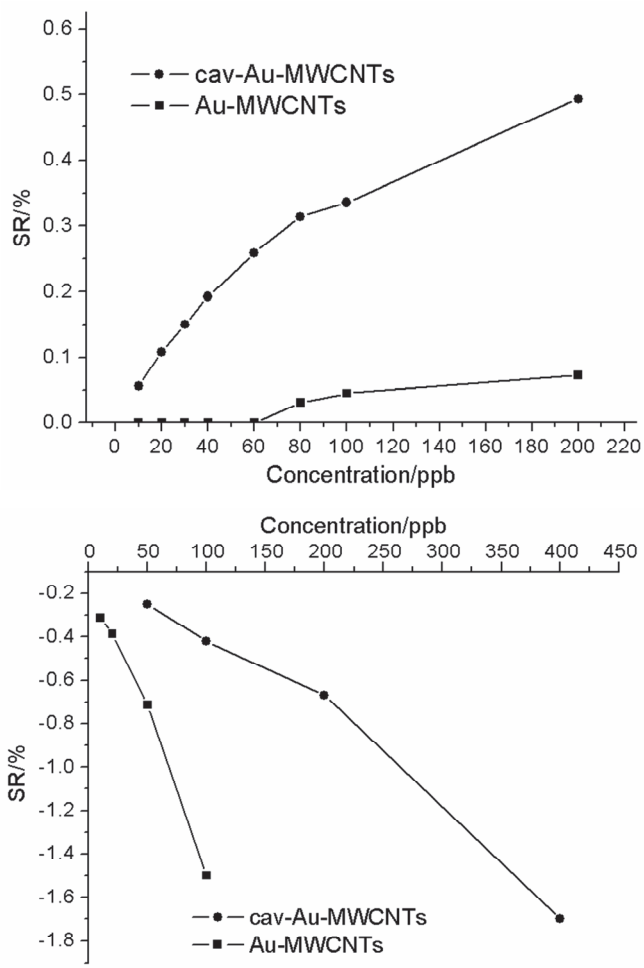

Figure 60. a) cav-Au-MWCNT sensor resistance response in function of NO_2 concentration in air; relative sensor response as a function of b) benzene vapor concentration and c) NO_2 gas concentration for cav-Au-MWCNTs and Au-MWCNTs sensors.

Au-MWCNTs show no response to benzene for concentrations below or equal to 60 ppb. For benzene concentrations up to 200 ppb, Au-MWCNTs show some response, but it remains more than ten times lower than that of cav-Au-MWCNTs. The response towards NO_2 displayed by cav-Au-MWCNT sensor is about two times lower than that exhibited by the Au-MWCNT sensor. However, NO_2 cross-

sensitivity of cavitand-functionalized sensors remains noticeable. The cav-Au-MWCNT may remain somewhat responsive to NO_2 because this molecule can be adsorbed directly onto Au-NPs. However, the important decrease in the response toward NO_2 observed for cav-Au-MWCNTs in comparison to that of Au-MWCNTs indicated that the presence of the cavitand significantly reduced the affinity of Au-NPs to adsorb NO_2 molecules. From a practical point of view, if the detection of benzene should be performed in an environment in which the presence of trace levels of nitrogen dioxide are likely, a detector comprised of two sensors, namely one cav-Au-MWCNT sensor and one Au-MWCNT sensor could be used for benzene level correction.

5.4. Conclusion

In conclusion, a simple technique for functionalizing the multiwall carbon nanotubes, in view of designing a gas sensor with a superior performance, has been introduced. A quinoxaline-walled thioether-legged cavitand **4** is attached onto oxygen plasma treated Au-NP decorated MWCNTs. The technique is suitable for the mass production of described hybrid sensing nanomaterial at low production costs, allowing cost-effective commercialization. The cavitand-functionalized MWCNT sensor shows unprecedented high sensitivity toward low levels of benzene in dry air at trace levels. The detection of 2.5 ppb is demonstrated experimentally and a theoretical LOD of 600 ppt was calculated. Furthermore, sensor response towards toluene and *o*-xylene is significantly lower, clearly showing

the strong response for benzene, what is the first example of such selective carbon nanotube based material. This was possible thanks to the molecular recognition introduced by quinoxaline-bridged cavitand **4**. The sensor shows significant cross-sensitivity to NO_2, but this can be compensated by combining a cav-Au-MWCNT sensor with an Au-MWCNT sensor, since the latter is more sensitive to NO_2 and while insensitive to benzene levels below 60 ppb. The cav-Au-MWCNT sensor response toward aromatic VOCs diminishes as the relative humidity in the gas flow increases. It remains responsive to benzene traces in presence of humidity but it becomes insensitive to toluene or *o*-xylene in the same range of concentrations. Possibilities to avoid the effect of moisture could be the dehumidification of the gas flow by employing a inexpensive filter, or keep the hydrophobic character of MWCNTs by using an alternative route to the oxygen plasma treatment used to anchor gold nanoparticles. Finally, it is worth mentioning that both the detection and the recovery of the baseline are performed at room temperature, which implies that these sensors can operate at very low power consumption. This makes the sensor suitable for being integrated in hand-held portable analysers, wearable detectors and semi-passive radio frequency identification tags with sensing capabilities or in the nodes of wireless sensor networks with a wide range of potential applications in environmental monitoring, workplace safety or medical devices, among others. These results have been published in [60].

References

[1] D. J. Cram, S. Karbach, H. E. Kim, C. B. Knobler, E. F. Maverick, J. L. Ericson*, et al.*, "Host-guest complexation. 46. Cavitands as open molecular vessels form solvates," *Journal of the American Chemical Society,* vol. 110, pp. 2229-2237, 1988/03/01 1988.

[2] M. Vincenti, E. Dalcanale, P. Soncini, and G. Guglielmetti, "Host-guest complexation in the gas phase by desorption chemical ionization mass spectrometry," *Journal of the American Chemical Society,* vol. 112, pp. 445-447, 1990.

[3] M. Vincenti and E. Dalcanale, "Host–guest complexation in the gas phase. Investigation of the mechanism of interaction between cavitands and neutral guest molecules," *J. Chem. Soc., Perkin Trans. 2,* pp. 1069-1076, 1995.

[4] E. U. Thoden van Velzen, J. F. Engbersen, and D. N. Reinhoudt, "Self-assembled monolayers of receptor adsorbates on gold: preparation and characterization," *Journal of the American Chemical Society,* vol. 116, pp. 3597-3598, 1994.

[5] E. U. Thoden van Velzen, J. F. Engbersen, P. J. de Lange, J. W. Mahy, and D. N. Reinhoudt, "Self-assembled monolayers of resorcin [4] arene tetrasulfides on gold," *Journal of the American Chemical Society,* vol. 117, pp. 6853-6862, 1995.

[6] E. U. Thoden van Velzen, J. F. Engbersen, and D. N. Reinhoudt, "Synthesis of self-assembling resorcin [4] arene tetrasulfide adsorbates," *Synthesis,* vol. 1995, pp. 989-997, 1995.

[7] F. Dickert and R. Sikorski, "Supramolecular strategies in chemical sensing," *Materials Science and Engineering: C,* vol. 10, pp. 39-46, 1999.

[8] Y. Yamakoshi, R. R. Schlittler, J. K. Gimzewski, and F. Diederich, "Synthesis of molecular-gripper-type dynamic receptors and STM-imaging of self-assembled monolayers on gold," *Journal of Materials Chemistry,* vol. 11, pp. 2895-2897, 2001.

[9] V. A. Azov, P. J. Skinner, Y. Yamakoshi, P. Seiler, V. Gramlich, and F. Diederich, "Functionalized and Partially or

Differentially Bridged Resorcin [4] arene Cavitands: Synthesis and Solid-State Structures," *Helvetica chimica acta,* vol. 86, pp. 3648-3670, 2003.

[10] E. B. Feresenbet, M. Busi, F. Ugozzoli, E. Dalcanale, and D. K. Shenoy, "Influence of Cavity Depth on the Responses of SPR Sensors Coated with Self-Assembled Monolayers of Cavitands," *Sensor Letters,* vol. 2, pp. 186-193, 2004.

[11] R. Capan, Z. Özbek, H. Göktaş, S. Şen, F. Ince, M. Özel*, et al.*, "Characterization of Langmuir–Blodgett films of a calix [8] arene and sensing properties towards volatile organic vapors," *Sensors and Actuators B: Chemical,* vol. 148, pp. 358-365, 2010.

[12] M. Erdoğan, R. Capan, and F. Davis, "Swelling behaviour of calixarene film exposed to various organic vapours by surface plasmon resonance technique," *Sensors and Actuators B: Chemical,* vol. 145, pp. 66-70, 2010.

[13] Y. Liu, T. Taira, M. C. Young, D. Ajami, J. Rebek Jr, Q. Cheng*, et al.*, "Protein Recognition by a Self-Assembled Deep Cavitand Monolayer on a Gold Substrate," *Langmuir,* vol. 28, pp. 1391-1398, 2011.

[14] A. Hassan, A. Ray, A. Nabok, and F. Davis, "Spun films of novel calix [4] resorcinarene derivatives for benzene vapour sensing," *Sensors and Actuators B: Chemical,* vol. 77, pp. 638-641, 2001.

[15] E. B. Feresenbet, E. Dalcanale, C. Dulcey, and D. K. Shenoy, "Optical sensing of the selective interaction of aromatic vapors with cavitands," *Sensors and Actuators B: Chemical,* vol. 97, pp. 211-220, 2004.

[16] O. B. Berryman, A. C. Sather, and J. Rebek Jr, "A Deep Cavitand with a Fluorescent Wall Functions as an Ion Sensor," *Organic letters,* vol. 13, pp. 5232-5235, 2011.

[17] T. Weiss, K. Schierbaum, U. T. van Velzen, D. Reinhoudt, and W. Göpel, "Self-assembled monolayers of supramolecular compounds for chemical sensors," *Sensors and Actuators B: Chemical,* vol. 26, pp. 203-207, 1995.

[18] J. Hartmann, J. Auge, R. Lucklum, S. Rösler, P. Hauptmann, B. Adler*, et al.*, "Supramolecular interactions on mass sensitive sensors in gas phases and liquids," *Sensors and Actuators B: Chemical,* vol. 34, pp. 305-311, 1996.

[19] J. Hartmann, P. Hauptmann, S. Levi, and E. Dalcanale, "Chemical sensing with cavitands: influence of cavity shape and dimensions on the detection of solvent vapors," *Sensors and Actuators B: Chemical,* vol. 35, pp. 154-157, 1996.

[20] R. Paolesse, C. Di Natale, S. Nardis, A. Macagnano, A. D'Amico, R. Pinalli*, et al.*, "Investigation of the Origin of Selectivity in Cavitand-Based Supramolecular Sensors," *Chemistry-A European Journal,* vol. 9, pp. 5388-5395, 2003.

[21] O. Mermer, S. Okur, F. Siimer, C. Ozbek, S. Sayin, and M. Yilmaz, "Gas Sensing Properties of Carbon Nanotubes Modified with Calixarene Molecules Measured by QCM Techniques," *Acta Physica Polonica-Series A General Physics,* vol. 121, p. 240, 2012.

[22] M. Ferrari, V. Ferrari, D. Marioli, A. Taroni, M. Suman, and E. Dalcanale, "Cavitand-coated PZT resonant piezo-layer sensors: properties, structure, and comparison with QCM sensors at different temperatures under exposure to organic vapors," *Sensors and Actuators B: Chemical,* vol. 103, pp. 240-246, 2004.

[23] F. Bianchi, A. Bedini, N. Riboni, R. Pinalli, A. Gregori, L. M. Sidisky*, et al.*, "Cavitand-based solid-phase microextraction coatings for the selective detection of nitroaromatic explosives in air and soil," *Analytical chemistry,* 2014.

[24] R. Pinalli, T. Barboza, F. Bianchi, C. Massera, F. Ugozzoli, and E. Dalcanale, "Detection of amphetamine precursors with quinoxaline-bridged cavitands," *Supramolecular Chemistry,* vol. 25, pp. 682-687, 2013.

[25] F. Bianchi, R. Pinalli, F. Ugozzoli, S. Spera, M. Careri, and E. Dalcanale, "Cavitands as superior sorbents for benzene detection at trace level," *New Journal of Chemistry,* vol. 27, pp. 502-509, 2003.

[26] S. Zampolli, I. Elmi, F. Mancarella, P. Betti, E. Dalcanale, G. Cardinali*, et al.*, "Real-time monitoring of sub-ppb concentrations of aromatic volatiles with a MEMS-enabled miniaturized gas-chromatograph," *Sensors and Actuators B: Chemical,* vol. 141, pp. 322-328, 2009.

[27] S. Zampolli, P. Betti, I. Elmi, and E. Dalcanale, "A supramolecular approach to sub-ppb aromatic VOC detection in air," *Chemical Communications,* pp. 2790-2792, 2007.

[28] F. Bianchi, M. Mattarozzi, P. Betti, F. Bisceglie, M. Careri, A. Mangia*, et al.*, "Innovative Cavitand-Based Sol−Gel Coatings for the Environmental Monitoring of Benzene and Chlorobenzenes via Solid-Phase Microextraction," *Analytical Chemistry,* vol. 80, pp. 6423-6430, 2008/08/01 2008.

[29] M. Dionisio, J. M. Schnorr, V. K. Michaelis, R. G. Griffin, T. M. Swager, and E. Dalcanale, "Cavitand-functionalized SWCNTs for N-methylammonium detection," *Journal of the American Chemical Society,* vol. 134, pp. 6540-6543, 2012.

[30] F. Wang and T. M. Swager, "Diverse chemiresistors based upon covalently modified multiwalled carbon nanotubes," *Journal of the American Chemical Society,* vol. 133, pp. 11181-11193, 2011.

[31] L. Kong, J. Wang, F. Meng, X. Chen, Z. Jin, M. Li*, et al.*, "Novel hybridized SWCNT–PCD: synthesis and host–guest inclusion for electrical sensing recognition of persistent organic pollutants," *Journal of Materials Chemistry,* vol. 21, pp. 11109-11115, 2011.

[32] J. M. Schnorr, D. van der Zwaag, J. J. Walish, Y. Weizmann, and T. M. Swager, "Sensory Arrays of Covalently Functionalized Single-Walled Carbon Nanotubes for Explosive Detection," *Advanced Functional Materials,* vol. 23, pp. 5285-5291, 2013.

[33] E. Llobet, "Gas sensors using carbon nanomaterials: A review," *Sensors and Actuators B: Chemical,* vol. 179, pp. 32-45, 2013.

[34] P. Clément, I. Hafaiedh, E. Parra, A. Thamri, J. Guillot, A. Abdelghani*, et al.*, "Iron oxide and oxygen plasma functionalized multi-walled carbon nanotubes for the discrimination of volatile organic compounds," *Carbon,* vol. 78, pp. 510-520, 2014.

[35] R. Leghrib, A. Felten, F. Demoisson, F. Reniers, J.-J. Pireaux, and E. Llobet, "Room-temperature, selective detection of benzene at trace levels using plasma-treated metal-decorated multiwalled carbon nanotubes," *Carbon,* vol. 48, pp. 3477-3484, 2010.

[36] R. Leghrib and E. Llobet, "Quantitative trace analysis of benzene using an array of plasma-treated metal-decorated carbon nanotubes and fuzzy adaptive resonant theory

techniques," *Analytica chimica acta,* vol. 708, pp. 19-27, 2011.

[37] Y. Zilberman, U. Tisch, G. Shuster, W. Pisula, X. Feng, K. Müllen*, et al.*, "Carbon Nanotube/Hexa-peri-hexabenzocoronene Bilayers for Discrimination Between Nonpolar Volatile Organic Compounds of Cancer and Humid Atmospheres," *Advanced Materials,* vol. 22, pp. 4317-4320, 2010.

[38] D. J. Cram, M. E. Tanner, and C. B. Knobler, "Host-guest complexation. 58. Guest release and capture by hemicarcerands introduces the phenomenon of constrictive binding," *Journal of the American Chemical Society,* vol. 113, pp. 7717-7727, 1991/09/01 1991.

[39] P. Soncini, S. Bonsignore, E. Dalcanale, and F. Ugozzoli, "Cavitands as versatile molecular receptors," *The Journal of Organic Chemistry,* vol. 57, pp. 4608-4612, 1992/08/01 1992.

[40] Y. Zhang, N. W. Franklin, R. J. Chen, and H. Dai, "Metal coating on suspended carbon nanotubes and its implication to metal–tube interaction," *Chemical Physics Letters,* vol. 331, pp. 35-41, 2000.

[41] J.-C. Charlier, L. Arnaud, I. Avilov, M. Delgado, F. Demoisson, E. Espinosa*, et al.*, "Carbon nanotubes randomly decorated with gold clusters: from nano2hybrid atomic structures to gas sensing prototypes," *Nanotechnology,* vol. 20, p. 375501, 2009.

[42] T. Prasomsri, D. Shi, and D. E. Resasco, "Anchoring Pd nanoclusters onto pristine and functionalized single-wall carbon nanotubes: A combined DFT and experimental study," *Chemical Physics Letters,* vol. 497, pp. 103-107, 9/10/ 2010.

[43] Z. Zanolli, R. Leghrib, A. Felten, J.-J. Pireaux, E. Llobet, and J.-C. Charlier, "Gas Sensing with Au-Decorated Carbon Nanotubes," *ACS Nano,* vol. 5, pp. 4592-4599, 2011/06/28 2011.

[44] J.-C. Charlier, "Defects in carbon nanotubes," *Accounts of chemical research,* vol. 35, pp. 1063-1069, 2002.

[45] A. Salehi-Khojin, F. Khalili-Araghi, M. A. Kuroda, K. Y. Lin, J.-P. Leburton, and R. I. Masel, "On the sensing mechanism in carbon nanotube chemiresistors," *ACS nano,* vol. 5, pp. 153-158, 2010.

[46] B. Wang, J. C. Cancilla, J. S. Torrecilla, and H. Haick, "Artificial sensing intelligence with silicon nanowires for ultraselective detection in the gas phase," *Nano letters,* vol. 14, pp. 933-938, 2014.

[47] G. Konvalina and H. Haick, "Sensors for breath testing: from nanomaterials to comprehensive disease detection," *Accounts of chemical research,* vol. 47, pp. 66-76, 2013.

[48] S. Kline, W. Reynolds, F. Schraub, and P. Runstadler, "The structure of turbulent boundary layers," *Journal of Fluid Mechanics,* vol. 30, pp. 741-773, 1967.

[49] D. MacDougall and W. B. Crummett, "Guidelines for data acquisition and data quality evaluation in environmental chemistry," *Analytical Chemistry,* vol. 52, pp. 2242-2249, 1980.

[50] D. M. Rudkevich, G. Hilmersson, and J. Rebek, "Self-folding cavitands," *Journal of the American Chemical Society,* vol. 120, pp. 12216-12225, 1998.

[51] D. M. Rudkevich, G. Hilmersson, and J. Rebek, "Intramolecular hydrogen bonding controls the exchange rates of guests in a cavitand," *Journal of the American Chemical Society,* vol. 119, pp. 9911-9912, 1997.

[52] P. J. Skinner, A. G. Cheetham, A. Beeby, V. Gramlich, and F. Diederich, "Conformational Switching of Resorcin [4] arene Cavitands by Protonation, Preliminary Communication," *Helvetica Chimica Acta,* vol. 84, pp. 2146-2153, 2001.

[53] K. Balasubramanian and K. Kern, "25th Anniversary Article: Label-Free Electrical Biodetection Using Carbon Nanostructures," *Advanced Materials,* vol. 26, pp. 1154-1175, 2014.

[54] J. Pawliszyn, *Handbook of Solid State Microextraction* vol. 8. London, UK: Elsevier, 2012.

[55] (April the 30th). *Humidity filtering tubes for PID detectors*. Available: http://www.rae.nl/files/pdf/FeedsEnclosure-Humidity_Tube_II_LR_051507.pdf

[56] T. Sainsbury, T. Ikuno, D. Okawa, D. Pacile, J. M. Frechet, and A. Zettl, "Self-assembly of gold nanoparticles at the surface of amine-and thiol-functionalized boron nitride nanotubes," *The Journal of Physical Chemistry C,* vol. 111, pp. 12992-12999, 2007.

[57] X. Guo, "Single-Molecule Electrical Biosensors Based on Single-Walled Carbon Nanotubes," *Advanced Materials,* vol. 25, pp. 3397-3408, 2013.

[58] A. D. Rushi, K. P. Datta, P. S. Ghosh, A. Mulchandani, and M. D. Shirsat, "Selective Discrimination among Benzene, Toluene, and Xylene: Probing Metalloporphyrin-Functionalized Single-Walled Carbon Nanotube-Based Field Effect Transistors," *The Journal of Physical Chemistry C,* vol. 118, pp. 24034-24041, 2014/10/16 2014.

[59] J. Li, Y. Lu, Q. Ye, M. Cinke, J. Han, and M. Meyyappan, "Carbon Nanotube Sensors for Gas and Organic Vapor Detection," *Nano Letters,* vol. 3, pp. 929-933, 2003/07/01 2003.

[60] P. Clément, S. Korom, C. Struzzi, E. J. Parra, C. Bittencourt, P. Ballester*, et al.*, "Deep Cavitand Self-Assembled on Au NPs-MWCNT as Highly Sensitive Benzene Sensing Interface," *Advanced Functional Materials,* vol. 25, pp. 4011-4020, 2015.

General conclusion

In this thesis two types of gas sensors using CNT nanomaterials have been studied (i.e. resistive and resonant). First of all, the design and the fabrication of a new test chamber were envisaged, which allowed us to study the performance of the different fabricated sensors in the best conditions. The screen printing technique allowed a fast and low cost fabrication of the transducer devices, while air-brushing was the method employed for coating these transducers with the gas-sensitive CNT films.

Oxygen plasma treated CNTs were first used as a reference sensitive layer and tested towards different toxic contaminants such as benzene, CO, NO_2, ethanol, methanol and acetone. Their performances were compared in terms of sensitivity, reproducibility, and response and recovery time. The O-MWCNTs resistive based sensors with interdigitated electrodes on alumina substrates showed repeatable and reversible responses. A significant faster kinetic response together with the difficulty for fully recovering the baseline resistance at room temperature experienced with methanol, ethanol and acetone seems to suggest that, for these vapors, the main mechanism of interaction with carbon nanotubes is chemisorption. Conversely, slower response kinetics and fully recovery of the baseline suggest that benzene and toluene are physisorbed onto carbon nanotubes.

The implementation of a double transduction on piezoelectric cantilever based sensors (i.e. monitoring both frequency shift and

resistance of the absorption layer) presents a real advantage compared to the simple transduction. Furthermore, it was shown that the changes in electrode geometry needed for implementing this double transduction in the new devices did not alter their piezoelectric properties for gas sensing application. The interest of the double transduction is shown first for the detection of CO. Resistance changes of O-MWCNTs films do not allow CO detection below 40 ppm, whereas the signal of the resonance frequency shift is already significant at 5 ppm. Additionally, thanks to the sign of the shifts experienced by the resistance of O-MWCNTs films it is possible to discriminate an oxidizing from a reducing contaminant. Nevertheless, gas detection remains seriously affected by changes in the humidity background that completely alters measurements due to the high mass effect.

Finally, the best improvement in terms of sensitivity and selectivity is shown with the functionalization of MWCNTs by gold nanoparticles and quinoxaline-walled thioether-legged cavitands. The simple technique used to functionalize them is suitable for the mass production of the described hybrid sensing nanomaterial at low production costs, allowing cost-effective commercialization. The cavitand-functionalized MWCNT sensors show unprecedented high sensitivity toward low levels of benzene in dry air at trace levels. The detection of 2.5 ppb is demonstrated experimentally and a theoretical LOD of 600 ppt was calculated. Furthermore, sensor response towards toluene and *o*-xylene is significantly lower, clearly showing the strong response for benzene, what is the first example of such inherent selectivity in a carbon nanotube based material. The

nanomaterial remains responsive to benzene traces in the presence of humidity but it becomes insensitive to toluene or *o*-xylene in the same range of concentrations.

Perspective: To avoid humidity effect of the cavitand-functionalized MWCNT sensor, it is possible to devise an alternative route to the oxygen plasma treatment used to anchor gold nanoparticles. Also, by varying the type of macromolecule grafted to carbon nanotube sidewalls, it should be possible to design other nanomaterials able to specifically interact to different target species keeping the molecular recognition strategy.

Annex I

Body of the sensors chamber:

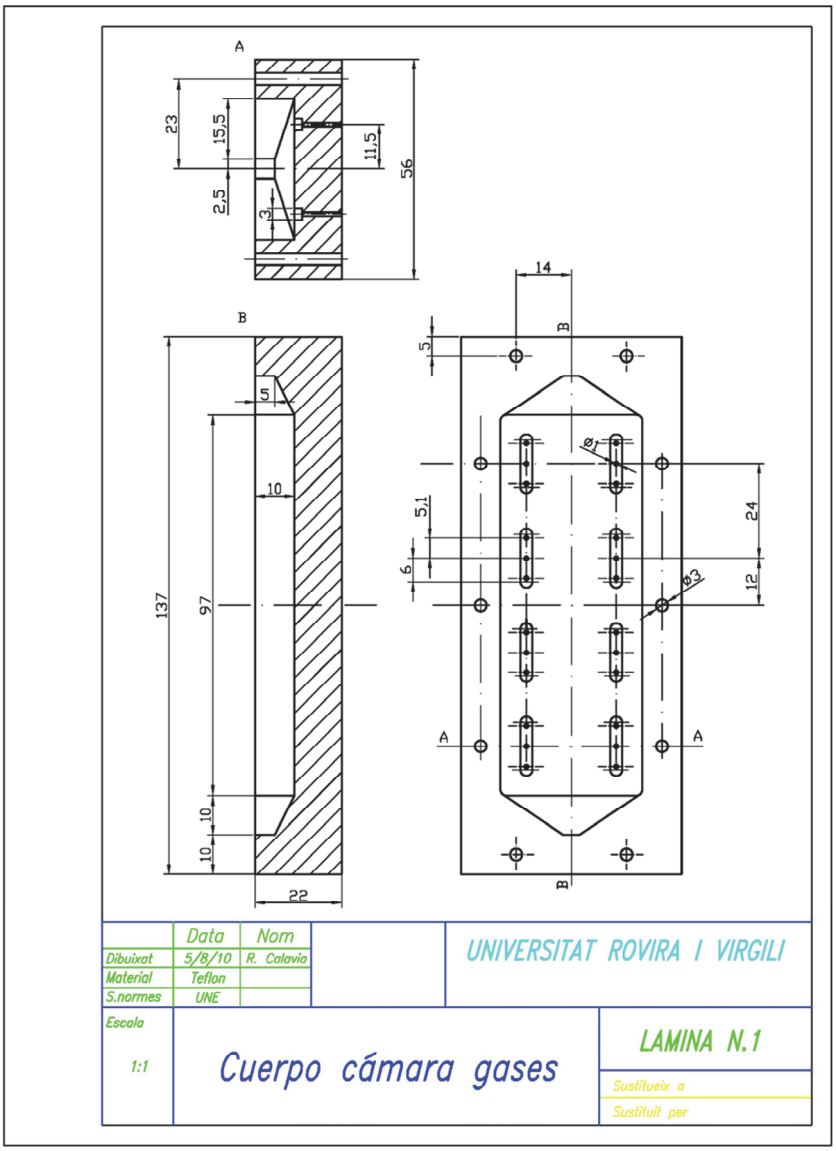

Sensors chamber cover:

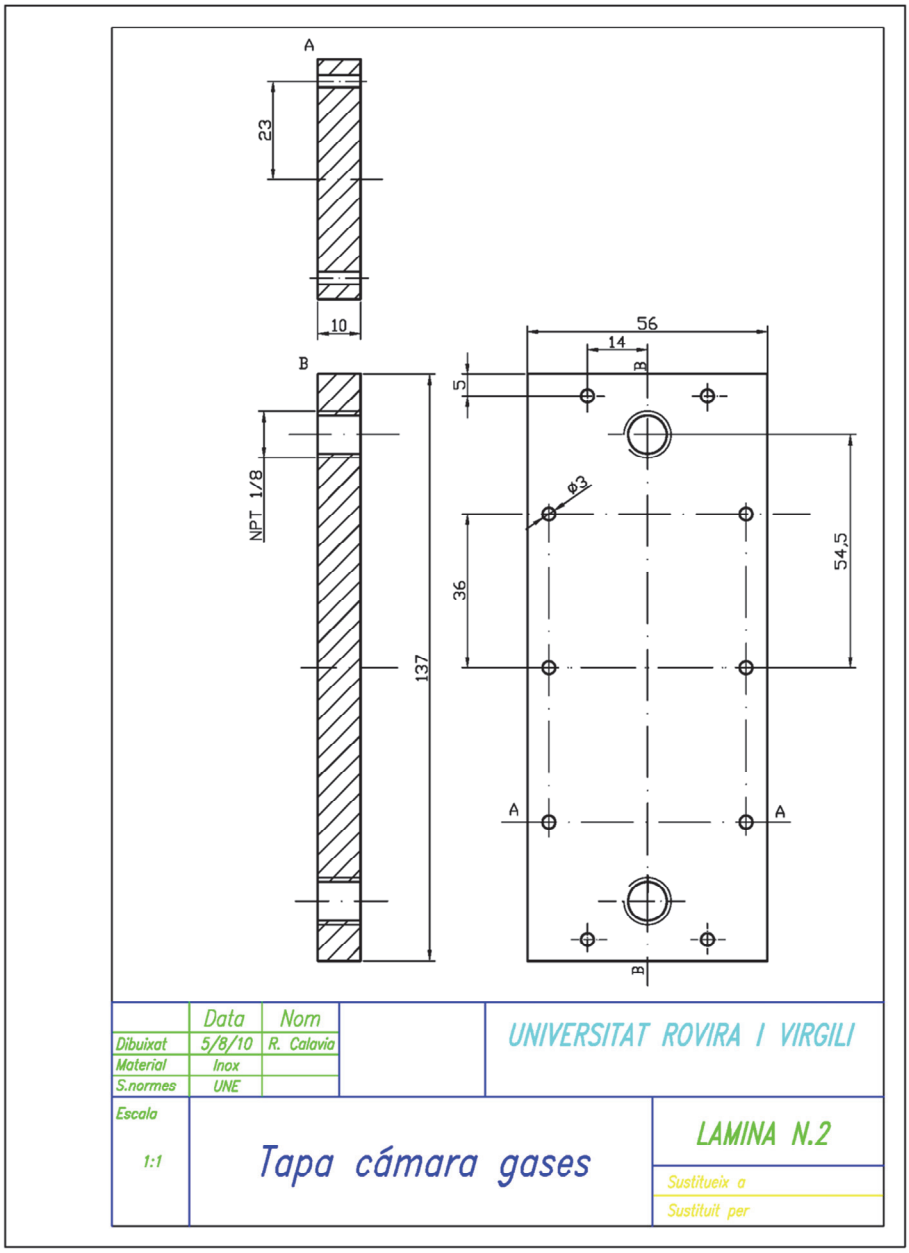

Annex II

Cavitand synthesis.

All reagents and solvents were obtained from commercial suppliers and used without further purification unless otherwise stated. 1H NMR spectra were recorded on a Bruker Avance 400 or a Bruker Avance 500 spectrometer. All deuterated solvents (Sigma-Aldrich) were used without any further purification. Chemical shifts are given in ppm and peaks were referenced relative to the solvent residual peak (δacetone = 2.04 ppm, δCDCl3 = 7.24 ppm). All NMR J values are given in Hz and are uncorrected.

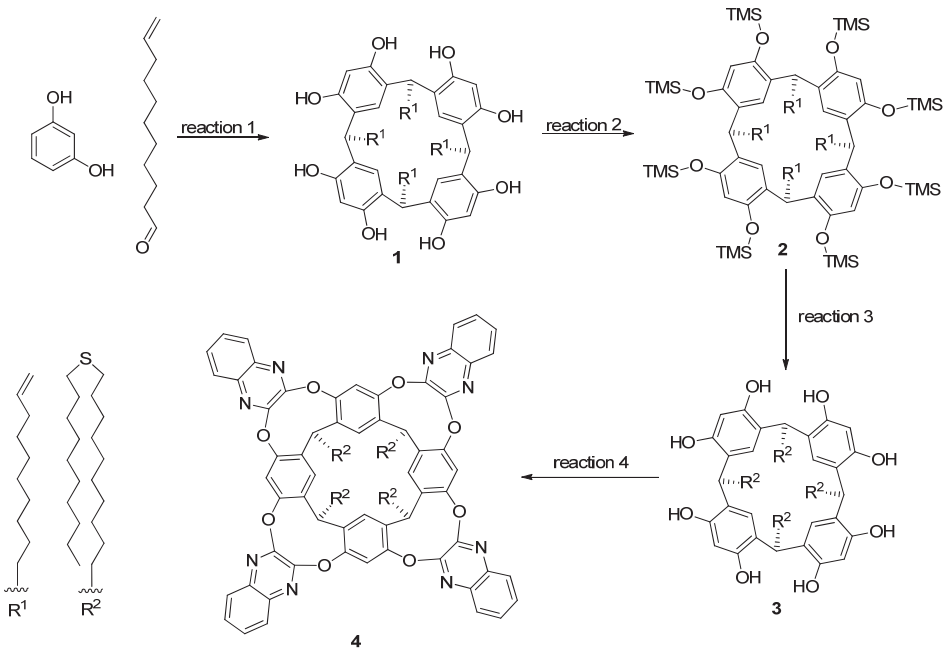

Figure II-1. Outcome of the four consecutive reactions employed to synthesize the deep-cavitand used to functionalize the Au-MWCNTs.

Cavitand 1: In 25 mL two-necked round bottomed flask resorcinol (2.000 g, 17.80 mmol) was dissolved in absolute ethanol (15 ml) followed by addition of hydrochloric acid (37%, 6 mL, 72.50 mmol). Then, to vigorously stirred reaction mixture undec-10-enal (4 mL, 18.97 mmol) was added drop-wise, and reaction mixture stirred at 60 °C for 24 h. Obtained hot red oil was poured slowly into vigorously stirred water, precipitate was collected by filtration, washed with hot water till pH 7 and absence of characteristic aldehyde scent. Pale yellow solid of the cavitand 1 was dried in vacuum for 24 h (3.842 g, 3.69 mmol, 83%). 1H NMR (500 MHz, acetone-d6): δ = 8.46 (s, 8H), 7.53 (s, 4H), 6.23 (s, 4H), 5.81 (ddt, *J* = 17.0, 10.2, 6.7 Hz, 4H), 4.98 (ddt, *J* = 17.1, 2.3, 1.6 Hz, 4H), 4.90 (ddt, *J* = 10.2, 2.3, 1.2 Hz, 4H), 4.30 (t, *J* = 7.9 Hz, 4H), 2.28 (q, *J* = 7.8 Hz, 8H), 1.43 - 1.26 (m, 56H) ppm. MS (ESI, +): calcd for C68H96O8 + Na+ 1063.7003; found 1063.6991.

Cavitand 2: Dried cavitand 1 (1.500 g, 1.44 mmol) was dissolved in anhydrous THF (15 mL) and cooled down to -25 °C. To this solution were added chlorotrimethylsilane (1.65 mL, 13.00 mmol) and triethylamine (3.00 mL, 21.52 mmol). Solution was left to warm up to room temperature and stirred overnight. Solvent was evacuated, residue suspended in hexanes and solid by product separated. Hexane was evacuated and product purified by flash chromatography over silica eluting product with a 8:2 mixture of methylene chloride and hexanes to afford a product as a pale yellow, low melting point solid (1.976 g, 1.22 mmol, 85%). 1H NMR (400 MHz, chloroform-d): δ = 7.11 (s, 2H), 6.23 (s, 2H), 6.13 (s, 2H), 5.95 (s, 2H), 5.77 (ddt, *J* = 16.9, 10.2, 6.7 Hz, 4H), 4.95 (dq, *J* = 17.1, 1.6 Hz, 4H), 4.89 (ddt, J = 10.2, 2.2, 1.1 Hz, 4H), 4.37

- 4.31 (m, 4H), 1.99 (q, *J* = 6.8 Hz, 8H), 1.76 (s, 4H), 1.65 (s, 4H), 1.38 - 1.07 (m, 52H), 0.33 (s, 40H), -0.05 (s, 32H) ppm.

Cavitand 3: In 5 mL flask under the nitrogen atmosphere, dry cavitand 2 (390.4 mg, 241 μmol) was dissolved in THF (2.70 mL) and solution cooled down to -60 °C. Then, hexane solution of 9-borabicyclo(3.3.1)nonane (BBN, 0.5 M, 1.95 mL, 975 μmol) was added and stirred till solution became pinkish. Then, decanethiol (1.95 mL, 8.85 mmol) was added and reaction carried out at the room temperature for two days. Solvent was evacuated, crude material dissolved in methylene chloride (20 mL) and three times washed with water. Solution was dried over anhydrous sodium sulfate, solvent evacuated and obtained cavitand 3 recrystallized from ethanol as a white solid. Compared to published procedure, TMS-protection fell off during reaction with (acidic) thiol (312 mg, 194 μmol, 80%). 1H NMR (500 MHz, chloroform-d): δ = 9.59 (bs, 4H), 9.31 (bs, 4H), 7.17 (bs, 4H), 6.09 (bs, 4H), 4.28 (bt, 4H), 2.47 (td, *J* = 7.6, 2.6 Hz, 16H), 2.19 (bm, 8H), 1.61 - 1.48 (m, 16H), 1.41 - 1.19 (m, 112H), 0.86 (t, *J* = 7.0 Hz, 12H) ppm.

Cavitand 4: In 25 mL Schlenk flask, dry cavitand 3 (500.0 mg, 288 μmol), 2,3-dichloroquinoxaline (387.0 mg, 1.94 mmol) and cesium carbonate (688.0 mg, 2.02 mmol) were added, vessel kept on vacuum at 60 °C for an hour followed by nitrogen purge. Anhydrous DMF (17 mL) was added and reaction carried at the room temperature overnight, followed by reaction at 60 °C for 2 days. Reaction mixture was poured into mixture of ice and water, pale-brown precipitate collected by filtration and washed with water. Solid product was extracted with methylene chloride, washed with water, dried over anhydrous sodium

sulfate and solvent evacuated. Obtained crude material was purified by flash chromatography on silica, using ethyl acetate in methylene chloride (2%, gradient 2 - 10%, 10%) to afford colorless flakes of the cavitand 4 (412.4 mg, 184 μmol, 63.9%). 1H NMR (300 MHz, chloroform-d): δ = 8.13 (s, 4H), 7.77 (dd, *J* = 6.4, 3.4 Hz, 8H), 7.45 (dd, *J* = 6.3, 3.5 Hz, 8H), 7.18 (s, 4H), 5.55 (t, *J* = 7.9 Hz, 4H), 2.49 (t, *J* = 7.2 Hz, 16H), 2.33 - 2.11 (m, 8H), 1.63 - 1.48 (m, 16H), 1.48 - 1.11 (m, 112H), 0.91 - 0.80 (m, 12H) ppm.

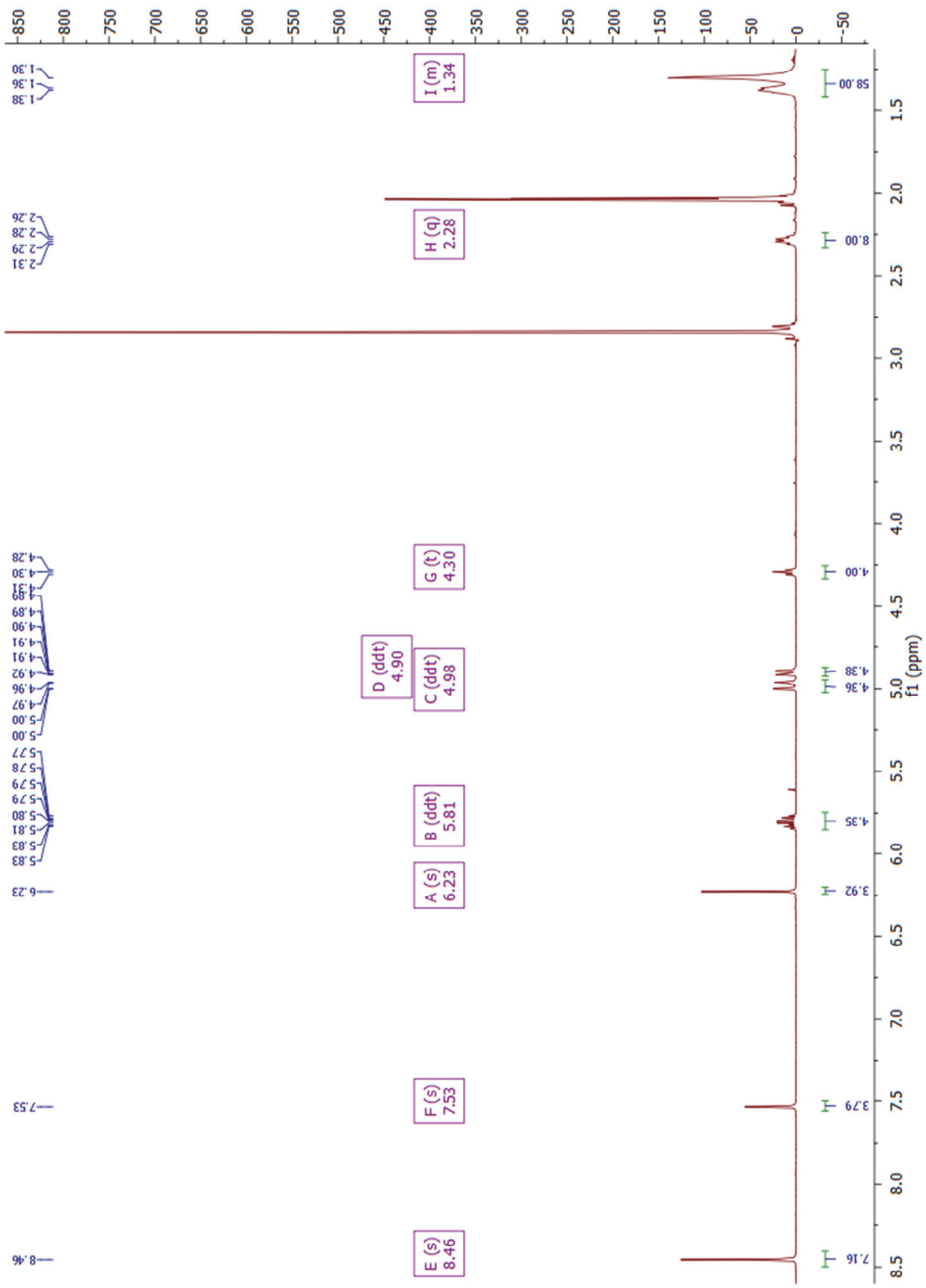

Figure II-2. ^{1}H NMR spectrum of cavitand **1**.

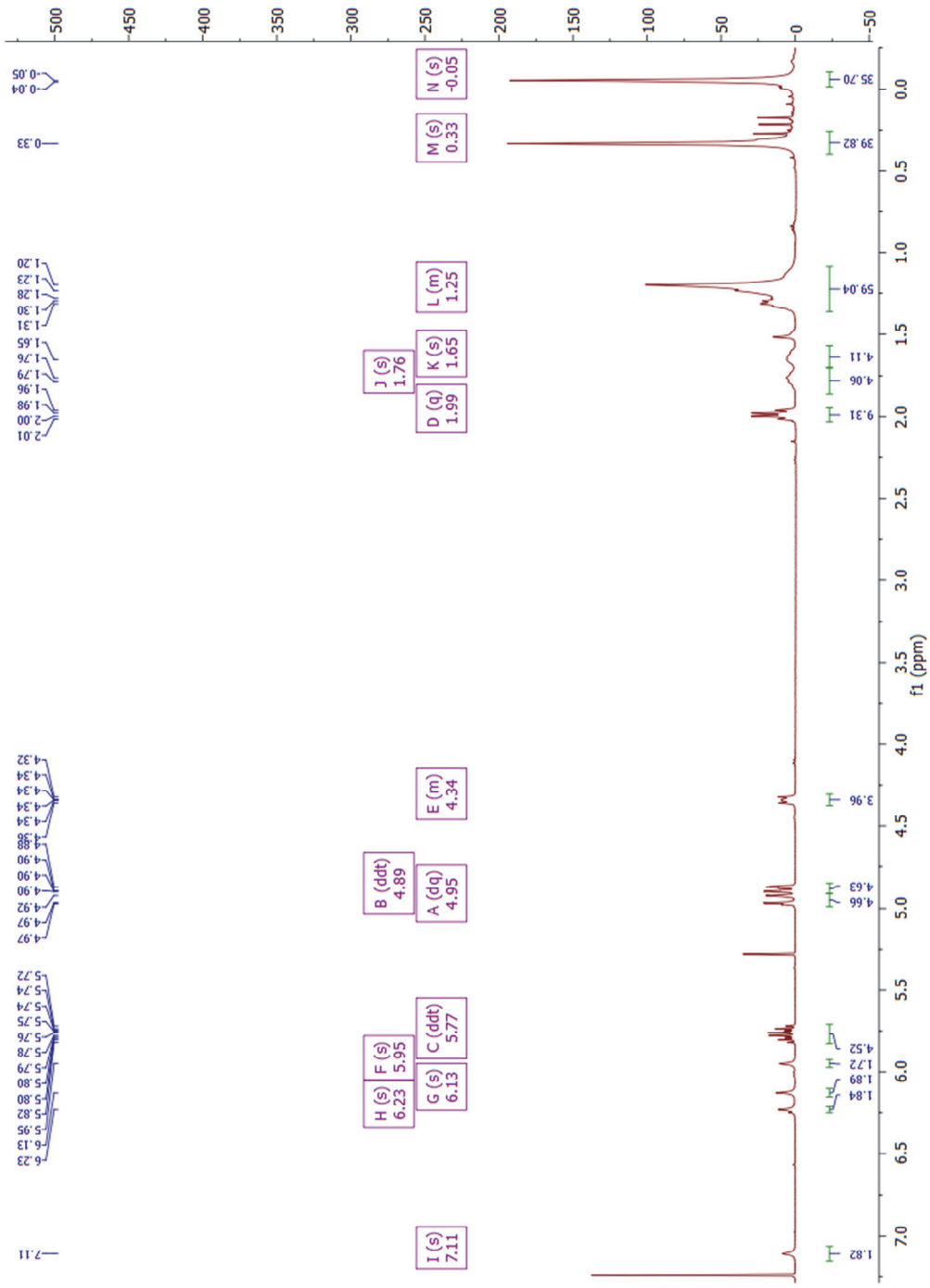

Figure II-3. ^{1}H NMR spectrum of cavitand **2**.

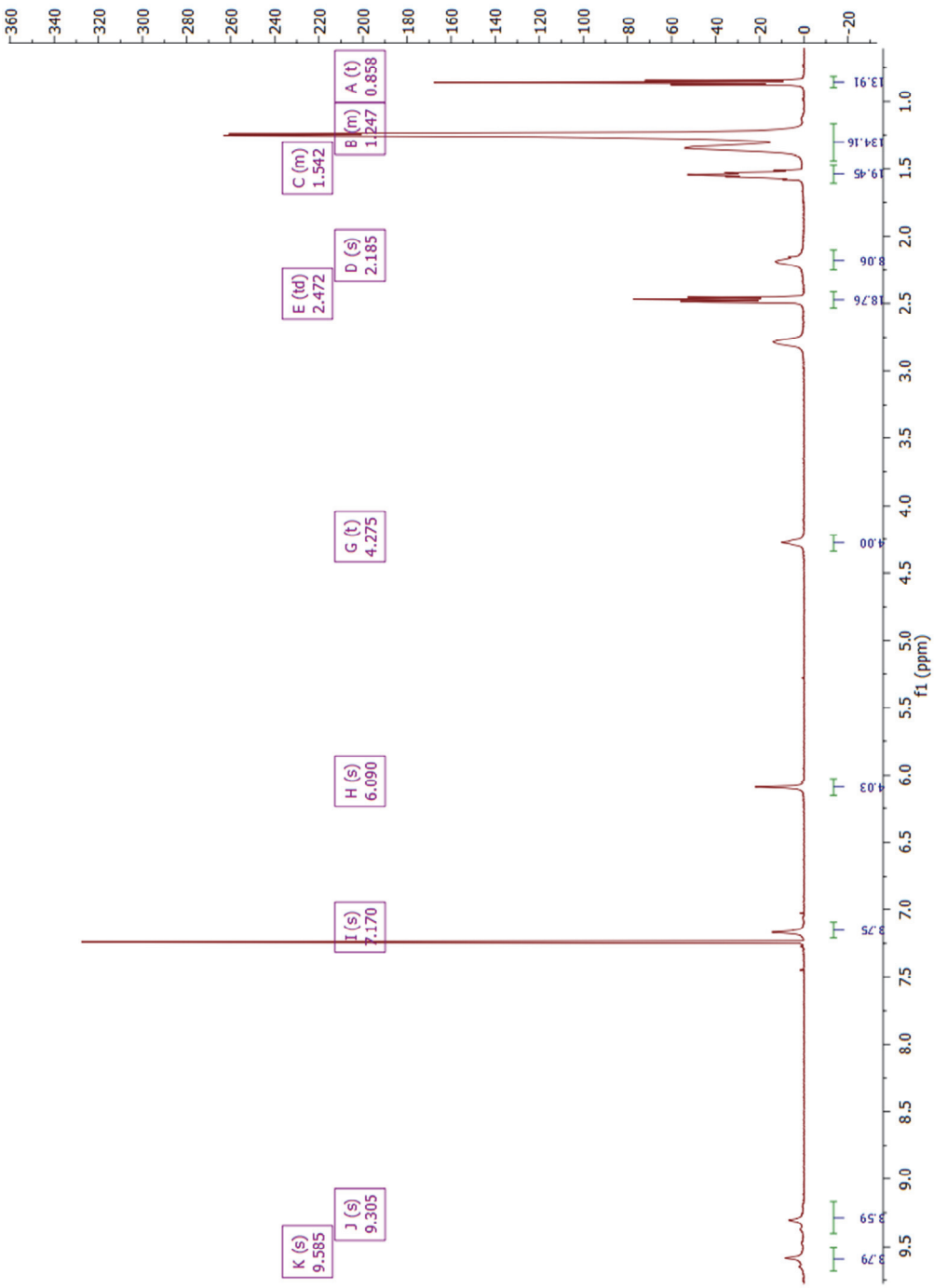

Figure II-4. ^{1}H NMR spectrum of cavitand **3**.

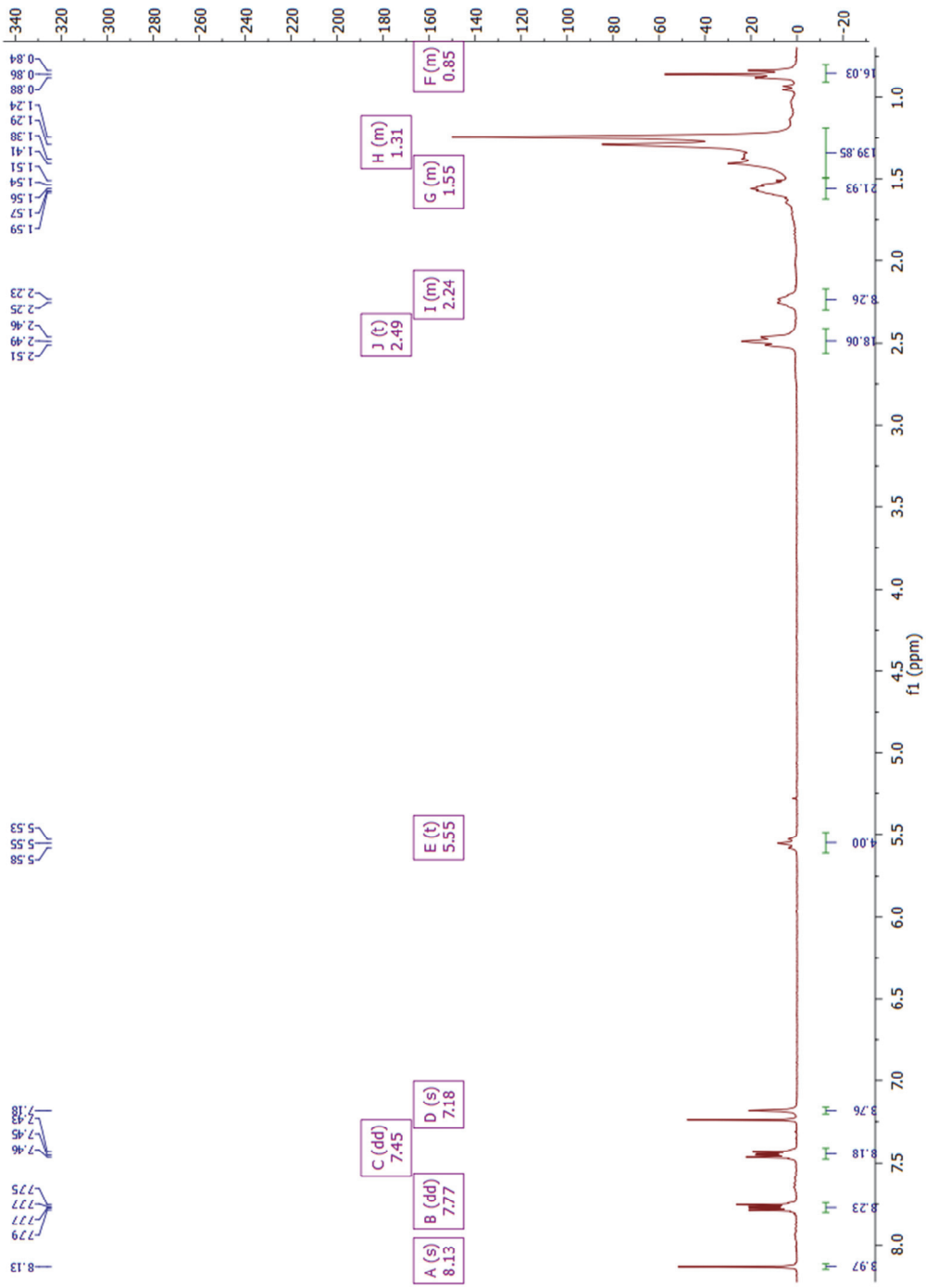

Figure II-5. ^{1}H NMR spectrum of cavitand **4**.

Annex III

Gold nanoparticle synthesis and SAM's of cavitand.

In 50 mL two-necked round bottomed flask, Gold(III) chloride trihydrate (8.5 mg) and cavitand 4 (28 mg, 0.5 mM) were dissolved in 20 mL of chloroform. The mixture was vigorously stirred during 30 min. Then, sodium borohydride (6 mg) dissolved in water (5 mL) cooled at 10°C was added drop-wise, and reaction stirred at room temperature. Characteristic red color appears due to gold nanoparticle growing (average size of 10-15 nm).

Publications in international Journals

- Accepted papers

1) **P. Clément**, S. Korom, C. Struzzi, Enrique J. Parra, C. Bittencourt, P. Ballester, E. Llobet, *"Deep Cavitand Self-Assembled on Au NPs-MWCNT as Highly Sensitive Benzene Sensing Interface"*. **Advanced functional materials** (2015); DOI: 10.1002/adfm.201501234 · 11.8 Impact factor

2) H. Baccar, A. Thamri, **P. Clément**, E. Llobet, A. Abdelghani,*"Pt- and Pd-decorated MWCNTs for vapour and gas detection at room temperature"*. **Beilstein journal of nanotechnology** (2015); 6:919-927. DOI:10.3762/bjnano.6.95 · 2.33 Impact Factor

3) Angel Ramos, **P. Clément**, Antonio Lazaro, Eduard Llobet, David Girbau, "*Nitrogen Dioxide Wireless Sensor based on Carbon Nanotubes and UWB RFID Technology"*. **ieee Antennas and wireless propagation letters** (2015); DOI:10.1109/LAWP.2015.2391293 ·1.95 Impact Factor

4) Atef Thamri, Hamdi Baccar, **P. Clément**, Eduard Llobet, Adnane Abdelghani, "*Rhodium-decorated MWCNTs for detecting organic vapours"*. **International journal of nanotechnology** (2015); 12(8/9):562 · 1.14 Impact Factor

5) H. Debéda, **P. Clément**, E. Llobet, V. Pommier-Budinger, I. Dufour, C. Lucat, **"***One-step firing for electroded PZT thick films applied to MEMS"*. **Smart materials and structures**

(2015); DOI:10.1088/0964-1726/24/2/025020 · 2.45 Impact Factor

6) **P. Clément**, Angel Ramos, Antonio Lazaro, Leopoldo Molina-Luna, Carla Bittencourt, David Girbau and Eduard Llobet, "*Oxygen plasma treated carbon nanotubes for the wireless monitoring of nitrogen dioxide levels".* **Sensors and actuators b chemical** (2014); 208:444-449. DOI:10.1016/j.snb.2014.11.059 · 3.84 Impact Factor

7) **P. Clément**, I. Hafaiedh, E.J. Parra, A. Thamri, J. Guillot, A. Abdelghani, E. Llobet. "*Iron oxide and oxygen plasma functionalized multi-walled carbon nanotubes for the discrimination of volatile organic compounds".* **Carbon** (2014); 78:510-520 · 5.87 Impact Factor

8) Debéda H., Lakhmi R., **Clément P.**, Llobet E., Zamarreño C.R., Arregui F.J., Lucat C. "*Inorganic and organic screen-printed cantilever-based gas sensors"*, **Sensors and transducers**, **173**, 6 (2014) 215-223 · 0.75 Impact Factor

9) Imen Hafaiedh, **P. Clément**, Hamdi Baccar, Eduard Llobet, Adnane Abdelghani. "*Functionalised multi-walled carbon nanotubes for chemical vapour detection".* **International journal of nanotechnology** (2013); 10(5/6/7):485 · 1.14 Impact Factor

10) Hafaiedh, W. Elleuch, **P. Clement**, E. Llobet, A. Abdelghani. "*Multi-walled carbon nanotubes for volatile organic compound detection".* **Sensors and actuators B: chemical** (2013); 182:344–350 · 3.84 Impact Factor

- Paper in progress

1) **P. Clément**, E. Del Castillo Perez, O. Ganzalez, R. Calavia, E. Llobet, C. Lucat, H. Debéda. *"Gas discrimination using screen-printed piezoelectric cantilevers coated with carbon nanotubes"*

Patent application

Inventor/s: **P. Clément**, S. Korom, Enrique J. Parra, E. Llobet, P. Ballester
Title: Selective detection of benzene traces in air
Application number: P27513ES00
First priority country: SPAIN
Date of priority: 11/2014
Main institution: ICREA, Universitat Rovira i Virgili, ICIQ

Contributions in National, European and International conferences

1) **P. Clément**, E. Llobet, C. Lucat, H. Debéda. Gas discrimination using screen-printed piezoelectric cantilevers coated with carbon nanotubes. Oral. EUROSENSORS XXIX. Freiburg (Germany), 2015

2) **P. Clément**, H. Debéda, C. Lucat, E. Llobet. Use of a CNT-coated cantilever with double transduction as a gas sensor for benzene detention at room temperature. Oral. The 28th European Conference on Solid-State Transducers, EUROSENSORS XXVIII. Brescia (Italy), 2014

3) **P. Clément**, H. Debéda, C. Lucat, M. P. Pina, E. Llobet. Combined resonance frequency and resistance measurements with a CNTs coated piezoelectric cantilever: application to benzene detection. Oral. 15th International Meeting on Chemical Sensors. Buenos Aires (Argentina), 2014

4) **P. Clément**, H. Debéda, E. Llobet, M.P. Pina, M.A.Urbiztondo. Screen-printed PZT cantilevers coated with inorganic nanopowders for benzene detection at room temperature. Oral. 3rd International Conference on Materials and Applications for Sensors and Transducers, IC-MAST. Prague (Czech Republic), 2013

5) J.W. Gardner, M. Cole, **P. Clément**, E. Llobet, Z. Ali and F. Udrea. Graphene SOI CMOS sensors for the detection of ppb levels of NO2 in air. Poster. Eurosensors XXVII – Transducers Barcelona (Spain), 2013

6) I. Hafaiedh, W. El Euch, **P. Clement**, A. Abdelghani, E. Llobet. Functionalized carbon nanotubes for the discrimination of volatile organic compounds. Poster.

Eurosensors XXVII –Transducers. Barcelona (Spain), 2013

7) **P. Clément**, H. Debéda, E. Llobet. Hybrid carbon nanotube as sensitive layer for resistive and resonant sensor Oral. PhD Institute of Bordeaux. Bordeaux (France), 2013

8) **P. Clément**, E. Llobet. RF sputtering as a tool for plasma treating and metal decorating CNTs for gas sensing applications. Oral. Graduate meeting. Tarragona (Spain), 2012

9) H. Debéda, R. Lakhmi, **P. Clément**, E. Llobet, C. Lucat. Gas detection using micro-structured organic and inorganic microcantilevers by screen printing. Oral. MADICA. Sousse (Tunisia), 2012

10) H. Debéda, R. Lakhmi, **P. Clément**, E. Llobet, M.P. Pina, M.A.Urbiztondo. VOC detection with screen-printed coated piezoelectric cantilevers. Comparison with Si cantilevers. Oral. Ibernam CMC2. Toulouse (France), 2012

11) **P. Clement**, E. Llobet, H. Debéda. RF sputtering as a tool for plasma treating and metal decorating CNTs for gas sensing applications. Oral. JNRDM. Marseille (France), 2012

12) R. Leghrib, **P. Clement**, E. Llobet. RF sputtering as a tool for plasma treating and metal decorating CNTs for gas sensing applications. Oral. Eurosensors XXV. Athens (Greece), 2011